AN ABSTRACT OF THE THESIS OF

Matthew McClintock for the degree of Master of Science in Soil Science presented on August 13, 2014

Title: Spatial Variability of Dust Deposition in the Luquillo Mountains, Puerto Rico

Abstract approved: _____

Julie Pett-Ridge

Dust deposition on ecosystems with highly weathered soils may provide vital rock-derived nutrients that maintain ecosystem productivity. Because of the difficulties in measuring temporally and spatially heterogeneous dust deposition over ecologically meaningful timescales, evaluations of the spatial variability in dust deposition are extremely rare. In the Luquillo Mountains of Puerto Rico, dust originates from the Sahara-Sahel region of Africa, travelling on trade winds from the east across the Atlantic Ocean. This thesis evaluates the spatial variability of dust deposition in two ways: 1) using two twenty-year weekly records of rainfall chemistry in conjunction with historical airmass trajectory provenance, and 2) Isotopic ratios of neodymium in soil that represent mixing between neodymium from bedrock sources and from African dust. Results from rainfall chemistry show deposition can vary from 0.7 to 2.6 g dust m^{-2} yr^{-1} along a 10 km east to west transect in the Luquillo Mountains. Across 31 ridgetop locations, soil neodymium isotope ratios reveal a spatial variability in dust deposition of 1.7 to 43.2 g m^{-2} yr^{-1} in an approximately 10 x 10 km area. An analysis of several key environmental variables has not revealed a key factor that determines long-term differences in dust deposition. The most probable control on dust deposition is a complex interaction of variables such as surface wind patterns and long-term canopy characteristics.

Spatial Variability of Dust Deposition in the Luquillo Mountains, Puerto Rico

by
Matthew McClintock

A THESIS

submitted to

Oregon State University

in partial fulfillment of
the requirements for the
degree of

Master of Science

Presented August 13, 2014
Commencement June 2015

Master of Science thesis of Matthew McClintock presented on August 13, 2014

APPROVED:

Major Professor, representing Soil Science

Head of the Department of Crop and Soil Science

Dean of the Graduate School

I understand that my thesis will become part of the permanent collection of Oregon State University libraries. My signature below authorizes release of my thesis to any reader upon request.

Matthew McClintock, Author

ACKNOWLEDGEMENTS

The author expresses sincere appreciation…..to everyone

CONTRIBUTION OF AUTHORS

Dr. Gilles Brocard contributed an understanding of geomorphology of the region as well as ^{10}Be data used in Chapter 2 of this thesis. Dr. Stephan Porder contributed to the understanding of the soil properties, phosphorus cycling at our site locations, and provided the physical soil samples used in Chapter 2 of this thesis.

TABLE OF CONTENTS

TABLE OF CONTENTS (Continued)

TABLE OF CONTENTS (Continued)

LIST OF FIGURES

LIST OF FIGURES

LIST OF TABLES

1 Thesis Introduction

Atmospheric mineral aerosol dust originates when mineral particles from the surface are ejected by wind erosion into the atmosphere. Most dust originates in deserts where dry environments facilitate entrainment of particles into the atmosphere. Understanding how dust behaves both in the atmosphere and after it settles on land or the ocean is important for understanding how the Earth System functions in many different ways. For example, pathogens plaguing coral reefs can be transported by dust [Shinn et al., 2000]. The radiative budget of the Earth can be drastically impacted by dust reflecting incoming radiation back out of the atmosphere [Tegen et al., 1996]. Increases in ocean productivity are directly caused by iron fertilization from dust deposition [Coale et al., 1996; Martin, 1990]. Finally, highly weathered terrestrial ecosystems that have limited rock-derived nutrients can be supplied with fresh minerals from long-range dust transport [e.g. Chadwick et al., 1999].

This thesis addresses the spatial and temporal variability of dust deposition to an ecosystem on highly weathered soil using two different methods. The specific ecosystem studied in this thesis is a montane tropical wet forest in the Luquillo Mountains of Puerto Rico. Evaluating the spatial variability of dust deposition is important for understanding the effect of dust in fertilizing of terrestrial ecosystems. Given the difficulty of measuring dust deposition, studies attempting to discern the spatial variability of long-range dust deposition are extremely rare. In addition to spatial variability, temporal variability of dust deposition can elucidate both how dust has affected past climates of the Earth System and how past climates have affected dust deposition rates. Few studies have such long-term measures of dust deposition in rainfall, and even fewer have attempted to

calculate a dust flux from isotopic measurements, which yield dust deposition averages for thousands of years.

The first method used in this thesis utilizes weekly records of rainfall chemistry from two separate rain-gauge stations 10 km apart in the Luquillo Mountains that have been operational for twenty years. The rainfall chemistry record includes three separate indicators of dust deposition, total suspended solids (TSS), non-seasalt calcium (nss-Ca) and dissolved silica ($dSiO_2$). Pairing this rainfall chemistry record with backward airmass trajectories to the Caribbean's main source of dust answers several important questions regarding: (1) relationships between nss-Ca, TSS, dSiO2, and backward airmass trajectories from the Sahara-Sahel region and the utility of each rainfall metric as a dust tracer, (2) variability in dust fluxes between two sites that are 10 km apart with similar rainfall, elevation, and forest type, (3) seasonal variation in dust deposition and its controls, and (4) rough estimates of dry deposition as calculated by difference, either between throughfall and openfall, or openfall and wet-only deposition.

The second method used in this thesis utilizes the isotopic ratio of neodymium (Nd) to trace dust deposition in 31 separate locations in the Luquillo Mountains. The Sahara-Sahel region of Africa has ratio of $^{143}Nd/^{144}Nd$ that is very different from the $^{143}Nd/^{144}Nd$ ratio found in Luquillo bedrock. This means that the ratio of $^{143}Nd/^{144}Nd$ in soil represents a two-endmember mixing calculation between dust and bedrock. Knowing the concentration of Nd in dust, and estimating the amount of dust associated Nd that has weathered out of the soil, we can calculate a dust flux that is an average over the residence time of the soil. Once an estimate of dust deposition is calculated for all site locations, correlations are examined between dust flux and several environmental

variables in an effort to answer questions regarding (1) the spatial variability of dust deposition over geologic timescales (2) if dust deposition is spatially variable, what factors control dust deposition over these longer timescales (3) how much P or other nutrients has this dust provided to the ecosystem and how does that compare to current bedrock nutrient contributions.

The primary relationship between both chapters in this thesis is the study of the spatial variability of dust deposition. Although both methods address this issue from a different approach, and over different timescales, both answer similar questions and open discussion on how dust is affecting terrestrial ecosystem processes. Both chapters also discuss the trans-oceanic relationship between the Sahara-Sahel region of Africa and highly productive ecosystems in the Americas.

Variability of African dust deposition in the Luquillo Mountains, Puerto Rico, based on rainfall chemistry and HYSPLIT airmass back-trajectory modeling

M. A. McClintock[1], W. H. McDowell[2], and J.C. Pett-Ridge[1]

[1]Department of Crop and Soil Science, Oregon State University, Corvallis, OR, USA.

[2]Department of Natural Resources and the Environment, University of New Hampshire, Durham, NH, USA

Corresponding author: M. McClintock, Agricultural & Life Sciences 3017, Oregon State University, Corvallis, OR, 97331-7306 (mcclinma@onid.oregonstate.edu)

Key Points

- Dissolved SiO_2 in rainwater reflects dust inputs more closely than non-seasalt Ca^{2+}
- Dust deposition after long-range transport is highly spatially variable on landscape scale
- Dust deposition fluxes in Puerto Rico are controlled by Sahel environmental conditions

2.1 Abstract

Dust deposition represents an important flux of rock-derived nutrients such as phosphorus to ecosystems on highly weathered soils. Direct measurements of dust deposition and its spatial variability are rare, yet they are essential for testing models of dust deposition processes and understanding the biogeochemical effects of dust. Long-term records of precipitation chemistry are available in the Luquillo Mountains of Puerto Rico, which are downwind of the world's largest dust source located in Northern Africa. We analyzed 20-year datasets of openfall, throughfall, and wet-only precipitation chemistry with weekly resolution at two different locations in the Luquillo Mountains to evaluate spatial and temporal variability of dust inputs. The measured dust flux varied by a factor of 2 over a distance of 10 km despite similarities between sites in elevation and rainfall amount. We evaluated which rainfall chemistry metrics best represented the flux of dust to the ecosystem by pairing these datasets with HYSPLIT (Hybrid Single Particle Lagrangian Integrated Trajectory) airmass back trajectory model calculations of airmasses coming from the Sahara-Sahel dust source region. Total suspended solids (TSS) and dissolved silica ($dSiO_2$) in openfall were higher at the eastern site in weeks with airmasses coming from the Sahara-Sahel region. Notably, non-seasalt calcium (nss-

Ca^{2+}) fluxes were not correlated with weeks in which airmasses originated from the Sahara-Sahel region, and did not vary between sites. Seasonal variation in the relationship between airmass origin and dissolved SiO_2 flux in openfall indicates that environmental conditions in the Sahel control variation in dust deposition in Caribbean.

Keywords

dust deposition; long-range transport; dissolved silica; Caribbean; rainfall chemistry; HYSPLIT

2.2 Introduction/Background

Mineral aerosol dust transport in the atmosphere has wide implications for Earth's climate and biogeochemical processes. The radiation budget of the Earth can be altered by atmospheric dust [Tegen et al., 1996], and ocean-dwelling photosynthetic life in high nutrient low chlorophyll zones relies on iron delivered to the water surface by dust deposition [Coale et al., 1996; Martin, 1990]. Dust can be a long-range vector for bacterial and fungal movement; for example, there is evidence that pathogens plaguing coral reefs in the Caribbean are transported from Africa by dust storms [Shinn et al., 2000]. Dust can also play a potential role in fertilizing certain terrestrial ecosystems by supplying phosphorus [e.g. Chadwick et al., 1999], or micronutrients [Bruijnzeel, 1991]. If dust is the main supplier of a limiting nutrient in highly productive ecosystems such as the Amazon Rainforest [Swap et al., 1992], then major carbon sinks can be controlled by climate factors affecting Sahara-Sahel dust production, transport, and deposition. However, before a link can be made between the Sahara-Sahel and other ecosystems, the

atmospheric removal processes that control how dust falls on a landscape must be understood [Prospero et al., 2010].

Modern atmospheric dust loading is monitored with remote sensing such as MODIS-based aerosol optical depth (AOD), or at specific field locations with air sampling stations that actively pass air through a filter [Prospero and Lamb, 2003]. In contrast to dust concentration in the air, however, there are very few available records of terrestrial dust deposition [Mahowald et al., 2008; and Kohfeld and Harrison, 2001]. Both modeling and direct measurement of dust deposition based on airmass dust concentration are hampered by multiple issues, including the high spatial and temporal variability in both transport and deposition. Dust deposition collectors cannot meaningfully measure the long-term average dust deposition a forested ecosystem receives, in part because they do not mimic the forest canopy structure and surface properties of leaves [Hicks et al., 1980; Lindberg and Lovett, 1985; Stoorvogel et al., 1997; White and Turner, 1970]. Deposition collectors may also miss significant portions of dust deposition if they are not exposed for long enough time periods, as dust deposition is highly episodic in nature [Prospero et al., 2001]. Particularly in montane topography, there are no clear relationships between dry deposition and leaf area index [De Longe et al., 2008]. Indirect estimates of dry deposition using the difference between measured openfall and throughfall are often confounded by foliar leaching or foliar uptake [Lindberg et al., 1988]. Model estimates of dust deposition are also problematic. Dry deposition of dust particles, which are predominately in the < 20 μm size range, is controlled by impaction and Brownian motion rather than by simple gravitational settling [Newman, 1995]. Model estimates of wet deposition are limited by considerable debate as to the choice of

scavenging ratio (defined as the ratio of the concentration of an element in dust to the concentration of that element in rain), and scavenging ratios can vary seasonally [Mahowald, 2005a, Prospero et al., 2010]. To simulate the poorly understood wet removal process, many researchers use simple scavenging ratios of between 200 and 1000 based on empirical observations [e.g., Tegen and Fung, 1994; Mahowald et al., 2003, Duce et al., 1991, and Jickells and Spokes 2001]. Attempts to identify and quantify contributions from specific dust source regions have been made with varying degrees of success based on comparison with ground–based measurements [Ginoux et al., 2001; Perez et al., 2006; Zhou et al., 2008]. As expected, there is greater confidence in determining sources of dust when the dust source and the site of deposition are in relatively close proximity [Jorquera & Barraza, 2013]. Longer distances between a dust source and an area of interest introduce large uncertainties with deposition sites often receiving different amounts of dust from different sources during different times of the year [Lawrence, 2009]. Problems with tracking long distance dust transport can be resolved with the use of chemical tracers unique to different source regions, or with computer models that identify source regions by tracking airmasses over longer time periods.

In this study we addressed questions specifically associated with quantifying dust deposition, including identifying appropriate chemical tracers of dust, temporal patterns, and spatial variability. We examined weekly resolution 20 year rainfall chemistry datasets from two different locations in the Luquillo Mountains of Puerto Rico, which are known to receive dust deposition from the Sahara-Sahel region of Africa [Stallard, 2012; Heartsill-Scalley, 2007; Pett-Ridge, 2009]. Specifically, we examined dissolved silica

($dSiO_2$), non sea-salt Ca^{2+} (nss-Ca^{2+}), and total suspended solids (TSS) in openfall, wet-only deposition, and throughfall as dust tracers. In addition to comparing $dSiO_2$, nss-Ca^{2+}, and TSS against each other, we also examined correlations between peaks in dust deposition with airmass back-trajectory analysis (HYSPLIT) to the Sahara-Sahel region of Africa, the primary dust source region for the Caribbean [Stallard, 2001; Kumar et al., 2014].

HYSPLIT uses meteorological data obtained from the National Centers for Environmental Prediction and the National Center for Atmospheric Research to calculate airmass trajectories both backward and forward in time [Draxler and Hess, 1998]. It has proven an invaluable tool for modeling the dispersion of dust as well as atmospheric contaminants [Yerramilli et al., 2012; Jorquera & Barraza, 2013]. A global analysis of sand and dust storms using the HYSPLIT model confirmed its effectiveness for predicting atmospheric dust concentrations on a global scale [Wang et al., 2011], and also verified accuracy in predicting seasonal variations in dust storm frequencies. Prior work using HYSPLIT back-trajectory modeling has been used to trace Sahara-Sahel dust to the Ecuadorean Andes and to Puerto Rico, over timescales of weeks [Boy and Wilke, 2008; Gioda, 2008; Reyes-Rodriguez, 2009; Gioda, 2011].

The Luquillo Mountains of Puerto Rico are well-suited for studying dust deposition because there is one dominant source region, the Sahara-Sahel region of Africa, and no other significant landmasses in the pathway of dust transport. The predominant wind direction is from the northeasterly trade winds off the Atlantic Ocean, minimizing the possibility of local anthropogenic influence. While previous studies have examined Luquillo Mountain's rainfall chemistry [e.g. McDowell et al, 1990; Stallard,

2001; Heartsill-Scaley et al, 2007; Gioda et al, 2013]; our approach brings a novel analysis of $dSiO_2$ and TSS as tracers of dust deposition in comparison to nss-Ca^{2+}. Our analysis of rainfall chemistry records and HYSPLIT modeling allows us to target four specific questions regarding: (1) relationships between non-seasalt Ca^{2+}, TSS, $dSiO_2$, and HYSPLIT trajectories from the Sahara-Sahel region and the utility of each rainfall metric as a dust tracer, (2) variability in dust fluxes between 2 sites that are 10 km apart with similar rainfall, elevation, and forest type, (3) seasonal variation in dust deposition and its controls, and (4) rough estimates of dry deposition as calculated by difference, either between throughfall and openfall, or between openfall and wet-only deposition.

2.3 Methods

2.3.1 Study Site and Rainfall Chemistry

The two rain gauges used in this study are located in the Bisley watershed and at the El Verde field station in the El Yunque National Forest in the Luquillo Mountains of northeastern Puerto Rico (Figure 1). These sites are part of the Luquillo Long Term Ecological Research (LTER) and Luquillo Critical Zone Observatory (CZO) programs. Both rainfall collection stations are located at approximately the same latitude; Bisley is approximately 10 km west of the northeastern coast and El Verde is approximately 24 km west of the northeastern coast. The Bisley and El Verde precipitation collectors are at approximately the same elevation (350 m) and have similar surrounding vegetation composed of a mixed forest of tabonuco, sierra palm, and colorado trees [Scatena, 1990]. The two sites have very similar temperature, relative humidity, and precipitation [Gioda et al., 2013]. At El Verde, weekly openfall (always open collector) and weekly wet-only rainfall flux and chemistry have been measured since 1983, and at Bisley weekly openfall

and weekly throughfall (passed through canopy) flux and chemistry have been measured since 1988. Bulk openfall measurements are taken at both sites from a tower >25 m above the forest canopy [Heartsill-Scalley et al., 2007; McDowell et al., 1990]. Throughfall was measured in a 3 ha area that surrounds the location of the openfall collector. As many as 35 throughfall collectors were operating at any one time for the duration of this study, each collector being randomly placed but located on ridges, hill-slopes, gaps and stream channels [Heartsill-Scalley, 2007]. Over the period of study, 1988 to 2009, total rainfall averaged 3.7 m yr^{-1} (± 0.7 m yr^{-1}) at the Bisley site and 3.5 m yr^{-1} (± 0.8 m yr^{-1}) at the El Verde Site.

Both weekly precipitation flux and chemistry including Ca^{2+} and $dSiO_2$ were obtained from the Luquillo Long Term Ecological Research database for the years 1988 through 2009 (http://luq.lternet.edu/data/datasets/all). All samples were filtered at ~0.7 μm (pre-combusted Whatman GF/F glass fiber filter) before chemical analysis. The silica detection limit was 0.1 mg L^{-1}, which is more than double typical glass fiber filter silica blanks [de Souza et al., 2012]. Calcium was measured by ion chromatography with colorimetric analysis (phenolhypochlorite), while $dSiO_2$ was measured by automated colorimetric analysis (molybdate blue), and Cl^- was measured by liquid chromatography with conductivity detection (http://luq.lternet.edu/data/luqmetadata174). Values below the detection limit were recorded as half the detection limit for statistical purposes. We adjusted Ca concentrations to remove seasalt contributions using the following equation [e.g. Stallard 2001],

$$non\ seasalt\ Ca^{2+} = Ca^{2+} - Cl^- \times (seasalt\ Ca^{2+}{:}\ Cl^-)$$

Fluxes were calculated by multiplying concentrations by the LTER rainfall flux records, which were co-located with chemical sampling. TSS in bulk rainfall was determined using the mass of total solids on the pre-weighed filter used to filter samples from the Bisley and El Verde sites prior to chemical analysis. In rare instances when filtering the entire volume of sample was difficult, a representative subsample of each week's shaken openfall rain was taken. Collection of TSS data began in the year 2000. To calculate a rough estimate of dry deposition at Bisley, openfall concentrations of nss-Ca^{2+} and $dSiO_2$ were subtracted from throughfall concentrations of nss-Ca^{2+} and $dSiO_2$ each week. To calculate a rough estimate of dry deposition at El Verde, wet-only precipitation concentrations of nss-Ca^{2+} and $dSiO_2$ were subtracted from openfall for each week.

2.3.2 HYSPLIT Trajectories

Hybrid Single-Particle Lagrangian Integrated Trajectories (HYSPLIT) is a model which takes historical meteorological data from archived sources and calculates the movement of airmasses for any latitude and longitude, and any elevation up to 10 km above ground level (access via NOAA ARL READY website, http://www.arl.noaa.gov/ready/hysplit4.html). We used the reanalysis meteorological dataset which merges several other datasets dating back to 1948. We calculated airmass trajectories once per day for years 1988-2009 at universal time code 0000. The starting latitude and longitude units were set to $18^{o}15'$N and $65^{o}45'$W, corresponding to northeastern Puerto Rico. Starting elevation was set to 600 m above-ground level, which is an elevation at which the cloud base of many trade winds from the Sahara-Sahel region pass over the island [Stallard, 2012]. When the model showed an airmass that came from any part of the African continent above ten degrees north, without passing over other

landmasses, it was given a value of 1. If the model showed that the airmass came from any other trajectory it was given a value of zero. Figure 2a shows an example of a back-calculated airmass trajectory that passes over the Sahara-Sahel region, which is counted for a value of 1. Figure 2b shows an example of a backward airmass trajectory that does not pass over the Sahara-Sahel, which was counted as a value of 0. This is similar to the model first proposed by Westphal et al. [1987], and subsequently utilized in several other studies [Escudero et al., 2006; Stein et al., 2011] where any airmass trajectory that passed over a geographic grid cell defined as desert, was considered to have potentially picked up dust. These values were added up over the same prior 7-day period corresponding to the weekly rainfall chemistry collection times. Over the study period, 7,671 backward airmass trajectories were calculated using HYSPLIT.

2.3.3 Statistical Analysis

A small number of nss-Ca^{2+}, TSS, and $dSiO_2$ data points had extremely elevated values, which may reflect sample contamination. We applied a simple threshold and removed data points that were greater than three standard deviations above the mean. A nearly identical subset of outliers were identified using either the rule of thumb of semistudentizied residuals absolute value >4, or using a threshold of three standard deviations above the median [Neter et al, 1996]. These datapoints were removed from consideration in further statistical analyses. For Bisley and El Verde $dSiO_2$, 7 out of 848 and 2 out of 818 data points were removed, respectively. For Bisley and El Verde nss-Ca^{2+}, 16 out of 830 and 23 out of 804 data points were removed, respectively. For Bisley and El Verde TSS, 6 out of 378 and 0 out of 371 data points were removed, respectively.

Because of the event-based nature of dust deposition, the nss-Ca^{2+}, $dSiO_2$, and TSS datasets are heavily weighted toward low or minimum detectable values. This creates non-normally distributed data. Due to the non-normal nature of the overall dataset, a Kruskal-Wallis test was performed to examine medians of datasets (log transformations still produced non-normal datasets). This tested the null hypothesis that there is no relationship between either location and dust deposition, or that there is no relationship between airmass provenance and dust deposition. Comparisons were made between openfall chemistry fluxes between sites, inter-season fluxes between and within each site, and between weeks with at least one Sahara-Sahel airmass present versus weeks without Sahara-Sahel airmasses. Nss-Ca^{2+}, $dSiO_2$, and TSS data were split into several groupings to be compared to each other. Seasonal groupings of data were in thirteen week increments, with the start of winter defined at the beginning of week 51. The HYSPLIT model was grouped by simple binary separation of whether northeastern Puerto Rico received at least one Saharan-Sahel-derived airmass (+), or no Saharan-Sahel-derived airmasses (-).

Missing data points encompass weeks where sites were inaccessible for logistic reasons, rainfall was insufficient to produce a sample large enough for chemical analysis, or when there was no Cl^- measurement that week to make the seasalt correction in the Ca data. These data points are evenly distributed across the study period. These missing data points constituted between 20 and 28% of all data across all categories. For both Bisley and El Verde weeks where the dry deposition calculation resulted in a negative value, it was assumed that dry deposition for that week equaled zero. At Bisley, there were 266 and 264 missing data points out of 1050 total in dry deposition for nss-Ca^{2+} and $dSiO_2$

respectively. At El Verde, there were 302 and 318 missing data points out of 1038 total for nss-Ca^{2+} and $dSiO_2$ respectively. These missing data points do not include data points missing due to Hurricane Hugo, which caused a gap in all measurements from September 18, 1989 to December 25, 1990.

2.4 Results

2.4.1 Average Weekly Fluxes

The yearly openfall nss-Ca^{2+} fluxes to Bisley and El Verde for the duration of the study were not significantly different, with averages of 0.423 and 0.443 kg ha^{-1} wk^{-1}, respectively (Table 1). In contrast, there was a significant difference between the two sites in the openfall flux of $dSiO_2$, which averaged 0.139 and 0.076 kg ha^{-1} wk^{-1} at Bisley and El Verde, respectively ($p<0.05$). A similar difference was evident in the openfall flux of TSS, which was 1.467 and 0.650 kg ha^{-1} wk^{-1} at Bisley and El Verde, respectively ($p<0.05$, Table 1). In the individual weekly data, TSS was not significantly correlated with either $dSiO_2$ or nss-Ca^{2+}, and $dSiO_2$ and nss-Ca^{2+} were not significantly correlated with each other.

The average throughfall flux of nss-Ca^{2+} at Bisley was 1.153 kg ha^{-1} wk^{-1} (2.7 times greater than the openfall flux), while the throughfall flux of $dSiO_2$ averaged 0.282 kg ha^{-1} wk^{-1}, (2.0 times greater than the openfall flux.) The average wet-only flux of nss-Ca^{2+} at El Verde was 0.193 kg ha^{-1} wk^{-1} (44% of the the openfall flux), while wet-only $dSiO_2$ averaged a flux of 0.061 kg ha^{-1} wk^{-1} (80% of the the openfall flux) (Table 1). The same set of statistical analyses was performed on concentration data without converting to flux numbers with rainfall amounts. These analyses yielded the same results in terms of when there were significant differences in comparisons between datasets.

2.4.2 HYSPLIT trajectories

Airmasses came from one of 3 regions: the Sahara-Sahel, the east-coast of the United States, or Southern Africa. More than 95% of the travel times from the Sahara-Sahel region to the Caribbean were between 3 to 10 days. When the HYSPLIT trajectory data were grouped based on whether or not an airmass had come from the Sahara-Sahel (+ or -), two significant results were apparent (Table 2). First, the median value of the Bisley openfall flux of $dSiO_2$ was significantly higher during weeks with Sahara-Sahel airmasses, (0.065 kg ha^{-1} wk^{-1} versus 0.048 kg ha^{-1} wk^{-1} during weeks without, $p<0.05$). Second, the median value of throughfall $dSiO_2$ flux at Bisley was also higher during weeks with a Sahara-Sahel airmass (0.154 kg ha^{-1} wk^{-1} versus 0.111 kg ha^{-1} wk^{-1}, $p<0.05$). The flux of nss-Ca^{2+} in openfall and throughfall at Bisley showed no significant change based on airmass origins. At Bisley, TSS flux in openfall was slightly higher during weeks that an airmass had come from the Sahara-Sahel (0.893 vs. 0.699, marginally significant $p=0.051$). Fluxes at El Verde did not vary based on where airmasses were originating. Similarly, the wet-only precipitation collector at El Verde also showed no significant changes in rainfall chemistry based on the presence or absence of airmasses coming from the Sahara-Sahel for the weeks the data represented. Dry deposition estimates for both Bisley and El Verde also did not show significantly different values during weeks with airmasses from the Sahara-Sahel (Table 2). The same statistical results were apparent when using concentration only data.

2.4.3 Seasonal Variations

Both Bisley and El Verde showed similar seasonal patterns in the openfall, throughfall, and wet-only fluxes of nss-Ca^{2+}, $dSiO_2$, and TSS (Table 3). Generally in the

winter and spring months of the year, fluxes of nss-Ca^{2+}, $dSiO_2$, and TSS were lowest. Summer fluxes were highest, and fluxes dropped again in the fall (Figure 3). The average number of airmass trajectories coming from the Sahara-Sahel region followed a different pattern where airmasses from the Sahara-Sahel were elevated throughout the summer and fall seasons (Figure 4). The only flux to follow the seasonal pattern of airmass origins is the throughfall $dSiO_2$ flux at Bisley. When comparing individual seasons between sites, there was still a significant difference in $dSiO_2$ concentrations, but not nss-Ca^{2+} concentrations (Table 3). During the summer, openfall $dSiO_2$ flux was 3 times higher at Bisley, and the $dSiO_2$ flux was always higher at Bisley than El Verde regardless of season. For example, during winter, the median openfall flux of $dSiO_2$ to Bisley was 2.3 times higher than the winter openfall flux of $dSiO_2$ to El Verde. The same patterns in seasonal distribution are apparent when examining concentration data.

2.5 Discussion

2.5.1 Rainfall Chemistry

Non sea-salt-Ca^{2+} has been used as an indicator of the dust component within rainfall chemistry as it is unlikely to be a significant component of other sources such as biomass burning or anthropogenic pollution aerosols, and Ca is known to be a significant component in desert soils from which dust is sourced [Stallard, 2001; Röthlisberger, 2002; Prospero, 2003, Lequy 2013]. Both Ca^{2+} and Cl^- are commonly measured ions in rainwater, making nss-Ca^{2+} a practical tracer of dust. On the other hand, $dSiO_2$ is measured much less frequently in rainwater, and subsequently rarely compared to nss-Ca^{2+}. If nss-Ca^{2+} was assumed to be a tracer of dust deposition, it would show that, on average, the same amount of dust fell on both the Bisley and El Verde sites in the

Luquillo Mountains (Figure 5). However, $dSiO_2$-based estimates of dust deposition indicated that Bisley received approximately two times as much dust in openfall as El Verde over the same time period (Figure 6). Backward airmass trajectories from the primary source of dust for Puerto Rico help reconcile whether dust deposition is spatially variable or not.

When comparing $dSiO_2$ and nss-Ca^{2+} in Bisley openfall, only $dSiO_2$ was significantly higher during weeks with airmass trajectories originating from the Sahara-Sahel and moving directly over Puerto Rico (Table 2). Higher TSS was also associated with positive HYSPLIT trajectories at Bisley ($p=0.051$), indicating mineral aerosol dust is an important component of particulate matter in precipitation. Throughfall at Bisley showed the same pattern, with $dSiO_2$ significantly higher during weeks that Sahara-Sahel airmasses were over Puerto Rico, while throughfall nss-Ca^{2+} was not. For these reasons, $dSiO_2$ appears to be a more accurate tracer of dust deposition than nss-Ca^{2+}. There are several reasons why this may be the case. Nss-Ca^{2+} may be affected by additional sources of atmospheric Ca not related to mineral aerosol dust such as volcanic ash from the Soufriere Hills in Montserrat, although little or no correlation between rainfall chemistry and ash events has been observed [Gioda et al., 2011, Heartsill-Scaley et al., 2007]. There could be fractionation between Ca and Cl during seasalt spray entrainment into the atmosphere, which could introduce error into the nss-Ca^{2+} sea salt correction. In general, the strength of correlations between rainfall chemistry or TSS and HYSPLIT trajectories are likely limited by several factors, including the fact that not all particulate matter is necessarily mineral aerosol dust, the time the dust can dissolve in the collector is variable from hours up to 7 days. The dominant factor limiting the correlation, however, is that

airmasses with the correct trajectory may or may not carry dust and may or may not encounter conditions that lead to deposition. An additional factor that likely controls the difference in correlations between $dSiO_2$ and nss-Ca^{2+} is the large variability in the Ca content of African dust relative to Si (for example, a range of 0.11 to 26.28 wt.% CaO versus a range of 20.5 to 79.2 wt.% SiO_2, Abouchami et al., 2013), and large variability in the degree of dissolution of the Ca in dust relative to Si. Calcium in African dust is present primarily as relatively soluble calcium carbonate or calcium sulfate minerals [Reid et al., 2003], whose solubility is highly dependent on pH and rainfall amount. In contrast, silica solubility, as either quartz or biogenic opal, is much smaller and is largely constant between pH 2.5 and 8.5 [Dove, 1995; Cornelis et al., 2011]. This variability in dust-derived dissolved Ca^{2+} likely obscures long-term patterns between HYSPLIT trajectories, dust deposition, and precipitation nss-Ca^{2+} inputs, despite earlier reports from a few years of data showing links between dust and nss-Ca^{2+} concentrations [McDowell et al., 1990].

2.5.2 Variability Between Sites

Dust deposition is highly variable on at least a scale of 10 km, based on openfall fluxes of $dSiO_2$ as the indicator of dust deposition, and based on the difference between Bisley and El Verde $dSiO_2$ fluxes. The approximately 2-fold variation in dust input based on the openfall fluxes of $dSiO_2$ between two Luquillo Mountain sites is much greater than the 33% total variation in dust input (based on Fe) that is observed across 9 stations spanning more than 800 km across the state of Florida, despite larger variability in rainfall amount across Florida [Prospero et al., 2010]. In addition to being spatially variable, the $dSiO_2$ fluxes at both Luquillo Mountain sites are large when compared to the

limited number of other rainfall silica measurements that are available. Compilations of temperate and tropical forests $dSiO_2$ inputs find a range from 0.03 to 5.6 kg ha^{-1} yr^{-1} [Cornelis et al. 2011, Sommer et al. 2006], with most values < 3 kg ha^{-1} yr^{-1}. For comparison, Bisley and El Verde have $dSiO_2$ inputs of 7.2 and 4.0 kg ha^{-1} yr^{-1} in openfall, respectively, similar to the $dSiO_2$ inputs measured on the island of Corsica in the Mediterranean Sea of 4.0 kg ha^{-1} yr^{-1} [Treguer 2012]. Overall, however, comparison is limited because $dSiO_2$ is not commonly measured in rainfall.

At the El Verde site, which is farther inland, neither nss-Ca^{2+}, $dSiO_2$, nor TSS changed significantly based on the presence or absence of Sahara-Sahel airmasses. The lack of correlations highlights the fact that having an airmass with a trajectory from the dust source area is only one of the three broad criteria – dust entrainment, transport, and deposition- which all must align for a dust deposition event to occur. The most likely explanation for the lack of correlation between rain chemistry and HYPLSIT trajectories is that dust deposition at El Verde is not as prominent as at Bisley, with smaller fluxes of both $dSiO_2$, and TSS in openfall. Seasonal patterns in openfall deposition also show Bisley receiving greater dust deposition than El Verde (Table 3). While both sites follow the same pattern of greater $dSiO_2$ deposition in the summer and less in other seasons, the ratio: Bisley $dSiO_2$:El Verde $dSiO_2$ changes from being two times higher in winter to three times higher in the summer. Since summer and fall have the highest numbers of airmass trajectories coming from the Sahara-Sahel, and other studies have shown summer and fall to be the dominant dust season in Puerto Rico [Stallard, 2001; Gioda et al., 2013], we conclude that Bisley receives more dust deposition than El Verde.

Based on Si and Ca content of dust of 26 wt.% and 4.8 wt % respectively [Reid et al., 2003], the total dust deposition estimates calculated based on the dissolved chemistry ($dSiO_2$ and nss-Ca^{2+} in rainfall) are equal to 13 and 458 kg ha^{-1} yr^{-1} , based on Si and Ca respectively, at Bisley, and 7.1 and 482 kg ha^{-1} yr^{-1} at El Verde. This calculation is clearly an underestimate, because it reflects only dissolved dust, not the total dust, but it provides a potential lower bound on dust inputs. When compared to the value of 210 ± 70 kg ha^{-1} yr^{-1} obtained from watershed-scale Sr isotope mass balance in Rio Icacos watershed within the Luquillo Mountains [Pett-Ridge, 2009], our $dSiO_2$ calculation of dust appears to greatly underestimate dust deposition, while nss-Ca^{2+} appears to overestimate dust deposition. An underestimate based on $dSiO_2$ is expected, as the majority of Si in dust deposition likely remains undissolved in the rainfall collectors. The solubility of both quartz and biogenic opal dissolution is limited, ranging from 36 to 250 μM for quartz, and 20 to 360 μM for biogenic opal [Bartoli and Wilding 1980]. In contrast, the $dSiO_2$ measured in Luquillo rain ranges from 1 to 30 μM.

If we assume that the TSS is composed entirely of mineral aerosol dust, and that the dust is 26 wt.% Si, then $dSiO_2$ represents on average 15% of the total Si in the openfall samples collected at Bisley. A Luquillo rainfall Si solubility of 15 % is slightly higher than the assumed 5-10% solubility of atmospheric dust-derived Si in seawater [Treguer 1995 and Harrison 2000]. The openfall value of 1.467 kg TSS ha^{-1} wk^{-1} can be converted to 76.284 kg dust ha^{-1} yr^{-1} that remained undissolved in rain collector. Adding the TSS dust in openfall to the $dSiO_2$ dust in openfall yields 89 kg dust ha^{-1} yr^{-1}, which represents the total dust calculated from dissolved and undissolved Si in openfall.

In addition to uncertainty regarding dust solubility, it is difficult to extrapolate directly from openfall to the dust deposition flux experienced by Luquillo Mountain ecosystems. Openfall is expected to under-sample dust inputs because a significant part of the dust deposition is likely in the form of dryfall, the magnitude of which is enhanced by interaction with the forest canopy. The higher estimates based on nss-Ca^{2+} likely reflect either problems with the assumption of sea salt ratios or additional sources of Ca in precipitation. Additionally, estimates could vary based on the timescale. The annual flux measurements of nss-Ca^{2+} from previous studies of Luquillo rainfall chemistry are smaller but similar to this study's annual flux of 22 kg nss-Ca^{2+} ha^{-1} yr^{-1} (±16.5 kg ha^{-1} yr^{-1} 1 s.d.) at Bisley. Gioda et al. [2013] calculated a nss-Ca^{2+} flux of 14.4 kg ha^{-1} yr^{-1} (±16.8 kg ha^{-1} yr^{-1} 1 s.d.) at Bisley (1988 to 2007), Heartsill-Scalley et al. [2007] calculated a flux of 16.06 kg ha^{-1} yr^{-1} at Bisley (1988-2002), and McDowell [1990] calculated a flux of 9.4 kg ha^{-1} yr^{-1} at El Verde (1984 to 1987). Other studies used different criteria for removing outliers, and some studies used different techniques to remove seasalt associated Ca^{2+} such as using sodium to remove sea-salt Ca^{2+} instead of Cl^{-}. Overall the most important factor causing a difference in annual flux measurements was the time period in which the study took place. The McDowell et al., [1990] measurement of nss-Ca^{2+} was almost half the flux found in this study despite similar rainfall (average of 3.4 m), highlighting the value of long-term data collection.

Given the similarities in site characteristics between Bisley and El Verde, differences in dust deposition cannot be attributed to differences in aspect, vegetation, precipitation (3.7 ±0 .7 m yr^{-1} at Bisley, 3.5 ± 0.8 m yr^{-1} at El Verde), or elevation (361 m at Bisley, 380 m at El Verde). The most likely explanation of differential dust deposition

between these two sites is that Bisley is approximately 10 km closer to the northeast corner of Puerto Rico where Saharan-Sahel airmasses approach from during dust periods [Scholl et al., 2009]. The sudden rise in elevation above sea level that the Puerto Rico landmass represents to Atlantic trade winds causes significant orographically driven precipitation, with at least 29% of total precipitation being orographically driven [Scholl et al., 2009, Daly et al., 2003]. This leads to enhanced dust deposition nearer the eastern coast as dust particles are scrubbed from the atmosphere. Despite the similar elevations between the two sites, a trade wind airmass travelling on a direct east-west trajectory from Bisley to El Verde would encounter elevations up to ~900 m between the two sites, causing further orographic rainfall and wet removal of dust particles.

The data presented here highlight the difference between measurements of atmospheric dust concentrations and the amount of dust falling on a landscape, which can potentially impact ecosystems and biogeochemical processes. Figure 7 shows the phenomenon where atmospheric concentrations of dust vary significantly from dust deposition measured as dissolved silica, total silica, or total suspended solids. The atmospheric measurements of silicon caught on a filter which had air actively passed through , are determined through the Virgin Islands Interagency Monitoring of Protected Visual Environments (IMPROVE) project on a three-day basis, only 80 km away from the Luquillo Mountains of Puerto Rico. The deviation between atmospheric dust and dust deposition is caused by several factors that enhance the deposition of dust to the ground, such as canopy trapping, rainfall amount, and meteorological conditions such as wind and turbulence.

2.5.3 Importance of the Sahel Region

Sr and Nd isotopic tracing of dust collected on air filters in the Caribbean show that mineral aerosol particles originate primarily from the Sahel region of North Africa [Kumar et al., 2014]. The temporal pattern of Luquillo Mountain rainfall chemistry likely reflects source region dynamics unique to the Sahel. The Sahel experiences a rainy season from approximately April until late October, with the most intense rainfall occurring from August through September (figure 8). At its peak, the western edge of the Sahel experiences on average 7.8 mm of rain per day, distributed over ~2.5 events per week, and an annual total rainfall of 300-400 mm [Lebel and Ali, 2009]. While this is a relatively small amount of rainfall, it reduces dust two different ways. First, rainfall directly increases soil moisture, which reduces ejection of dust into the atmosphere [Mahowald, 2009]. Second, rainfall spurs the growth of vegetation; enough to alter satellite based measurements of vegetation greening of the region for two months after the rainy season has halted [Nicholson et al., 1990]. The greening of vegetation and increased plant growth hinders dust entrainment to the atmosphere.

A comparison of the $dSiO_2$ and HYSPLIT data (Figure 9) shows that the seasonal pattern in dust deposition based on measured rainfall chemistry in the Luquillo Mountains of Puerto Rico deviates from the seasonal pattern of airmasses coming from the Sahara-Sahel region. The number of airmasses coming from the Sahara-Sahel region remains elevated during the fall season, as expected based on the seasonal shift in the intertropical convergence zone across the Atlantic [Perry et al., 1997]. However, the openfall fluxes of nss-Ca^{2+} and $dSiO_2$ decline in fall relative to summer, despite the fact that this continues to be a time of peak atmospheric transport from the dust source region to the Caribbean. Figure 9 shows that at approximately the 33rd week of the year (mid-

August) rainfall in the Western Sahel is at its peak, and the amount of dust in openfall begins to decrease despite the continued prevalence of airmasses from the Sahara-Sahel region passing over the Luquillo Mountains. Changes in the surface conditions at the dust source must control the decreased dust deposition in fall. In other words, during the fall Caribbean "dust season", positive HYSPLIT trajectories from the Sahara-Sahel region are counter-intuitively less likely to carry dust from Africa to the Caribbean [Prospero, 2003].

This highlights the sensitivity of Caribbean dust deposition fluxes to land-use change or climate change affecting dust production in the Sahel region, such as agricultural plowing or vegetation loss to desertification [Mulitza et al., 2010]. Before intensive agricultural practices in the Sahel region, there was a stronger correlation between drought and dust emissions [Tegan and Fung, 1996]. During the 20th century, dust fluxes from the Sahara-Sahel region have doubled, although large uncertainties remain regarding the relative importance of direct human impacts and climate change [Mahowald et al., 2010]. The connection between seasonal patterns in Luquillo precipitation chemistry and environmental conditions in the Sahel supports the potential cross-Atlantic dependence of downwind ecosystems in the Amazon and Caribbean on dust production in Africa [Swap, 1992].

2.5.3 Wet vs. Dry Deposition

The proportion of dust that comes into an ecosystem as dry deposition or wet deposition is poorly known. In reality, each ecosystem is likely to vary in proportion based on several factors such as proximity to the dust source and climate. Calculating a rough estimate of dry deposition at El Verde based on the difference between openfall

and wet-only deposition yields 0.299 kg nss-Ca^{2+} ha^{-1} yr^{-1} and 0.040 kg $dSiO_2$ ha^{-1} yr^{-1}. Calculating a rough estimate of dry deposition at Bisley based on the difference between throughfall and openfall, (assuming throughfall washes dust off the canopy) yields 0.816 kg nss-Ca^{2+} ha^{-1} yr^{-1} and 0.204 kg $dSiO_2$ ha^{-1} yr^{-1}. Comparing this estimate with openfall, the percentage that dry deposition contributes to the flux of $dSiO_2$ and nss-Ca^{2+} to Bisley respectively is 72% and 71%. The percentage that dry deposition contributes to the flux of $dSiO_2$ and nss-Ca^{2+} to El Verde respectively is 53% and 67%. These methods of dry deposition estimation are very rough and each has shortcomings. Throughfall oversamples dry deposition inputs because of canopy leaching, while openfall collectors undersample dry deposition inputs because they do not reflect forest canopy surface area and structure that traps airborne particles. Previous studies comparing the two forms of deposition often find wet deposition contributes more deposition than dry deposition, but also that dry deposition is highly variable [e.g. Inomata et al., 2009; Balestrini et al., 2000]. In Florida, a network of 9 precipitation collectors where African dust inputs were analyzed showed that wet deposition consistently represented between 70 and 80% of total deposition based on the difference between openfall and wet-only precipitation [Prospero et al., 2010]. In contrast, our results based on Luquillo Mountain precipitation suggest that dry deposition at two different sites is >50% of total dust deposition.

The seasonal variability of dry deposition evident in Luquillo precipitation is dependent on whether the calculation used $dSiO_2$ or nss-Ca^{2+}. The proportion of deposition inputs that are dry based on $dSiO_2$ shows significant variability between 'dust seasons' (summer and fall) and non-dust seasons (winter and spring), while nss-Ca^{2+} remains relatively constant (Table 4). This comparison solidifies the assertion that nss-

Ca^{2+} is confounded by either inputs other than dust or by variability in Ca content and Ca dissolution from dust.

While rainfall is not strongly seasonal in the Luquillo Mountains, there are patterns in the rainfall volume, average cloud height, and the $\partial^{2}H$ and $\partial^{18}O$ signature of rainfall [Scholl et al., 2009]. In particular, the stable isotope values of rain are consistent with lower equilibration times during fall rain storms, indicating a difference in rainfall style such as increased droplet size [Scholl et al., 2009]. While total deposition is highest in summer, a notable fall maximum in the proportion of dry to total deposition is observed based on the $dSiO_2$ dry deposition estimate at Bisley (Table 4). In fall, mean dry deposition accounts for 74% of total deposition while in summer dry deposition is only 64% of total deposition. However, median values of dry deposition show much more contrast between seasonal dry deposition, 52% in fall and only 16% in summer. This characterizes dry deposition in the summer as being large singular events, whereas fall dry deposition is consistently large. Together these results suggest that the proportion of total dust deposition that occurs as dry deposition is quite sensitive to specific rainfall dynamics, not just the mean annual precipitation.

2.6 Conclusion

By delivering key rock-derived nutrients, dust deposition has the potential to affect the productivity of tropical ecosystems that represent an important fraction of biological diversity and terrestrial carbon storage [Chadwick et al., 1999]. Determining the spatial variability of dust deposition across a landscape is a key first-step in understanding how to quantitatively measure the effects dust has on ecosystems, and is essential for improving models to predict dust deposition.

In Puerto Rico, the main source of mineral aerosol dust is the Sahara-Sahel region of Africa, and there appears to be little aerosol contamination from other sources such as ash or anthropogenic pollution. Data from two rainfall stations with records of nss-Ca^{2+} and $dSiO_2$ deposition going back more than twenty years at two different locations along an east-west wind trajectory, as well as the calculated backward airmass trajectories, revealed that rainfall $dSiO_2$ is more closely reflects dust deposition than nss-Ca^{2+}. The $dSiO_2$ record shows that in as little as 10 km, the dust deposition flux evident in openfall chemistry can be reduced in half. This difference in dust deposition rate between two sites 10 km apart in the Luquillo Mountains of Puerto Rico, with similar rainfall and elevation, is as large as the differences in dust deposition fluxes across 100s of km found in other studies [Brahney et al., 2014; Prospero, 2012]. While the two sites varied in overall dust deposition, they both exhibited similar seasonal patterns. Based on the coincident timing in the decline of Caribbean dust inputs and the Sahel rainy season, we find that Caribbean dust fluxes are particularly sensitive to environmental conditions in this region of Africa.

The measurement of $dSiO_2$ provides a useful and important potential tracer for dust deposition in rainfall with $dSiO_2$ being a more reliable tracer than nss-Ca^{2+}. With $dSiO_2$ as a dust tracer, we use rainfall chemistry records to estimate dust fluxes, and complement and greatly extend what can be inferred about the amount and spatial variability in dust deposition beyond our current understanding from airborne filtration, modeling, or satellite observations alone. For example, in dust deposition models, the spatial resolution is such that the island of Puerto Rico uniformly receives the same relatively low rainfall flux as the open ocean [Mahowald et al., 2010], missing orographic

enhancement of dust deposition in the high rainfall Luquillo Mountains. Better understanding of dust deposition processes and spatial and temporal variability is needed, and rainfall $dSiO_2$ measurements provide one tool for assessing dust variability and comparing dust deposition measurements with dust models.

2.7 Acknowledgments

We thank Julia Jones and Cynthia Twohy for useful discussions. Collection and analysis of rainfall was supported by grants BSR-8811902, DEB 9411973, DEB 0080538, DEB 0218039, DEB 0620910 and DEB 0963447 from NSF to the Institute for Tropical Ecosystem Studies, University of Puerto Rico, and to the International Institute of Tropical Forestry USDA Forest Service, as part of the Luquillo Long-Term Ecological Research Program. Additional support was provided by the Luquillo Critical Zone Observatory, NSF EAR-1331841. Special thanks go to Alonso Ramírez, John Bithorn, Grizelle González, Carlos Estrada, Carlos Torrens, and Miriam Salgado for maintaining the ongoing weekly sampling. The U.S. Forest Service (Dept. of Agriculture), ITIF and the University of Puerto Rico gave additional support.

2.8 Citations

Abouchami W, Naethe K, Kumar A, Galer SJG, Jochum KP, Williams E, et al. Geochemical and isotopic characterization of the Bodele Depression dust source and implications for transatlantic dust transport to the Amazon Basin. Earth and Planetary Science Letters. 2013;380:112-23.

Baker AR, French M, Linge KL. Trends in aerosol nutrient solubility along a west-east transect of the Saharan dust plume. Geophysical Research Letters. 2006;33.

Balestrini R, Consuma A, Polesello S, Tartari G. Comparison between dry deposition fluxes measured with water and solid surfaces, and estimated by an inferential model. Annali Di Chimica. 2000;90:467-78.

Bartoli F, Wilding LP. Dissolution of biogenic opal as a function of its physical and chemical-properties. Soil Science Society of America Journal. 1980;44:873-8.

Boy J, Wilcke W. Tropical Andean forest derives calcium and magnesium from Saharan dust. Global Biogeochemical Cycles. 2008;22.

Bruijnzeel LA. Nutrient input output budgets of tropical forest ecosystems - a review. Journal of Tropical Ecology. 1991;7:1-24.

Chadwick OA, Derry LA, Vitousek PM, Huebert BJ, Hedin LO. Changing sources of nutrients during four million years of ecosystem development. Nature. 1999;397:491-7.

Coale KH, Johnson KS, Fitzwater SE, Gordon RM, Tanner S, Chavez FP, et al. A massive phytoplankton bloom induced by an ecosystem-scale iron fertilization experiment in the equatorial Pacific Ocean. Nature. 1996;383:495-501.

Cornelis JT, Delvaux B, Georg RB, Lucas Y, Ranger J, Opfergelt S. Tracing the origin of dissolved silicon transferred from various soil-plant systems towards rivers: a review. Biogeosciences. 2011;8:89-112.

G.F. de Souza, B.C. Reynolds, G.C. Johnson, J.L. Bullister, B. Bourdon Silicon stable isotope distribution traces Southern Ocean export of Si to the eastern South Pacific thermocline Biogeosciences, 9 (2012), pp. 4199–4213

Daly, C., Helmer, E. H. & Quinones, M. 2003. Mapping the climate of Puerto Rico, Vieques and Culebra. International Journal of Climatology, 23, 1359-1381.

DeLonge M, D'Odorico P, Lawrence D. Feedbacks between phosphorus deposition and canopy cover: The emergence of multiple stable states in tropical dry forests. Global Change Biology. 2008;14:154-60.

Dove PM. Kinetic and thermodynamic controls on silica reactivity in weathering environments. Chemical Weathering Rates of Silicate Minerals. 1995;31:235-90.

Draxier RR, Hess GD. An overview of the HYSPLIT_4 modelling system for trajectories, dispersion and deposition. Australian Meteorological Magazine. 1998;47:295-308.

Escudero M, Stein A, Draxler RR, Querol X, Alastuey A, Castillo S, et al. Determination of the contribution of northern Africa dust source areas to PM10 concentrations over the central Iberian Peninsula using the Hybrid Single-Particle Lagrangian Integrated Trajectory model (HYSPLIT) model. Journal of Geophysical Research-Atmospheres. 2006;111.

Escudero M, Stein AF, Draxler RR, Querol X, Alastuey A, Castillo S, et al. Source apportionment for African dust outbreaks over the Western Mediterranean using the HYSPLIT model. Atmospheric Research. 2011;99:518-27.

Ginoux P, Chin M, Tegen I, Prospero JM, Holben B, Dubovik O, et al. Sources and distributions of dust aerosols simulated with the GOCART model. Journal of Geophysical Research-Atmospheres. 2001;106:20255-73.

Gioda A, Amaral BS, Goncalves Monteiro IL, Saint'Pierre TD. Chemical composition, sources, solubility, and transport of aerosol trace elements in a tropical region. Journal of Environmental Monitoring. 2011;13:2134-42.

Gioda A, Mayol-Bracero OL, Reyes-Rodriguez GJ, Santos-Figueroa G, Collett JL, Jr. Water-soluble organic and nitrogen levels in cloud and rainwater in a background marine environment under influence of different air masses. Journal of Atmospheric Chemistry. 2008;61:85-99.

Gioda A, Mayol-Bracero OL, Scatena FN, Weathers KC, Mateus VL, McDowell WH. Chemical constituents in clouds and rainwater in the Puerto Rican rainforest: Potential sources and seasonal drivers. Atmospheric Environment. 2013;68:208-20.

Heartsill-Scalley T, Scatena FN, Estrada C, McDowell WH, Lugo AE. Disturbance and long-term patterns of rainfall and throughfall nutrient fluxes in a subtropical wet forest in Puerto Rico. Journal of Hydrology. 2007;333:472-85.

Hicks DJ. Intrastand distribution patterns of southern Appalachian cove forest herbaceous species. American Midland Naturalist. 1980;104:209-23.

Jickells, T. D. and Spokes, L. J. The Biogeochemistry of Iron in Seawater, edited by: Turner, D. R. and Hunter, K., Wiley, UK, 85–121, 2001.

Johnson-Maynard JL, Graham RC, Shouse PJ, Quideau SA. Base cation and silicon biogeochemistry under pine and scrub oak monocultures: implications for weathering rates. Geoderma. 2005;126:353-65.

Jorquera H, Barraza F. Source apportionment of PM10 and PM2.5 in a desert region in northern Chile. Science of the Total Environment. 2013;444:327-35.

Kohfeld KE, Harrison SP. DIRTMAP: the geological record of dust. Earth-Science Reviews. 2001;54:81-114.

Kumar A, Abouchami W, Galer SJG, Garrison VH, Williams E, Andreae MO. A radiogenic isotope tracer study of transatlantic dust transport from Africa to the Caribbean. Atmospheric Environment. 2014;82:130-43.

Lawrence CR, Neff JC. The contemporary physical and chemical flux of aeolian dust: A synthesis of direct measurements of dust deposition. Chemical Geology. 2009;267:46-63.

Lebel T, Ali A. Recent trends in the Central and Western Sahel rainfall regime (1990-2007). Journal of Hydrology. 2009;375:52-64.

Lequy E, Nicolas M, Conil S, Turpault M-P. Relationship Between Atmospheric Dissolved Deposition and Mineral Dust Deposition in French Forests. Water Air and Soil Pollution. 2013;224.

Lindberg SE, Lovett GM. Field-measurements of particle dry deposition rates to foliage and inert surfaces in a forest canopy. Environmental Science & Technology. 1985;19:238-44.

Lindberg SE, Lovett GM, Schaefer DA, Bredemeier M. Dry deposition velocities and surface-to-canopy scaling factors for aerosol calcium from forest canopy throughfall. Journal of Aerosol Science. 1988;19:1187-90.

Mahowald N, Albani S, Engelstaedter S, Winckler G, Goman M. Model insight into glacial-interglacial paleodust records. Quaternary Science Reviews. 2011;30:832-54.

Mahowald, N. M., S. Kloster, S. Engelstaedter, J. K. Moore, S. Mukhopadhyay, J. R. McConnell, S. Albani, S. C. Doney, A. Bhattacharya, M. A. J. Curran, M. G. Flanner, F. M. Hoffman, D. M. Lawrence, K. Lindsay, P. A. Mayewski, J. Neff, D. Rothenberg, E. Thomas, P. E. Thornton, and C. S. Zender. Observed 20th century desert dust variability: impact on climate and biogeochemistry. Atmospheric Chemistry and Physics. 2010; 10 (22):10875-10893.

Mahowald N, Jickells TD, Baker AR, Artaxo P, Benitez-Nelson CR, Bergametti G, et al. Global distribution of atmospheric phosphorus sources, concentrations and

deposition rates, and anthropogenic impacts. Global Biogeochemical Cycles. 2008;22.

Mahowald NM, Artaxo P, Baker AR, Jickells TD, Okin GS, Randerson JT, et al. Impacts of biomass burning emissions and land use change on Amazonian atmospheric phosphorus cycling and deposition. Global Biogeochemical Cycles. 2005a;19.

Mahowald NM, Baker AR, Bergametti G, Brooks N, Duce RA, Jickells TD, et al. Atmospheric global dust cycle and iron inputs to the ocean. Global Biogeochemical Cycles. 2005b;19.

Martin JH. Glacial-interglacial CO_2 change: the iron hypothesis. Paleoceanography. 1990;5:1-13.

Mcdowell, W. H., Sanchez, C. G., Asbury, C. E. & Perez, C. R. R. 1990. Influence of sea salt aerosols and long-range transport on precipitation chemistry at el-verde, puerto-rico. Atmospheric Environment Part a-General Topics, 24, 2813-2821

McDowell WH. Internal nutrient fluxes in a Puerto Rican rain forest. Journal of Tropical Ecology. 1998;14:521-36.

Mulitza S, Heslop D, Pittauerova D, Fischer HW, Meyer I, Stuut J-B, et al. Increase in African dust flux at the onset of commercial agriculture in the Sahel region. Nature. 2010;466:226-8.

J. Neter, M.H Kutner, C.J. Nachtsheim, and W. Wasserman. Applied Linear Statistical Models, McGraw Hill, New York, New York, 1996.

Newman EI. Phosphorus inputs to terrestrial ecosystems. Journal of Ecology. 1995;83:713-26.

Nicholson SE, Davenport ML, Malo AR. A comparison of the vegetation response to rainfall in the Sahel and East-Africa, using normalized difference vegetation index from NOAA AVHRR. Climatic Change. 1990;17:209-41.

Perez C, Nickovic S, Pejanovic G, Baldasano JM, Ozsoy E. Interactive dust-radiation modeling: A step to improve weather forecasts. Journal of Geophysical Research-Atmospheres. 2006;111:17.

Perry KD, Cahill TA, Eldred RA, Dutcher DD, Gill TE. Long-range transport of North African dust to the eastern United States. Journal of Geophysical Research-Atmospheres. 1997;102:11225-38.

Pett-Ridge, J. C. 2009. Contributions of dust to phosphorus cycling in tropical forests of the Luquillo Mountains, Puerto Rico. Biogeochemistry, 94, 63-80.

Prospero JM, Olmez I, Ames M. Al and Fe in PM2.5 and PM10 in suspended particles in south-central Florida: the impact of the long range transport of African mineral dust. Water Air Soil Pollution 2001, 125:291-317.

Prospero JM, Lamb PJ. African droughts and dust transport to the Caribbean: Climate change implications. Science. 2003;302:1024-7.

Prospero JM, Landing WM, Schulz M. African dust deposition to Florida: Temporal and spatial variability and comparisons to models. Journal of Geophysical Research-Atmospheres. 2010;115.

Reid EA, Reid JS, Meier MM, Dunlap MR, Cliff SS, Broumas A, et al. Characterization of African dust transported to Puerto Rico by individual particle and size segregated bulk analysis. Journal of Geophysical Research-Atmospheres. 2003;108.

Reyes-Rodriguez GJ, Gioda A, Mayol-Bracero OL, Collett J, Jr. Organic carbon, total nitrogen, and water-soluble ions in clouds from a tropical montane cloud forest in Puerto Rico. Atmospheric Environment. 2009;43:4171-7.

Rodriguez S, Querol X, Alastuey A, Kallos G, Kakaliagou O. Saharan dust contributions to PM10 and TSP levels in Southern and Eastern Spain. Atmospheric Environment. 2001;35:2433-47.

Rothlisberger R, Mulvaney R, Wolff EW, Hutterli MA, Bigler M, Sommer S, et al. Dust and sea salt variability in central East Antarctica (Dome C) over the last 45 kyrs and its implications for southern high-latitude climate. Geophysical Research Letters. 2002;29:4.

Scatena FN. Watershed scale rainfall interception on 2 forested watersheds in the Luquillo Mountains of Puerto-Rico. Journal of Hydrology. 1990;113:89-102.

Scholl MA, Shanley JB, Zegarra JP, Coplen TB. The stable isotope amount effect: New insights from NEXRAD echo tops, Luquillo Mountains, Puerto Rico. Water Resources Research. 2009;45.

Shinn EA, Smith GW, Prospero JM, Betzer P, Hayes ML, Garrison V, et al. African dust and the demise of Caribbean coral reefs. Geophysical Research Letters. 2000;27:3029-32.

Sommer M, Kaczorek D, Kuzyakov Y, Breuer J. Silicon pools and fluxes in soils and landscapes - a review. Journal of Plant Nutrition and Soil Science-Zeitschrift Fur Pflanzenernahrung Und Bodenkunde. 2006;169:310-29.

Stallard RF. Possible environmental factors underlying amphibian decline in eastern Puerto Rico: Analysis of US government data archives. Conservation Biology. 2001;15:943-53.

Stallard RF. Weathering, landscape, and carbon in four paired research watersheds in eastern Puerto Rico. Applied Geochemistry. 2011;26:S370-S372.

Stallard, R.F., 2012, Atmospheric inputs to watersheds of the Luquillo Mountains in eastern Puerto Rico—Chapter D, *in* Murphy, S.F., and Stallard, R.F., Editors, Water quality and landscape processes of four watersheds in eastern Puerto Rico: Reston, VA, U. S. Geological Survey, USGS Professional Paper 1789–D, p. 85-112.

Stegmann PM, Tindale NW. Global distribution of aerosols over the open ocean as derived from the coastal zone color scanner. Global Biogeochemical Cycles. 1999;13:383-97.

Stein AF, Wang Y, de la Rosa JD, Sanchez de la Campa AM, Castell N, Draxler RR. Modeling PM10 Originating from Dust Intrusions in the Southern Iberian Peninsula Using HYSPLIT. Weather and Forecasting. 2011;26:236-42.

Stoorvogel JJ, VanBreemen N, Janssen BH. The nutrient input by Harmattan dust to a forest ecosystem in Cote d'Ivoire, Africa. Biogeochemistry. 1997;37:145-57.

Swap R, Garstang M, Greco S, Talbot R, Kallberg P. Saharan dust in the Amazon Basin. Tellus Series B-Chemical and Physical Meteorology. 1992;44:133-49.

Tegen I, Lacis AA, Fung I. The influence on climate forcing of mineral aerosols from disturbed soils. Nature. 1996;380:419-22.

Treguer PJ, De La Rocha CL. The World Ocean Silica Cycle. Annual Review of Marine Science, Vol 5. 2013;5:477-501.

Wang YH, Liu YM. Hydrological characteristics of a moso-bamboo (*phyllostachys pubescents*) forest in South China. Hydrological Processes. 1995;9:797-808.

Wang YQ, Stein AF, Draxler RR, de la Rosa JD, Zhang XY. Global sand and dust storms in 2008: Observation and HYSPLIT model verification. Atmospheric Environment. 2011;45:6368-81.

Westphal DL, Toon OB, Carlson TN. A two-dimensional numerical investigation of the dynamics and microphysics of Saharan dust storms. Journal of Geophysical Research-Atmospheres. 1987;92:3027-49.

White EJ, Turner F. Method of estimating income of nutrients in a catch of airborne particles by a woodland canopy. Journal of Applied Ecology. 1970;7:441-&.

Yerramilli A, Dodla VBR, Challa VS, Myles L, Pendergrass WR, Vogel CA, et al. An integrated WRF/HYSPLIT modeling approach for the assessment of PM2.5 source regions over the Mississippi Gulf Coast region. Air Quality Atmosphere and Health. 2012;5:401-12.

Yoshioka M, Mahowald NM, Conley AJ, Collins WD, Fillmore DW, Zender CS, et al. Impact of desert dust radiative forcing on Sahel precipitation: Relative importance of dust compared to sea surface temperature variations, vegetation changes, and greenhouse gas warming. Journal of Climate. 2007;20:1445-67.

Zhou CH, Gong SL, Zhang XY, Wang YQ, Niu T, Liu HL, et al. Development and evaluation of an operational SDS forecasting system for East Asia: CUACE/Dust. Atmospheric Chemistry and Physics. 2008;8:787-98.

2.9 Tables

Table 1. Average weekly fluxes of nss-Ca and $dSiO_2$ in rainfall fractions

Openfall (kg ha^{-1} wk^{-1})								
	Bisley				El Verde			
	n	Mean	Median	SD	n	Mean	Median	SD
nss-Ca	814	0.423	0.342	0.318	804	0.443	0.365	0.331
$dSiO_2$	841	0.139	***0.055***	0.305	818	0.076	***0.022***	0.233
TSS	390	1.467	***0.759***	3.399	367	0.65	***0.468***	0.709
	Bisley				El Verde			
Throughfall (kg $ha^{-1}wk^{-1}$)					Wet Only (kg $ha^{-1}wk^{-1}$)			
	n	Mean	Median	SD	n	Mean	Median	SD
nss-Ca	1058	1.153	0.979	0.714	800	0.193	0.127	0.195
$dSiO_2$	907	0.282	0.14	0.513	761	0.061	0.017	0.145
Dry Deposition Estimates (kg $ha^{-1}wk^{-1}$)								
	Bisley				El Verde			
	n	Mean	Median	SD	n	Mean	Median	SD
nss-Ca	773	0.816	0.672	0.687	737	0.299	0.222	0.317
dSiO2	775	0.204	0.056	0.437	721	0.04	0	0.183

Bolded italics indicate a significant ($p<0.05$) difference between Bisley and El Verde

Table 2. Median values of all rainfall chemistry in weeks with and without. Sahara-Sahel airmasses

	(-)	(+)
Bisley Openfall (kg $ha^{-1}wk^{-1}$)		
nss-Ca	0.357	0.332
$dSiO_2$	***0.048***	***0.065***
TSS	0.699*	0.893*
El Verde Openfall (kg $ha^{-1}wk^{-1}$)		
nss-Ca	0.341	0.376
$dSiO_2$	0.021	0.024
TSS	0.297	0.294
Bisley Throughfall (kg $ha^{-1}wk^{-1}$)		
nss-Ca	1.061	0.985
$dSiO_2$	***0.111***	***0.154***
El Verde WetOnly (kg $ha^{-1}wk^{-1}$)		
nss-Ca	0.118	0.131
$dSiO_2$	0.017	0.017
Bisley Dry Estimate (kg $ha^{-1}wk^{-1}$)		
nss-Ca	0.682	0.675
$dSiO_2$	0.061	0.051
El Verde Dry Estimate (kg $ha^{-1}wk^{-1}$)		
nss-Ca	0.196	0.234
$dSiO_2$	0	0

(+) indicates presence of Sahara-Sahel airmass.
(-) indicates absence of Sahara-Sahel airmass. Bolded italics denote there was a significant difference ($p<0.05$) between weeks that did have a Saharan airmass vs. weeks that did not.
*=marginally significant ($p<0.051$)

Table 3. Seasonal distribution of rainfall chemistry for all rainwater collectors

nss-Ca Openfall (kg ha^{-1} wk^{-1})								
	Bisley				El Verde			
	Winter	Spring	Summer	Fall	Winter	Spring	Summer	Fall
n	189	201	206	218	184	191	217	212
Mean	0.400	0.427	0.532	0.338	0.407	0.465	0.554	0.339
Median	0.326	0.33	0.479	0.27	0.336	0.368	0.474	0.29
SD	0.309	0.33	0.337	0.264	0.315	0.356	0.371	0.225
$dSiO_2$ Openfall (kg ha^{-1} wk^{-1})								
	Bisley				El Verde			
	Winter	Spring	Summer	Fall	Winter	Spring	Summer	Fall
n	202	208	215	216	203	196	221	198
Mean	0.129	0.133	0.172	0.123	0.064	0.101	0.082	0.056
Median	***0.039***	***0.046***	***0.091***	***0.066***	***0.017***	***0.022***	***0.028***	***0.025***
SD	0.414	0.276	0.322	0.158	0.285	0.333	0.133	0.108
TSS Openfall (kg ha^{-1} wk^{-1})								
	Bisley				El Verde			
	Winter	Spring	Summer	Fall	Winter	Spring	Summer	Fall
n	94	105	111	81	74	96	112	84
Mean	0.697	1.293	1.672	1.390	0.434	0.675	0.896	0.491
Median	***0.517***	***0.941***	***0.964***	***0.718***	***0.296***	***0.486***	***0.684***	***0.413***
SD	0.576	1.196	2.002	1.918	0.453	0.692	0.913	0.469
Bisley Throughfall								
	nss-Ca (kg $ha^{-1}wk^{-1}$)				$dSiO_2$ (kg $ha^{-1}wk^{-1}$)			
	Winter	Spring	Summer	Fall	Winter	Spring	Summer	Fall
n	228	248	254	242	209	221	221	223
Mean	1.293	1.172	1.259	1.042	0.235	0.262	0.315	0.325
Median	1.154	0.959	1.148	0.905	***0.110***	***0.103***	***0.148***	***0.197***
SD	0.728	0.725	0.691	0.658	0.478	0.433	0.581	0.557
El Verde Wet Only								
	nss-Ca (kg $ha^{-1}wk^{-1}$)				$dSiO_2$ (kg $ha^{-1}wk^{-1}$)			
	Winter	Spring	Summer	Fall	Winter	Spring	Summer	Fall
n	192	181	224	201	183	182	211	186
Mean	0.161	0.184	0.26	0.155	0.053	0.055	0.072	0.063
Median	0.1	0.124	0.203	0.095	0.013	0.018	0.02	0.017
SD	0.169	0.193	0.224	0.167	0.165	0.118	0.122	0.17

Bolded italics indicate the median value for that season at one site is significantly ($p<0.05$) different from the same season at the other site. All metrics tested had seasonality, indicating at least one season showed a significant difference ($p<0.05$) from the other seasons.

Table 4. Seasonal distribution of dry deposition $dSiO_2$ and nss-Ca at Bisley and El Verde

nss-Ca (kg ha^{-1} wk^{-1})								
	Bisley				El Verde			
	Winter	Spring	Summer	Fall	Winter	Spring	Summer	Fall
n	173	189	201	210	166	174	202	194
Mean	0.898	0.773	0.869	0.738	0.296	0.343	0.337	0.221
Median	***0.782***	***0.619***	***0.707***	***0.583***	***0.216***	***0.245***	***0.282***	***0.186***
SD	0.709	0.724	0.67	0.644	0.328	0.354	0.348	0.205
$dSiO_2$ (kg ha^{-1} wk^{-1})								
	Bisley				El Verde			
	Winter	Spring	Summer	Fall	Winter	Spring	Summer	Fall
n	178	188	202	207	166	172	206	176
Mean	0.165	0.199	0.204	0.243	0.015	0.073	0.041	0.029
Median	***0.061***	***0.057***	***0.024***	***0.104***	***0***	***0***	***0***	***0***
SD	0.309	0.372	0.509	0.503	0.041	0.34	0.095	0.101

Bolded italics indicate the median value for that season at one site is significantly ($p<0.05$) different from the same season at the other site. All metrics tested had seasonality, indicating at least one season showed a significant difference ($p<0.05$) from the other seasons.

2.10 Figures

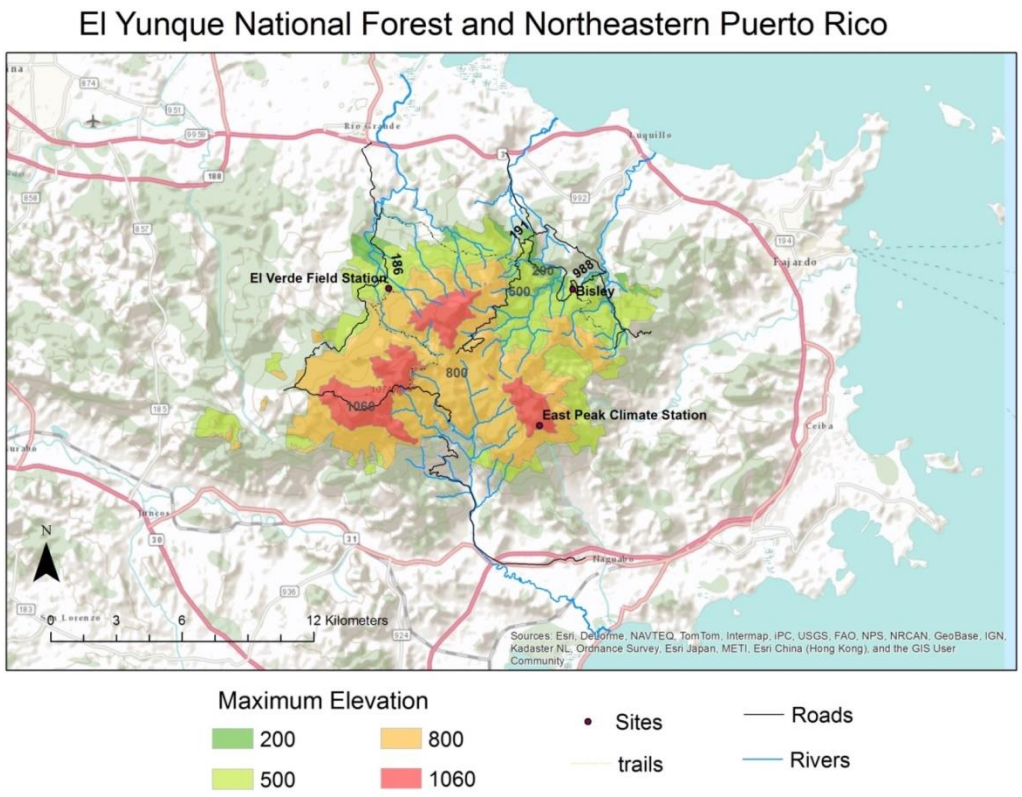

Figure 1. Locations of the two rain gauges used to gather bulk rainfall measurements and rain chemistry data in the Luquillo Mountains in northeastern Puerto Rico. Approximate distance between El Verde and Bisley = 10km.

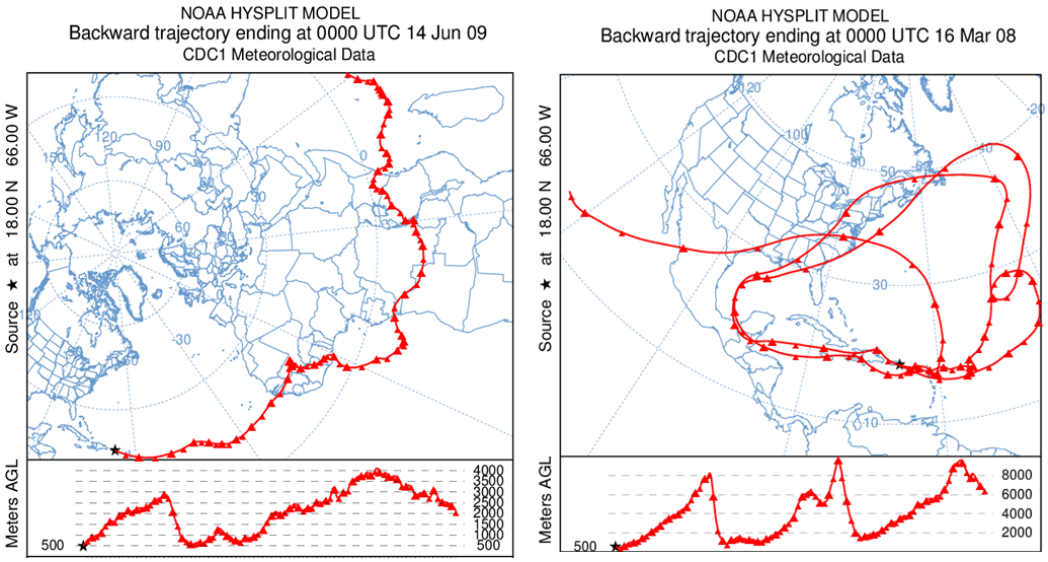

Figures 2a and 2b. Backward airmass trajectories from Puerto Rico. Figure 2 shows the airmass passing directly over the Sahara before moving to Puerto Rico. Figure 3 shows the airmass moving around the eastern seaboard of the United States, not going near the Saharan Desert.

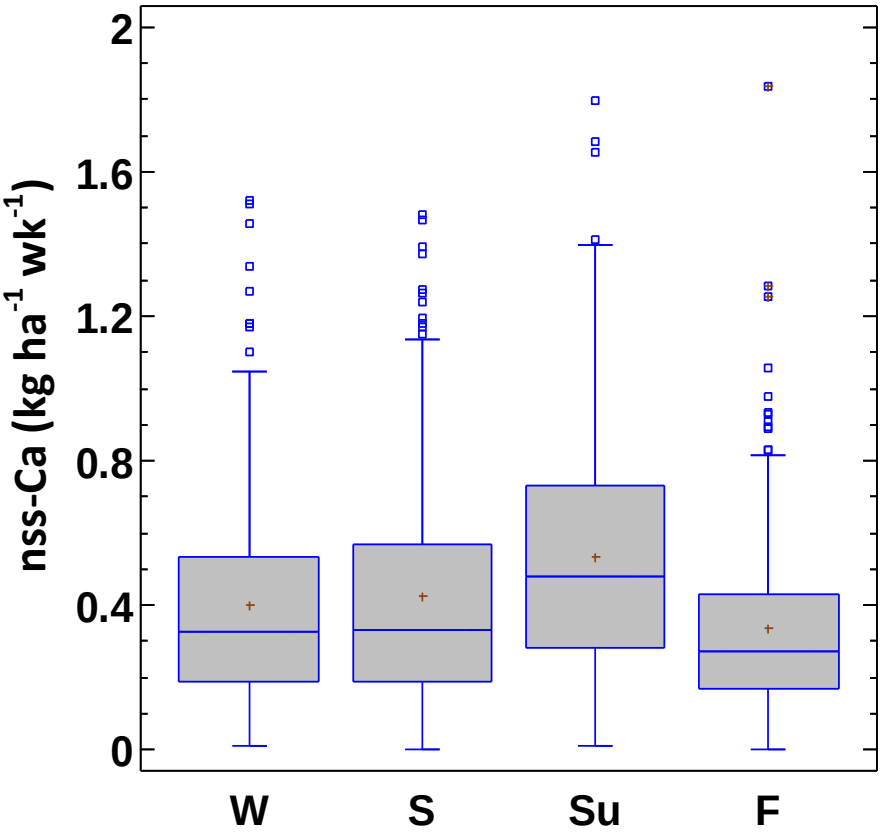

Figure 3. Seasonal distribution of nss-Ca in openfall at Bisley 1988-2009. The rectangular part of the plot extends from the lower quartile to the upper quartile, covering the center half of the sample. The center line within the box shows the location of the sample median. The plus sign indicates the location of the sample mean. The whiskers extend from the box to the minimum and maximum values in the sample, except for any outside or far outside points, which will be plotted separately. Outside points are points which lie more than 1.5 times the interquartile range above or below the box and are shown as small squares. Far outside points are points which lie more than 3.0 times the interquartile range above or below the box and are shown as small squares with plus signs through them. The y-axis has been shortened for graphical purposes to show changes in seasonality, which cuts off many of the far outside points. Seasons are split into 13 week increments with winter beginning on the 51st week of the year. The decrease in Fall flux is characteristic of most seasonal flux patterns. Tests for seasonality show that summer is significantly ($p<0.05$) different from other seasons.

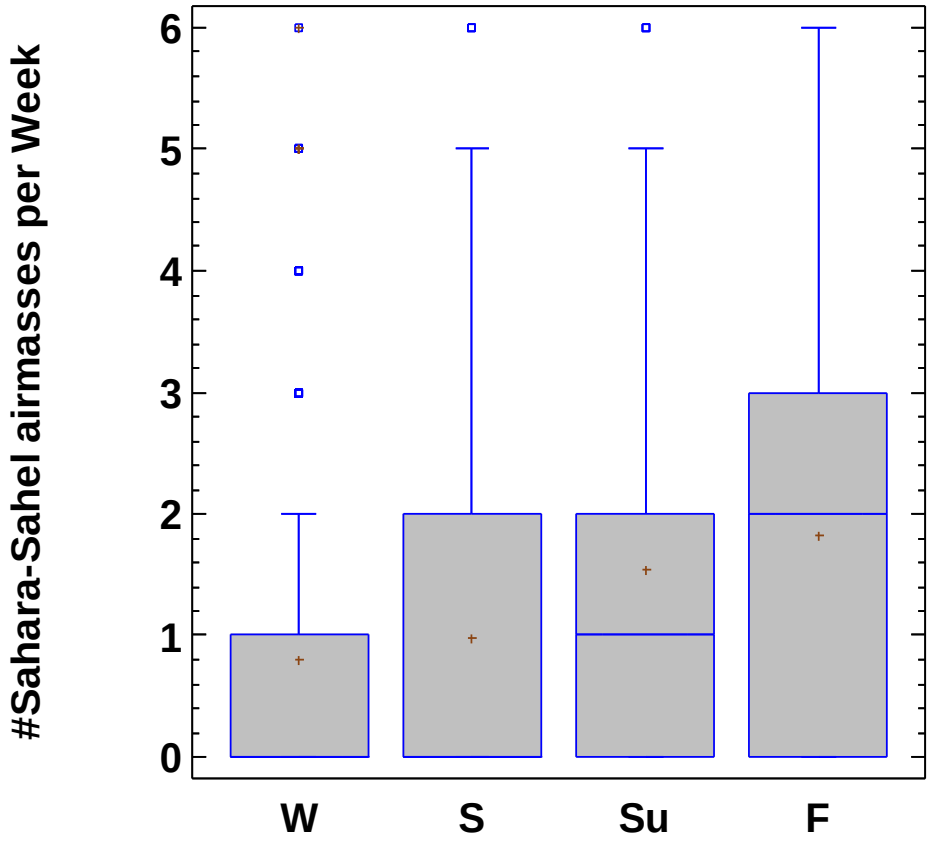

Figure 4. The number of airmasses coming from the Sahara-Sahel region per week during each season of the year, averaged for the duration of this study, 1988-2009. The rectangular part of the plot extends from the lower quartile to the upper quartile, covering the center half of the sample. The center line within the box shows the location of the sample median. The plus sign indicates the location of the sample mean. The whiskers extend from the box to the minimum and maximum values in the sample, except for any outside or far outside points, which will be plotted separately. Outside points are points which lie more than 1.5 times the interquartile range above or below the box and are shown as small squares. Far outside points are points which lie more than 3.0 times the interquartile range above or below the box and are shown as small squares with plus signs through them. The y-axis has been shortened for graphical purposes to show changes in seasonality, which cuts off some of the far outside points. Seasons are split into 13 week increments with winter beginning on the 51st week of the year. Median values for winter and spring are zero.

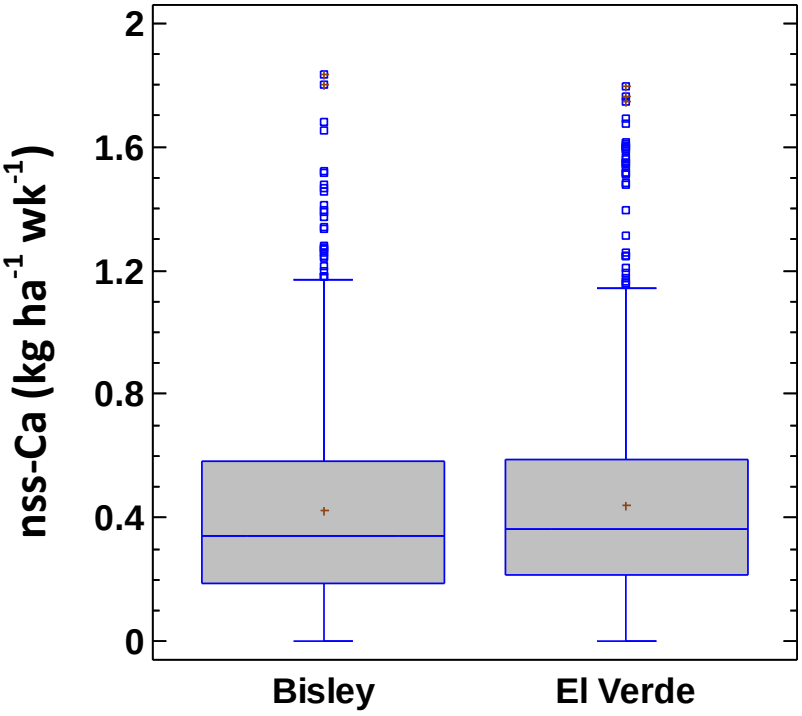

Figure 5. Weekly openfall non-seasalt-Ca^{2+} deposition at Bisley and El Verde 1988-2009. The rectangular part of the plot extends from the lower quartile to the upper quartile, covering the center half of the sample. The center line within the box shows the location of the sample median. The plus sign indicates the location of the sample mean. The whiskers extend from the box to the minimum and maximum values in the sample, except for any outside or far outside points, which will be plotted separately. Outside points are points which lie more than 1.5 times the interquartile range above or below the box and are shown as small squares. Far outside points are points which lie more than 3.0 times the interquartile range above or below the box and are shown as small squares with plus signs through them. The y-axis has been shortened for graphical purposes to show changes in seasonality, which cuts off some of the far outside points. Median value at Bisley is 0.342; median value at El Verde is 0.365. These values are not significantly different from each other ($p>0.05$).

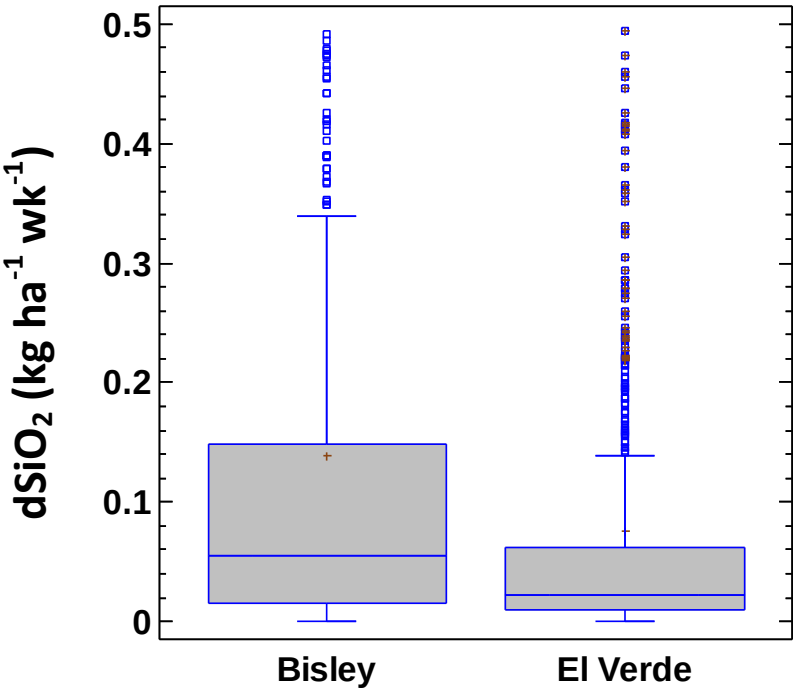

Figure 6. Weekly openfall $dSiO_2$ deposition at Bisley and El Verde 1988-2009. The rectangular part of the plot extends from the lower quartile to the upper quartile, covering the center half of the sample. The center line within the box shows the location of the sample median. The plus sign indicates the location of the sample mean. The whiskers extend from the box to the minimum and maximum values in the sample, except for any outside or far outside points, which will be plotted separately. Outside points are points which lie more than 1.5 times the interquartile range above or below the box and are shown as small squares. Far outside points are points which lie more than 3.0 times the interquartile range above or below the box and are shown as small squares with plus signs through them. The y-axis has been shortened for graphical purposes to show changes in seasonality, which cuts off some of the far outside points. Median value at Bisley is 0.055; median value at El Verde is 0.022. These values are significantly different from each other ($p<0.05$).

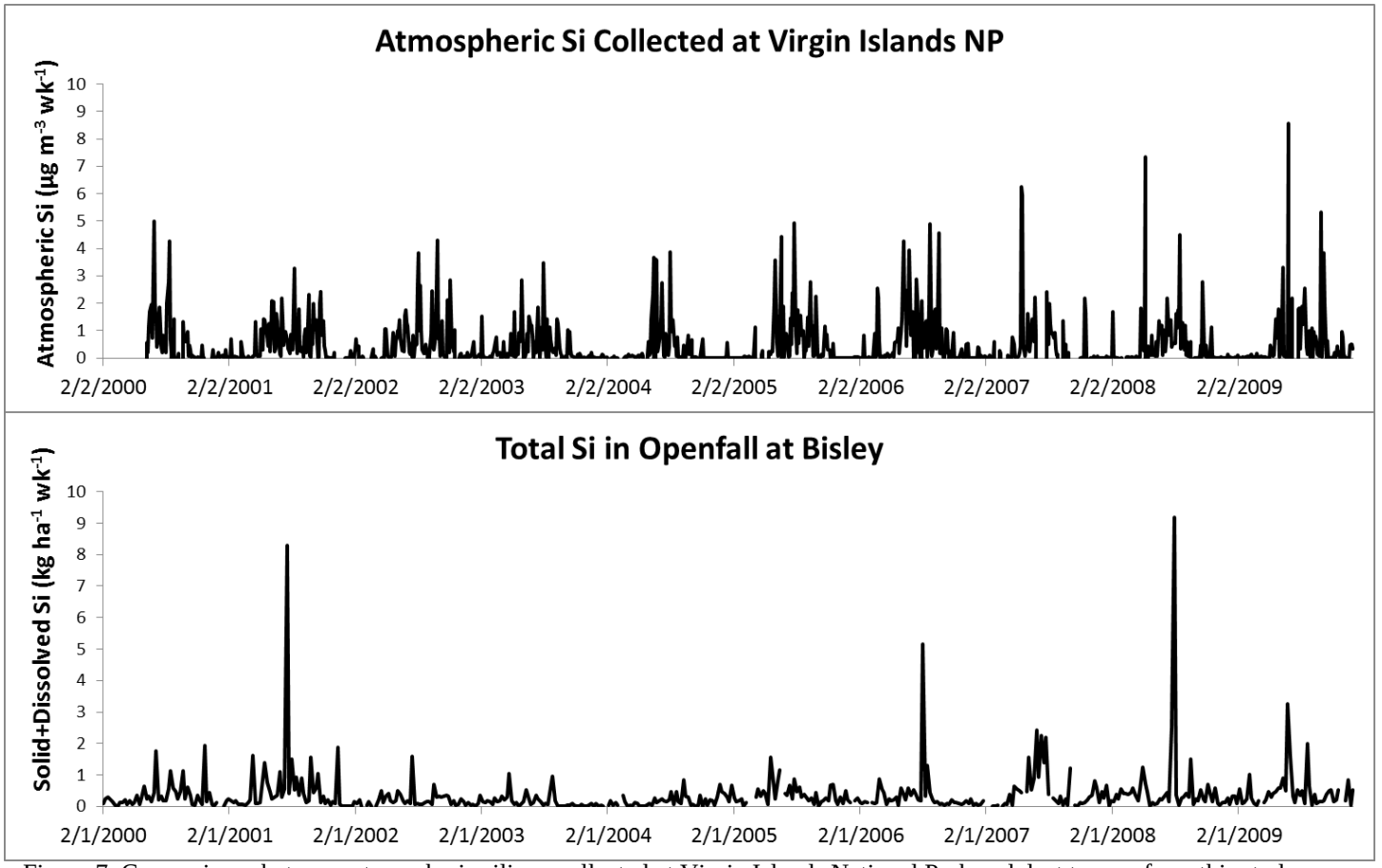

Figure 7. Comparisons between atmospheric silicon collected at Virgin Islands National Park and dust tracers from this study, TSS and $dSiO_2$, for the same time period. The Si in the atmosphere representing dust contains very few outliers and is very regular temporally. The TSS and $dSiO_2$ measured in openfall at Bisley in comparison frequently have outlying values far exceeding seasonal peaks.

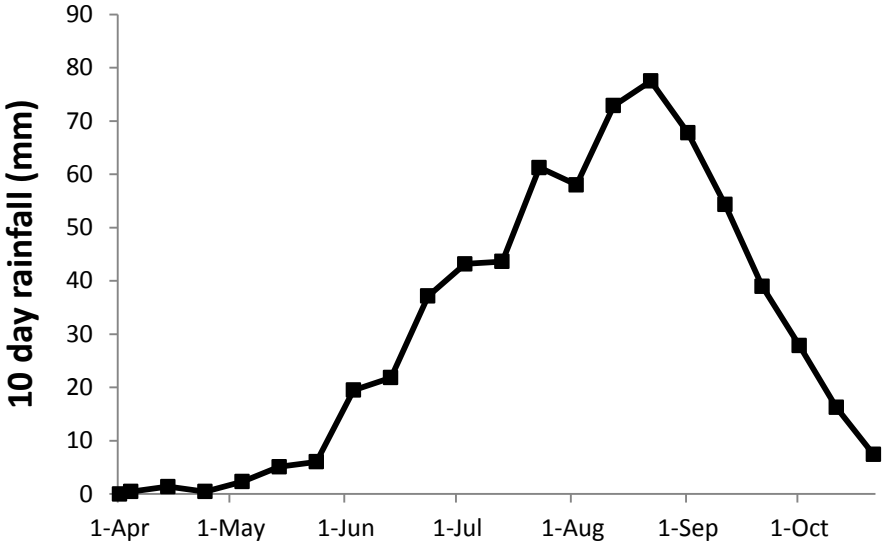

Figure 8. Average amount of rainfall experienced in ten days in the Western Sahel region from 1990 to 2007 [adapted from Lebel and Ali, 2009].

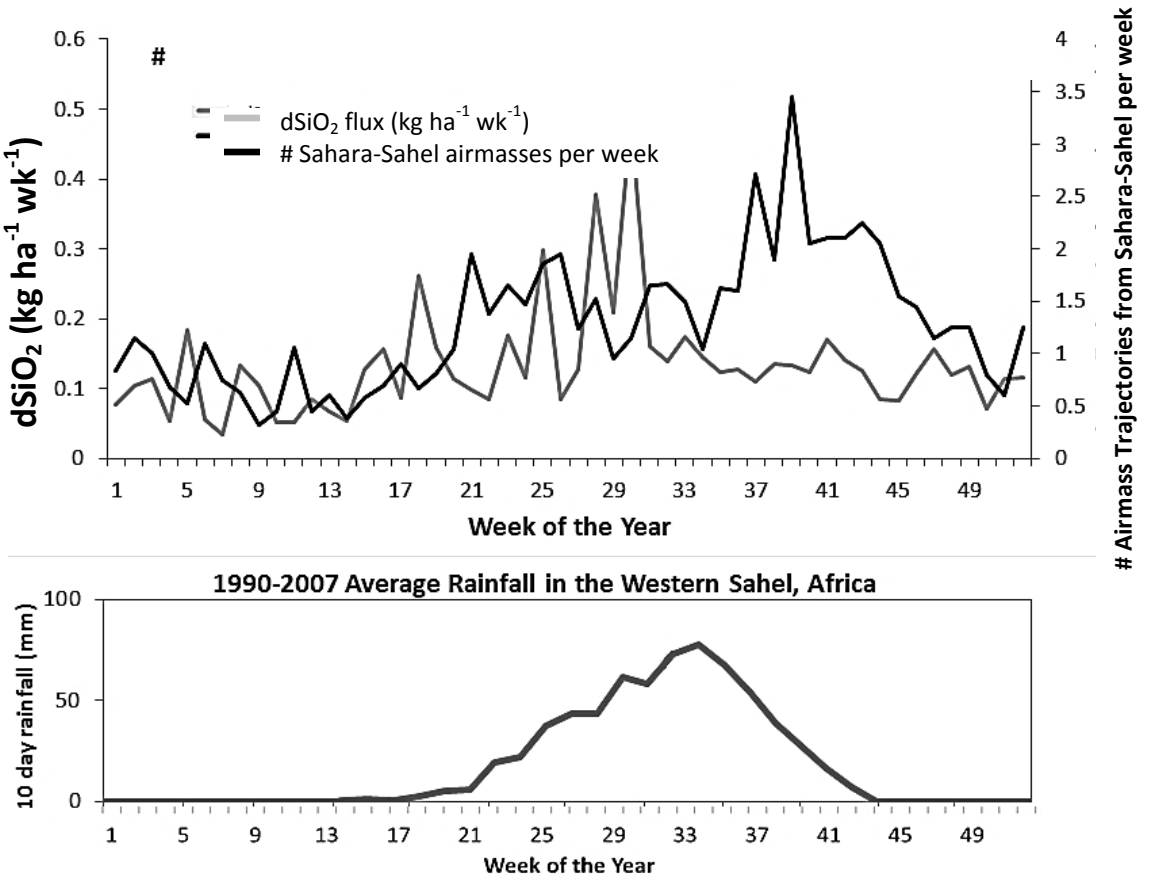

Figures 9. (Top) A time series of the average number of Sahara-Sahel airmasses per week of the year and the average weekly flux of $dSiO_2$ both taken from approximately twenty years of weekly measurements. Both measurements are closely linked until approximately the 33rd week of the year, where airmass provenance no longer correlates to the flux of $dSiO_2$ to Puerto Rico. (Bottom) The equivalent of figure 9, expanded to show the entire year of rainfall in the Western Sahel. Peak rainfall is centered around the 33rd week of the year, however, greening of vegetation in the region persists for up to two months after precipitation has halted [Nicholson et al., 1990]. The expanded leaf area has the potential to prevent dust entrainment into the atmosphere.

Spatial variability of African dust deposition in the Luquillo Mountains, Puerto Rico, based on soil neodymium isotopes and rare earth element patterns

M.A. McClintock and J.C. Pett-Ridge, Department of Crop and Soil Science, Oregon State University, Corvallis, OR, USA.

Corresponding author: M. A. McClintock, Agricultural & Life Sciences 3017, Oregon State University, Corvallis, OR, 97331-7306 (mcclinma@onid.oregonstate.edu)

Key Points

- ε_{Nd} reflects high variability in the amount of African dust present in surface soil at 31 ridgetop locations across a ~100 km^2 landscape in the Luquillo Mountains, Puerto Rico.
- Nd weathering losses, combined with soil ε_{Nd} and estimates for denudation rates, can be used to estimate dust deposition fluxes.
- Dust deposition after long-range transport is highly spatially variable on landscape scales in mountainous terrain, and translates to spatial variability in phosphorus supply to ecosystems.

3.1 Abstract

Dust deposition provides rock-derived nutrients such as phosphorus (P) to terrestrial ecosystems. Over pedogenic timescales, as bedrock sources of P are depleted, dust sources of P can support productivity in certain ecosystems, but both dust deposition rates and the spatial variability of dust deposition rates are largely unknown. This study evaluates the spatial variability of dust deposition using neodymium (Nd) isotope ratios and the distribution of rare earth elements (REE) in soil in the Luquillo Mountains, Puerto Rico. Dust from the Sahara-Sahel region of Africa carries a distinct isotopic signature of -12 ε_{Nd}, and a characteristic enrichment of light REEs, with a La/Yb ratio of 30. Local bedrock, in contrast, has a ε_{Nd} signature of 7, and a La/Yb ratio of 5.5 to 5.7. End-member mixing calculations for 31 ridgetop sites across the Luquillo Mountains based on ε_{Nd} reveal a wide range in dust influence on surface soils, with between 6% and 89% of soil Nd being African dust-derived. Using ε_{Nd} paired with surface soil residence times from ^{10}Be-based or other estimates of denudation rates, dust fluxes to the Luquillo

Mountains were calculated, ranging from 0.48 – 71 g m^{-2} yr^{-1} at different locations within a ~100 km^2 area. Based on the P content of African dust, this represents a dust-derived P input of 0.53 - 78 mg P m^{-2} yr^{-1}. Current dust content of soil is positively correlated with biologically cycled fractions of soil P on quartz diorite bedrock (r^2=0.47 and p=0.0015 for $NaHCO_3$-P_i, r^2=0.23 and p=0.030 for NaOH-P_t). Dust content of soil is also positively correlated with ridgetop width (r^2=0.67 and p=0.011). However, dust content of soil is not correlated with denudation rate, meaning that variation in dust deposition flux controls dust content in addition to variation in soil residence time across the landscape. Soil dust content is not simply correlated with elevation, rainfall, longitude, forest type, or bedrock type, suggesting that other factors such as wind speed, turbulence, and forest canopy structure influence local dust deposition rates.

3.2 Introduction

Dust emissions from desert areas total as much as 2 billion tons yr^{-1} globally, with important implications for Earth surface processes [Jickells et al, 2005]. The radiation budget of the Earth can be altered by atmospheric dust [Tegen et al., 1996], and in high nutrient low chlorophyll zones, the productivity of ocean-dwelling photosynthetic life relies on iron delivered to the water surface by dust deposition [Coale et al., 1996; Martin, 1990]. Mineral aerosols can also be a long-range vector for bacterial and fungal movement, which can cause mortality of coral reefs [Shinn et al., 2000]. Dust is also hypothesized to play an important role in certain terrestrial ecosystems, but few records exist with which to examine the spatial variability of dust deposition at a landscape scale.

Dust has the potential to fertilize ecosystems that nutrient limited in either phosphorus (P) [e.g. Chadwick et al., 1999], or calcium (Ca^{2+}) [Avila et al., 1998]. Over time, ecosystems on highly weathered soils may experience decline in rock-derived nutrients such as P due to leaching, or through formation of insoluble complexes with metal oxides [Walker and Syers, 1976]. Despite efficient nutrient recycling, over longer timescales small losses of rock-derived nutrients from soils must be replenished by new inputs, such as long-range dust transport or erosion-induced rejuvenation of soil primary minerals, in order to maintain ecosystem productivity [Porder et al., 2005, Pett-Ridge 2009]. It has been proposed that dust is an ecologically significant supplier of limiting nutrients to highly productive ecosystems such as the Amazon Basin [Swap et al., 1992]. In this manner the size of major carbon pools can be linked to factors affecting dust production, transport, and deposition.

Long-term dust flux measurements are needed to assess the potential impact of dust fertilization on terrestrial ecosystems. Short term dust deposition can be estimated directly and indirectly using different techniques, such as measuring non-seasalt calcium in rainwater [Stallard, 2001], collecting atmospheric samples passed through an active filter [Prospero and Lamb, 2003], or using ocean-basin scale modeling techniques [Ginoux et al., 2001; Mahowald, 2008]. These methods are limited by multiple issues, including the high spatial and temporal variability in both transport and deposition [Prospero 1999]. Direct collection of dust using ground-based deposition collectors cannot meaningfully measure the long-term average dust deposition a forested ecosystem receives, in part because they do not mimic the forest canopy structure and surface properties of leaves [Hicks et al., 1980; Lindberg and Lovett, 1985; Stoorvogel et al., 1997; White and Turner, 1970]. Modern deposition studies are also limited in their temporal scale; longer timescales are required to understand how dust affects terrestrial ecosystems, and to understand how decadal-scale changes such as the North Atlantic Oscillation (NAO) or other significant variations in climate affect dust inputs to ecosystems.

Isotopic tracers in soils can be used to identify the presence of long-range transported dust [Kurtz et al., 2001, Jahn et al., 2001, Borg and Banner 1996, Dia et al., 2006, Pett-Ridge et al., 2009], and to calculate long term average rates of dust deposition [Pett-Ridge, 2009]. Two different isotope systems, strontium ($^{86}Sr/^{87}Sr$) and neodymium ($^{143}Nd/^{144}Nd$) are commonly used to determine dust provenance [e.g. Kumar et al., . 2014]. When the dust source region has a unique isotopic signature relative to the deposition region's bedrock, mixing model calculations can be used to calculate dust

flux. These calculations work best in situations where only two end-members exist, dust and underlying parent material. This is more often the case with Nd isotopes as compared to Sr isotopes, because sea-salt derived aerosols are presumed to have negligible Nd content [Grousset and Biscaye 2005].

Other techniques for estimating the influence of dust on soil chemistry involve measuring a suite of rare earth element (REE) concentrations and immobile elements such as Zr, Nb, or Th [Kurtz et al., 2001, Aubert et al., 2002, Muhs et al., 2009]. REEs form stable 3^+ ions, which have a small (but steady) decrease in ionic size with increasing atomic number. A result is that certain lithologies will have their own unique REE signatures and differences in these geologic origins can be quantified by examining ratios of particular REEs. For instance, there is a noticeable enrichment of light rare earth elements (LREEs) in Saharan dust [Herwitz et al., 1993], which can be imprinted on a soil REE pattern, altering the overall distribution of REEs in soil. "Immobile" elements such as Zr, Nb, and Th are less susceptible to leaching and transport in a soil profile relative to REEs, and can be used in combination with REE patterns to distinguish between enrichment or depletion due to soil weathering or additions to soil from dust or other potential sources [Bern and White 2011].

The Luquillo Mountains of Puerto Rico are well-suited for studying dust deposition because there is one dominant dust source region, the Sahara-Sahel region of Africa, and no other significant landmasses in the pathway of dust transport. The predominant wind direction is northeasterly trade winds off the Atlantic Ocean, minimizing the possibility of local or anthropogenic influence on atmospheric inputs in the Luquillo Mountains. This study investigates dust deposition in Luquillo using the

isotopic ratio of Nd (in units of ε_{Nd}, eq.1 where CHUR is the chondritic uniform reservoir of the Earth) in soil samples to calculate the amount of dust that has been deposited over long timescales.

$$\text{Eq. 1} \quad \varepsilon_{Nd} = \left[\frac{\left(\frac{^{143}Nd}{^{144}Nd}\right)_{sample}}{\left(\frac{^{143}Nd}{^{144}Nd}\right)_{CHUR}} - 1 \right] * 10000$$

Bedrock formations throughout the Luquillo Mountians have an average ε_{Nd} of +7 [Smith et al., 1998]. The primary dust source in the Luquillo Mountains is the Sahara-Sahel region, which has a ε_{Nd} value of -12 [Kumar et al., 2014]. This creates the opportunity to create a simple two end-member mixing calculation to determine the fraction of Nd in soil that came from dust. This result, when combined with the average Nd concentration in dust, the Nd concentration in soil, and an estimate of the amount of dust that has weathered out of the soil, is used to calculate the mass of the dust that has fallen on a soil over the residence time of the soil. We then convert these values into estimates of dust deposition rate using estimates of denudation rates. These results are compared with REE concentrations of topsoil and bedrock to establish patterns in soil weathering and dust fluxes. Using these measurements we seek to address three main aspects of dust deposition in the Luquillo Mountains of Puerto Rico: (1) the spatial variability of dust deposition over approximately hundred to thousand year timescales (2) the factors controlling spatial variability of dust deposition, and (3) the role of dust deposition in supplying P to Luquillo ecosystems.

3.3 Methods

3.3.1 Study Site

The Luquillo Mountains are located in the El Yunque National Forest of NE Puerto Rico in the Caribbean and are covered by lower montane, montane, and dwarf rainforest. The climate in El Yunque is classified as tropical, with 2.5 to 5 meters of orographically driven rainfall with little seasonality throughout the year and a mean annual temperature of 24°C at 370m elevation, and 19°C at 1000m elevation. Trade winds that carry mineral aerosol dust typically travel in a NEE to SWW direction and originate from the Sahara-Sahel region of Africa [Chapter 2 of this thesis, Gioda et al., 2013]. This area is a Critical Zone Observatory in addition to a Long-Term Ecological Research site, and has been the focus of extensive ecology and biogeochemistry research. Over our study area, which spans approximately 100 km^2, there are two different types of bedrock, which correspond to two different primary classifications of soil. Andesitic to basaltic volcaniclastic sandstone, breccia, and mudstone bedrock is overlain by Humic Hapludoxes, while intrusive quartz diorite bedrock is overlain by Aquic Dystrudepts. Two common forest types covering the sample sites are classified as either being dominated by either palo colorado trees (average canopy height 15 m) or tabonuco trees (average canopy height 30 m) [Scatena 1990]. The samples used by this study cover an elevation range between 376 and 815 meters above sea level.

3.3.2 Sample Collection

Ridgetop soils were collected from a total of 31 locations across the Luquillo Mountains. Soils from a fully-factorial investigation of rock type and forest type covering both quartz diorite and volcaniclastic bedrock, and tabonuco and palo colorado forest, were collected from 16 ridgetop locations (4 of each combination) in the summer of 2010 [Mage and Porder 2013]. Sample SM82 was originally classified as having a quartz

diorite parent material, but further analysis revealed the parent material of that soil was volcaniclastic in origin. A second sampling campaign collected soils from an additional 15 sites, all on quartz diorite bedrock with palo colorado forest type. The second set of sites were chosen to constitute a gradient of ridgetop-width, between 5 and 54 m, holding other soil-forming factors constant. Denudation rates have been determined on 11 of the 15 ridge-width gradient soils based on ^{10}Be in 250-500 µm quartz grains from the soils [Tamayo, 2014]. Ridge-top sites were defined as having <10% slope, and being local topographic high areas where colluvial deposition of soil from a higher topographical location was unlikely. At all 31 locations, 0-20 cm depth soil was collected in three pits approximately 10 m apart in a transect along the spine of the ridge. The soil excludes large roots and surface litter layer. Soils were air-dried and sieved (<2 mm) within 2 weeks of collection. The three samples at each site were composited prior to our analysis. A 25 cm by 25 cm quantitative pit was dug to a depth of 20 cm at each site to calculate bulk density.

3.3.3 Soil Digestion

Prior to soil digestion organic matter was removed by placing soil in crucibles and heating them to 550 degrees Celsius for five hours. Approximately 0.4 grams of the ashed soil was placed in a Teflon microwave vessel with concentrated acids: 6 ml HNO_3, 2 ml HCl, and 2 ml HF. Samples were then digested in the microwave for 70 minutes, reaching 200 °C and 60 bars of pressure. After the microwave digestion, samples were transferred to Teflon vials and dried down on a hotplate. Samples were re-dissolved in combination of concentrated HCl, HNO_3. Samples were stored in concentrated aqua regia prior to dilution and analysis.

3.3.4 REE Analysis

Rare earth element and trace element concentrations were analyzed on a Thermo Scientific X-Series II Quadrupole ICP-MS in the William P. Keck Lab for Plasma Spectrometry at Oregon State University. A multi-element standard solution in dilute nitric acid from Inorganic Ventures was used to calculate concentrations of all the rare earth elements as well as uranium and thorium. Spex multi-element standards were used for all other elements measured in this study. Single element standards were monitored for oxide formation. For each element measured, the amount of oxides that formed in the single element standard was subtracted as a proportion from the sample. An internal indium standard was used to monitor and correct for changes in uptake and instrument sensitivity throughout the experiment. Procedural blanks measured in concentration data were at similar levels to the instrumental blanks for all REE analytes, <5 pg g^{-1}. REE concentration pattern data are normalized to the REE concentrations of the underlying bedrock, averaged from several different rock samples for each bedrock type [Pett-Ridge 2007 and Porder, S.P., unpublished data]. Analytical uncertainty of concentration data is 5% based on multiple digestions (n=10) of the NIST 2709a soil standard. Procedural blanks were monitored and never exceeded 1% of sample concentrations.

3.3.5 $^{143}Nd/^{144}Nd$ Measurements

Nd was isolated from the remainder of the soil sample using a two-stage column procedure. AG50-HCl form resin was used to remove major cations and separate rare-earth fractions from other fractions. The REE elements were then run through Eichrom Ln-spec resin to separate Nd from other REEs. The procedural blank for Nd was <5 pg g^{-1}. The final solutions were all brought to 50 ng g^{-1}concentration and run on a Nu

instruments multi-collector ICP-MS. Long-term precision of the Nu MC-ICPMS based on 155 analyses of an in-house standard is 0.511205 +/- 0.000014 $^{143}Nd/^{144}Nd$. This corresponds to an analytical precision of 0.3 ε_{Nd} (where ε_{Nd} is the deviation of $^{143}Nd/^{144}Nd$ from a bulk earth value, CHUR 0.512638, in parts-per-ten thousand; [Jacobsen and Wasserburg, 1979]). Analyses of JNdi-1, used for instrumental offset correction, gave similar long-term external reproducibility (0.2 ε_{Nd}; n = 174).

3.3.6 Dust Flux Calculations

The total amount of dust that has been added to the top 20 cm of soil can be calculated with several known variables and assumptions. From the time bedrock begins weathering to the time our measurements were made, the total loss of Nd can be determined using several different methods. One method is to normalize Nd to an immobile element such as Zr or Nb in an elemental open-system transport function, known as a τ value (Equation 2) [Brimhall and Dietrich 1987]

$$\text{Eq. 2} \quad \tau_{j,h} = [(C_{j,h}/C_{i,h})/(C_{j,p}/C_{i,p})]\text{-}1$$

Changes in the concentration, *C*, of an element, *j*, in soil horizon, *h*, are normalized to changes in the concentration of an index element, *i*. The subscript *p* refers to concentrations in the unweathered parent material. The τ calculation has limitations because it relies on the assumption of immobility of the index element and does not take atmospheric inputs into account, both of which are important factors in the Luquillo Mountains [Pett-Ridge et al, 2009]. Instead, we employ an alternative method based on bedrock concentrations of the element of interest can be used to estimate how much bedrock Nd has weathered out of a profile. This measurement calculates the total percent

loss of Nd using an assumption of isovolumetric weathering (meaning no strain or soil collapse during weathering), which has previously been shown to be the case for the Luquillo quartz diorite [White et al., 1998].

$$\text{Eq. 3} \qquad X_{soil}^{Nd} = C_{soil}^{Nd} * \rho_{soil} * z_{soil}$$

$$\text{Eq. 4} \qquad X_{bedrock}^{Nd} = C_{bedrock}^{Nd} * \rho_{bedrock} * z_{bedrock}$$

The amount of Nd in either soil or bedrock is based on the concentration of Nd (*C*), the density (ρ), and the thickness (*z*), and has units of mg Nd cm^{-2} (equations 3 and 4). The Nd in soil is a combination of dust-derived Nd ($Nd_{soil\text{-}dust}$) and bedrock-derived Nd ($Nd_{soil\text{-}bedrock}$). Using ε_{Nd}, we can determine the fraction of total Nd derived from both dust and rock, using their endmembers of -12 and 7 respectively. The fraction of soil Nd that is derived from dust is calculated using a simple two end-member mixing formula (equation 5), where:

$$\text{Eq. 5} \quad f_{soil-dust}^{Nd} = \left(\frac{\varepsilon_{Nd}^{soil} - \varepsilon_{Nd}^{bedrock}}{\varepsilon_{Nd}^{dust} - \varepsilon_{Nd}^{bedrock}}\right)$$

The dust content of the soil (%Dust) is calculated based on the average Nd concentration of the dust (43 ug g^{-1} , (Herwitz 1993)) in equation 6. The difference between 1 and f_{dust}^{Nd} is used to calculate the fraction of soil Nd that is derived from bedrock (equation 7).

$$\text{Eq. 6} \quad \%Dust = 100 * \left[\left(\frac{f_{soil-dust}^{Nd} * C_{soil}^{Nd} * soil\ mass}{C_{dust}^{Nd}}\right) \div soil\ mass\ \right]$$

$$\text{Eq. 7} \quad f_{soil-bedrock}^{Nd} = 1 - f_{dust}^{Nd}$$

$$\text{Eq. 8} \quad f_{soil-bedrock}^{Nd} * X_{soil}^{Nd} = X_{soil,bedrock-derived}^{Nd}$$

$$\text{Eq. 9} \quad f_{soil-dust}^{Nd} * X_{soil}^{Nd} = X_{soil,dust-derived}^{Nd}$$

$$\text{Eq. 10} \quad \left(\left(\frac{X_{soil,bedrock-derived}^{Nd}}{X_{bedrock}^{Nd}}\right) - 1\right) * 100 = \%loss\ Nd_{bedrock}$$

$$\text{Eq. 11} \quad \%loss\ Nd_{bedrock} = \%loss\ Nd_{dust}$$

$$\text{Eq. 12} \quad \left(\left(\frac{X^{Nd}_{soil}}{X^{Nd}_{bedrock}+X^{Nd}_{dust}}\right)-1\right)*100 = \%loss\ Nd_{total}$$

Using the original mass of bedrock Nd ($X^{Nd}_{bedrock}$) and the current mass of bedrock-derived Nd in soil ($X^{Nd}_{soil,\ bedrock\text{-}derived}$), we establish the percentage of $Nd_{bedrock}$ lost during weathering (%loss $Nd_{bedrock}$, Eq. 10). Because there is no clear reason to believe Nd weathering rate would differ between dust-derived and bedrock-derived Nd in this system, we assume that the %loss($Nd_{bedrock}$) =%loss(Nd_{dust}).

Using the %loss (Nd_{dust}) we extrapolate from the current inventory of dust-derived Nd in the soil ($X^{Nd}_{soil,\ dust\text{-}derived}$) to the total amount of dust-derived Nd that was deposited during the residence time of the top 20 cm of soil at the surface (Eq. 13).

$$\text{Eq. 13} \quad \left[\frac{X^{Nd}_{soil,dust-derived}}{1-(\%\text{loss}(Nd_{dust}/100))}\right] = \textit{mass total dust-derived Nd deposited}$$

The mass of total dust-derived Nd deposited is then converted to a mass of dust deposited by dividing by the average concentration of Nd in African dust, 43 µg g^{-1} (equation 14) [Herwitz 1993].

$$\text{Eq. 14} \quad \frac{mass\ total\ dust-derived\ Nd\ deposited}{C^{Nd}_{dust}} = total\ dust\ deposited$$

The dust amount can be expressed as a dust deposition rate using the soil residence time calculated using either a ^{10}Be-based denudation estimate [Tamayo, 2014 data], or other estimates of denudation rates specific to each bedrock type (equation 15) [Riebe et al., 2004, Brown et al., 1995, Pett-Ridge et al., 2009 and Dosseto et al., 2013].

$$\text{Eq. 15} \quad \frac{total\ dust\ deposited}{residence\ time} = \textit{dust deposition flux}$$

3.4 Results

3.4.1 Soil REE Data

A wide range of soil REE, Zr, and Nb concentrations is evident across the 31 ridgetop sites as shown in Table 1. Nd concentrations in the soil ranged from 0.28 to 14.25 μg g^{-1}, and averaged 2.79 μg g^{-1} with a standard deviation of 2.74 μg g^{-1}. The quartz diorite bedrock had 7.86 μg g^{-1} Nd and the volcaniclastic bedrock had 16.10 μg g^{-1} Nd. Between soils developed on different bedrock types, a t-test assuming unequal variances revealed that volcaniclastic and quartz diorite derived soils did not have significantly ($p>0.05$) different concentrations of Nd. Tables 2 and 3 show soil concentration values of all REEs + Y normalized to the those concentrations in their underlying bedrock. Table 4 shows the τ values showing large depletion of Nd relative to the immobile element Nb, with most sites have lost >90% of bedrock-derived Nd. Table 4 also shows the calculations of $\%loss Nd_{total}$, and $\%loss Nd_{dust}$. $\%\ loss Nd_{dust}$ for the soil samples are large, all but two samples are >90%, with no relation to rock type. REE patterns normalized to underlying bedrock were plotted in Figures 1-3.

3.4.2 Nd isotopes

Nd isotope ratios of all 0-20 cm depth ridgetop soil are presented in ε_{Nd} units, and shown in Table 5. ε_{Nd} values for soil samples displayed a wide range from -10.3 to 7.0 with a mean of -1.2 and a standard deviation of 5.0. The values encompass most of the range between the two end-members; dust has a ε_{Nd} of -12 [Kumar et al., 2014], while both bedrock types in Luquillo have a ε_{Nd} of +7 [Smith et al., 1998].

Using equation 5, the fraction of Nd that comes from dust for these soils ranges from 0.06 to 0.89 (meaning 6 to 89% dust-derived Nd in soil) with a mean of 0.47 and a standard deviation of 0.24. Figure 4 shows a map of % dust-derived Nd in the soil at each

site. The average ε_{Nd} values between bedrock types were not significantly ($p>0.05$) different from each other. ε_{Nd} is not correlated to elevation, latitude, longitude, or forest type based on multiple linear regression analysis. The % dust derived Nd in soil did show a positive correlation with ridge width (Figure 12), but not with elevation, latitude, longitude, or forest type.

3.4.3 Dust flux calculations

Dust flux calculations were done using both $\tau_{Nd\ (Nb)}$ as a weathering indicator and $\%lossNd_{bedrock}$. In the ridgetop-width gradient subset of samples (PR-CT), for which ^{10}Be data are available, the dust flux calculations are more reliable because the denudation rate and soil Nd have been determined at the same sites [Tamayo 2014]. On these samples, using $\%lossNd_{bedrock}$ the dust flux ranges from 1.7 to 43 g m^{-2} yr^{-1} with an average of 18.1 ± 12.6 g m^{-2} yr^{-1} (Table 5). A likely range in dust flux values for the other samples on quartz diorite bedrock (SM73 through SM136) was calculated from two different estimates denudation rates of 26 m Ma^{-1} (the lowest rate in the quartz diorite ridgetop width set of samples) and 65 m Ma^{-1} (the average rate for the monolithologic quartz diorite Rio Icacos watershed)[Pett-Ridge et al., 2009]. Dust flux numbers were not calculated for volcaniclastic soils, as the only available estimate of soil denudation rate, based on a single regolith profile is extremely rapid, 360 m Ma^{-1} [Dosseto et al., 2013] and yields unrealistically high dust deposition fluxes of up to 3700 g m^{-2} yr^{-1}. The total mass of dust that has been deposited during the residence time of the surface 20 cm of all soils (Table 5) is similar, suggesting that the soil residence times at volcaniclastic sites are likely not dramatically different from those on quartz diorite bedrock.

3.5 Discussion

3.5.1 Nd isotopes

Calculated dust fluxes based on ε_{Nd} values reveal that dust deposition is highly variable across the Luquillo Mountains. Previous research has found that dust deposition can vary 1.8-fold across nine stations spanning 800 km in Florida [Prospero et al., 2010], up to three-fold at 3 stations across a spatial scale of 125 km in the Wind River Range in Wyoming [Brahney, 2014], and 5-fold at six stations over a scale of 1 km on winter snowpack in the Spanish Pyrenees [Bacardit and Camerero, 2010]. In the Luquillo Mountains, we have measured dust deposition that varies almost 26 fold within an approximately 100 km^2 area. Dust deposition fluxes range from 1.7 to 43 g m^{-2} yr^{-1} with an average of 18.1 ± 12.6 g m^{-2} yr^{-1} on the quartz diorite soils.

Comparing dust deposition fluxes on quartz diorite soils with the environmental variables of slope, aspect, latitude, longitude, elevation, or forest type revealed no clear patterns to explain wide spatial variation in dust deposition (Figures 5-8, and Table 6). Analysis of variance showed that no single variable tested had a significant control on dust deposition. Longitude was the most significant at p=0.09. Longitude was hypothesized to control dust deposition, because airmasses average an east to west track, with orographically-driven rainfall potentially removing dust along that path. Multiple regression analysis also revealed that no combination of measured environmental variables controlled dust deposition significantly. Rainfall estimated using the PRISM climate model [Daly et al., 2003] had no correlation with dust deposition measured from the ^{10}Be paired dataset.

There are several other explanatory variables that could be controlling dust deposition. Surface wind speed and wind turbulence data were not available, but are a

likely factor controlling local scale variation in dust deposition. Historical surface wind patterns would be even more difficult to estimate for the measured residence times of our soil. Another potential explanation of dust deposition variability would be surface canopy characteristics. Although dominant vegetation type plays a major determining factor in surface canopy character, variations exist in these sites within forest types. The historical variation of surface canopy characteristics could be even more varied between these site locations, leading to a wide variety of dust deposition rates over the thousand year residence times of the surface 0-20 cm of soil. Regardless of why variation of dust deposition exists on the spatial scales addressed by this study, ~100 km^2, this variation can translate to a wide variation in atmospheric rock-derived nutrient delivery to ecosystems. In terms of phosphorus (P), assuming a concentration of 1100 μg P g $dust^{-1}$ [Pett-Ridge 2009], a 1.7 to 44 g m^{-2} yr^{-1} variation in dust deposition represents a variation of between 1.9 to 48.4 mg P m^{-2} yr^{-1}. For reference, the other input of P to ecosystems, the conversion of saprolite to soil, provides approximately 23 mg P m^{-2} yr^{-1} in the quartz diorite Rio Icacos watershed in the Luquillo Mountains [Pett-Ridge, 2009].

3.5.2 Dust impact on phosphorus cycling

Based on fertilization studies of nutrient limitation in Puerto Rico [Fetcher et al., 1996], and an extensive evaluation of soil nutrient status [Silver et al., 1994], there is evidence that Luquillo ecosystems are P-limited. Several key measures of soil nutrient status previously measured on these ridgetop soils correlate well with the measures of current dust status in the soil [Tamayo 2014, Mage and Porder 2013]. Figure 9 shows that the total soil dust content ($f_{soil-dust}^{Nd} * 100$) is correlated with biologically cycled P fractions, as defined by $NaHCO_3$ and NaOH-extractable P on quartz diorite soils. Figure

10 shows that the organic P fraction is not a function of % C in soil, which suggests that the correlation between organic P and soil dust content is driven by dust deposition, instead of the amount of organic matter in the soil. This implies that dust inputs increase the amount of biologically cycled P in ecosystems and soils on the quartz diorite bedrock. On the other hand, dust content in volcaniclastic derived soil does not correlate with the organic and labile P fractions in soil. This is most likely because both volcaniclastic bedrock and volcaniclastic soils have a higher P content than quartz diorite bedrock and soils [Mage and Porder 2013]. Our data suggest that the P-poor quartz diorite systems are more sensitive to dust-derived P inputs.

Two additional soil factors, ridgetop width and τ_{Si} (where Nb is the immobile index element eq. 2), correlate with the current soil dust content (Figures 11 and 12 and Table 5). Ridgetop width is positively correlated with soil dust content ($r^2 = 0.68$; $p < 0.05$). The τ_{Si} values for all soils with precise denudation rates are negatively correlated with current soil dust content ($r^2 = 0.41$; $p < 0.05$). However, denudation rates calculated from ^{10}Be data do not correlate with current soil dust content (Figure 13). This suggests that the soil weathering status based on τ_{Si} values on the ridgetop width gradient of sites is not a function of slower denudation on wider ridges, and instead may be related to different hydrology and soil hydraulic connectivity on wider ridges [Tamayo 2014]. It is not known what causes higher current soil dust content on wider ridges, but in the absence of a residence time effect, it appears that small-scale meteorological factors related to airmass interactions with ridges, or differences in forest canopy structure may play a role. Nevertheless, the relationship between increased soil dust content and wider

ridges appears to explain the paradox of increased pools of biologically cycled P on the more highly weathered soils on wider ridges.

3.5.3 REE Patterns

The patterns of REE reveal several characteristics that point to dust deposition being highly variable from site to site. Dust from the Sahara-Sahel region has a characteristically high La:Yb relative to both bedrock types of Luquillo. High dust deposition would cause the REE distribution in soil to appear similar to the REE distribution in dust. This is shown clearly with a depth profile of REE distribution patterns in Figure 14 [Pett-Ridge 2007]. However, this could also indicate that soil weathering is causing the distribution of REEs to change and not dust deposition, since dust is essentially weathered soil. The dust deposition calculated from ε_{Nd} when plotted against La/Yb for soil samples with known denudation rates from ^{10}Be, shows a significant ($p<0.05$) positive relationship between La/Yb and dust flux (Figure 15). While dust deposition and degree of soil weathering may co-vary to some degree (Figure 12), this suggests that dust deposition at least contributes to surface soil REE patterns. The general shape of the pattern for dust is heavily enriched with LREEs, while soils with more dust or more weathering are also enriched in LREEs. Because the patterns are normalized to bedrock, soils that are unweathered with respect to REEs remain flat with a normalized value of 1. Of particular interest is the La/Yb for each soil, representing a light to heavy REE ratio. This value in our soils ranges from 1.7 to 23.6, with an average of 8.9 and standard deviation of 4.9 (Table 4). Dust has a La/Yb of 29.5 while the quartz diorite and volcaniclastic bedrocks have a La/Yb of 5.5 and 5.7 respectively.

Plots of ridgetop surface soil La/Yb versus spatial variables Figures 16-18 show variation between volcaniclastic and quartz diorite derived soils. Latitude and longitude plots (Figure 16 and 17) reveal the spatial extent of quartz diorite across the landscape controls variability in La/Yb ratios. Quartz diorite soils show a wider range in La/Yb, and volcaniclastic soils have lower La/Yb and are more uniform. Within just quartz diorite soils, variability in La/Yb is higher at higher elevations (Figure 18) likely caused by either more weathered soils at higher elevations due to a regional knickpoint in denudation rates [Porder et al, in review], increased dust inputs at higher elevations, or a combination of both. Figure 18 shows there is a point in elevation where dust flux increases drastically, potentially from intercepting airmasses carrying dust.

3.5.4 Comparison of methods for determining dust deposition

Several other dust flux estimates have been made using other techniques, which incorporate different timescales. The dust flux estimated using a Sr isotope watershed scale mass balance in the Rio Icacos watershed of the Luquillo Mountains shows that dust is deposited at a rate of 21 $\pm$ 7 g m^{-2} yr^{-1} [Pett-Ridge, 2009], which is similar to the average deposition rate from this study, 18 $\pm$ 12 g m^{-2} yr^{-1}. A study by Mahowald [2005], estimates the dust flux to the Caribbean as approximately 5 g m^{-2} yr^{-1} using a model of global deposition rates. The model resolution encompasses a large area of ocean however, with average rainfall that is 4-fold lower that that over the Luquillo Mountains. Yet another approach calculates dust flux using dissolved silica ($dSiO_2$) and non-seasalt calcium (nss-Ca) in rainwater as a tracer (Chapter 2, this thesis). These dust flux estimates ranged from 0.7 to 48 g m^{-2} yr^{-1} at the El Verde rain station for $dSiO_2$ and nss-Ca respectively, and between 2.6 and 125.4 g m^{-2} yr^{-1} for $dSiO_2$ and nss-Ca respectively

at Bisley. $dSiO_2$ is thought to be an underestimate of dust deposition because much of the SiO_2 in dust does not dissolve, and nss-Ca is thought to be an overestimate because removing seasalt calcium using Cl^- as a seasalt tracer is likely imperfect. Several other studies measuring deposition using these rainwater based dust tracers at this location had similar values [Heartscill-Scaley, 2007; Stallard, 2001; Gioda, 2013]. The range of dust deposition calculated using these rainwater proxies does fall in the ranges of deposition fluxes at the soil sites in this chapter. It is important to note that the study by Maholwald [2005] and the previous chapter of this thesis are modern decadal estimates of dust deposition, while the dust deposition fluxes presented here represent dust deposition averaged over hundreds to thousands of years.

3.6 Conclusion

Dust deposition has been quantified in multiple locations within the Luquillo Mountains of Puerto Rico using Nd isotopes and Nd concentrations in both soil and bedrock. ^{10}Be data has provided precise soil residence times for several of these samples to calculate accurate dust fluxes. Other soils used an average denudation rate from Riebe et al., [2004], Brown et al., [1995], Pett-Ridge et al., [2009] and Dosseto et al., [2013] to calculate soil residence times. Soils that were paired with ^{10}Be residence times had an average dust deposition rate of 18.10 ± 12.63 g m^{-2} yr^{-1}. These dust fluxes are highly variable throughout this landscape, but do not follow a regular pattern with longitude, latitude, or elevation. The dust deposition rates paired with ^{10}Be data do correlate strongly other factors such as the amounts of labile and organic P in surface soil. Organic P does not correlate with soil C, implying there is another source of P not associated with organic matter, most probably dust. With the more varied dataset covered by La/Yb

measurements, a pattern occurs where both longitude and elevation become major determining factors in dust deposition.

3.7 Citations:

Abouchami, W., Naethe, K., Kumar, A., Galer, S. J. G., Jochum, K. P., Williams, E., Horbe, A. M. C., Rosa, J. W. C., Balsam, W., Adams, D., Mezger, K. & Andreae, M. O. 2013. Geochemical and isotopic characterization of the Bodele Depression dust source and implications for transatlantic dust transport to the Amazon Basin. *Earth and Planetary Science Letters,* 380**,** 112-123.

Aubert, D., Stille, P., Probst, A., Gauthier-Lafaye, F., Pourcelot, L. & Del Nero, M. 2002. Characterization and migration of atmospheric REE in soils and surface waters. *Geochimica Et Cosmochimica Acta,* 66**,** 3339-3350.

Avila, A., Alarcon, M. & Queralt, I. 1998. The chemical composition of dust transported in red rains - Its contribution to the biogeochemical cycle of a Holm oak forest in Catalonia (Spain). *Atmospheric Environment,* 32**,** 179-191.

Bacardit, M. & Camarero, L. 2010. Atmospherically deposited major and trace elements in the winter snowpack along a gradient of altitude in the Central Pyrenees: The seasonal record of long-range fluxes over SW Europe. *Atmospheric Environment,* 44**,**582-595.

Bataille, C. P., Laffoon, J. & Bowen, G. J. 2012. Mapping multiple source effects on the strontium isotopic signatures of ecosystems from the circum-Caribbean region. *Ecosphere,* 3.

Bern, C. R. & White, A. F. 2011. A model for assessing, quantifying, and correcting for index element mobility in weathering studies. *Applied Geochemistry,* 26**,** S9-S11.

Brahney, J., Ballantyne, A.P., Kociolek, P., Spaulding S., Otu, M., Porwoll, T., Neff, J.C. 2014. Dust mediated transfer of phosphorus to alpine lake ecosystems of the Wind River Range, Wyoming, USA. Biogeochemistry, 120:259-278.

Brimhall, G. H. & Dietrich, W. E. 1987. Constitutive mass balance relations between chemical-composition, volume, density, porosity, and strain in metasomatic hydrochemical systems - results on weathering and pedogenesis. *Geochimica Et Cosmochimica Acta,* 51**,** 567-587.

Brown ET, Stallard RF, Larsen MC, Raisbeck GM, Yiou F (1995) Denudation rates determined from the accumulation of in situ produced 10Be in the Luquillo Experimental Forest, Puerto Rico. Earth Planet Sci Lett 129:193–202. doi:10.1016/0012-821X(94)00249-X

Borg, L. E. & Banner, J. L. 1996. Neodymium and strontium isotopic constraints on soil sources in Barbados, West Indies. *Geochimica Et Cosmochimica Acta,* 60**,**4193-4206.

Boy, J. & Wilcke, W. 2008. Tropical Andean forest derives calcium and magnesium from Saharan dust. *Global Biogeochemical Cycles,* 22.

Chabaux, F., Blaes, E., Stille, P., Roupert, R. D. C., Pelt, E., Dosseto, A., MA, L., Buss, H. L. & Brantley, S. L. 2013. Regolith formation rate from U-series nuclides: Implications from the study of a spheroidal weathering profile in the Rio Icacos watershed (Puerto Rico). *Geochimica Et Cosmochimica Acta,* 100**,** 73-95.

Chadwick, O. A., Derry, L. A., Vitousek, P. M., Huebert, B. J. & Hedin, L. O. 1999. Changing sources of nutrients during four million years of ecosystem development. *Nature,* 397**,** 491-497.

Coale, K. H., Johnson, K. S., Fitzwater, S. E., Gordon, R. M., Tanner, S., Chavez, F. P., FeriolI, L., Sakamoto, C., Rogers, P., Millero, F., Steinberg, P., Nightingale, P., Cooper, D., Cochlan, W. P., Landry, M. R., Constantinou, J., Rollwagen, G., Trasvina, A. & Kudela, R. 1996. A massive phytoplankton bloom induced by an ecosystem-scale iron fertilization experiment in the equatorial Pacific Ocean. *Nature,* 383**,** 495-501.

Cox, S. B., Willig, M. R. & Scatena, F. N. 2002. Variation in nutrient characteristics of surface soils from the Luquillo Experimental Forest of Puerto Rico: A multivariate perspective. *Plant and Soil,* 247**,** 189-198.

Daly, C., Helmer, E.H., Quiñones, M. 2003. Mapping the Climate of Puerto Rico, Vieques and Culebra. *International Journal of Climatology,* 23: 1359-1381.

Dia, A., Chauvel, C., Bulourde, M. & Gerard, M. 2006. Eolian contribution to soils on Mount Cameroon: Isotopic and trace element records. *Chemical Geology,* 226**,** 232-252.

Dosseto, A., Buss, H. L. & Suresh, P. O. 2012. Rapid regolith formation over volcanic bedrock and implications for landscape evolution. *Earth and Planetary Science Letters,* 337**,** 47-55.

Fetcher, N., Haines, B. L., Cordero, R. A., Lodge, D. J., Walker, L. R., Fernandez, D. S. & Lawrence, W. T. 1996. Responses of tropical plants to nutrients and light on a landslide in Puerto Rico. *Journal of Ecology,* 84**,** 331-341.

Ginoux, P., Chin, M., Tegen, I., Prospero, J. M., Holben, B., Dubovik, O. & Lin, S. J. 2001. Sources and distributions of dust aerosols simulated with the GOCART model. *Journal of Geophysical Research-Atmospheres,* 106, 20255-20273.

Gioda, A., Mayol-Bracero, O. L., Scatena, F. N., Weathers, K. C., Mateus, V. L. & Mcdowell, W. H. 2013. Chemical constituents in clouds and rainwater in the Puerto Rican rainforest: Potential sources and seasonal drivers. *Atmospheric Environment,* 68**,** 208-220.

Grousset, F. E. & Biscaye, P. E. 2005. Tracing dust sources and transport patterns using Sr, Nd and Pb isotopes. *Chemical Geology,* 222**,** 149-167.

Guieu, C., Loye-Pilot, M. D., Ridame, C. & Thomas, C. 2002. Chemical characterization of the Saharan dust end-member: Some biogeochemical implications for the western Mediterranean Sea. *Journal of Geophysical Research-Atmospheres,* 107.

Hedin, L. O., Vitousek, P. M. & Matson, P. A. 2003. Nutrient losses over four million years of tropical forest development. *Ecology,* 84**,** 2231-2255.

Herwitz SR, Muhs DR, Prospero JM, Mahan S, Vaughn B (1996) Origin of Bermuda's clay-rich quaternary paleosols and their paleoclimatic significance. J Geophys Res Atmos 101(D18):23389–23400. doi:10.1029/96JD02333

Hicks, D. J. 1980. Intrastand distribution patterns of southern appalachian cove forest herbaceous species. *American Midland Naturalist,* 104**,** 209-223.

Jacobsen, S. B. & Wasserburg, G. J. 1979. Nd and Sr isotopic study of the bay of islands ophiolite complex and the evolution of the source of midocean ridge basalts. *Journal of Geophysical Research,* 84**,** 7429-7445.

Jahn, B. M., Gallet, S. & Han, J. M. 2001. Geochemistry of the Xining, Xifeng and Jixian sections, Loess Plateau of China: eolian dust provenance and paleosol evolution during the last 140 ka. *Chemical Geology,* 178**,** 71-94.

Jickells, T. D., An, Z. S., Andersen, K. K., Baker, A. R., Bergametti, G., Brooks, N., Cao, J. J., Boyd, P. W., Duce, R. A., Hunter, K. A., Kawahata, H., Kubilay, N., Laroche, J., Liss, P. S., Mahowald, N., Prospero, J. M., Ridgwell, A. J., Tegen, I. & Torres, R. 2005. Global iron connections between desert dust, ocean biogeochemistry, and climate. *Science,* 308**,** 67-71.

Kumar, A., Abouchami, W., Galer, S. J. G., Garrison, V. H., Williams, E. & Andreae, M. O. 2014. A radiogenic isotope tracer study of transatlantic dust transport from Africa to the Caribbean. *Atmospheric Environment,* 82**,** 130-143.

Kurtz, A. C., Derry, L. A. & Chadwick, O. A. 2001. Accretion of Asian dust to Hawaiian soils: Isotopic, elemental, and mineral mass balances. *Geochimica Et Cosmochimica Acta,* 65**,** 1971-1983.

Larsen M. C. 2012. Landslides and sediment budgets in four watersheds in Eastern Puerto Rico. In: Water Quality and Landscape Processes of Four Watersheds in Eastern Puerto Rico (eds. S.F. Murphy and R. F. Stallard). p. 292.

Li, J.-W., Zhang, G.-L. & Gong, Z.-T. 2013. Nd isotope evidence for dust accretion to a soil chronosequence in Hainan Island. *Catena,* 101**,** 24-30.

Lindberg, S. E. & Lovett, G. M. 1985. Field-measurements of particle dry deposition rates to foliage and inert surfaces in a forest canopy.*Environmental Science & Technology,* 19**,** 238-244.

Mage, S. M. & Porder, S. 2013. Parent Material and Topography Determine Soil Phosphorus Status in the Luquillo Mountains of Puerto Rico. *Ecosystems,* 16**,** 284-294.

Mahowald, N., Jickells, T. D., Baker, A. R., Artaxo, P., Benitez-Nelson, C. R., Bergametti, G., Bond, T. C., Chen, Y., Cohen, D. D., Herut, B., Kubilay, N., Losno, R., Luo, C., Maenhaut, W., Mcgee, K. A., Okin, G. S., Siefert, R. L. & Tsukuda, S. 2008. Global distribution of atmospheric phosphorus sources, concentrations and deposition rates, and anthropogenic impacts. *Global Biogeochemical Cycles,* 22.

Mahowald, N. M., Baker, A. R., Bergametti, G., Brooks, N., Duce, R. A., Jickells, T. D., Kubilay, N., Prospero, J. M. & Tegen, I. 2005. Atmospheric global dust cycle and iron inputs to the ocean. *Global Biogeochemical Cycles,* 19.

Martin, J. H. 1990. glacial-interglacial CO_2 change: the iron hypothesis.*Paleoceanography,* 5**,** 1-13.

Muhs, D. R. & Budahn, J. R. 2009. Geochemical evidence for African dust and volcanic ash inputs to terra rossa soils on carbonate reef terraces, northern Jamaica, West Indies.*Quaternary International,* 196**,** 13-35.

Pett-Ridge, J. C., Derry, L. A. & Kurtz, A. C. 2007. Quantifying mineral aerosol inputs and the mobility of "immobile" elements in weathering studies. *Geochimica Et Cosmochimica Acta,* 71**,** A782-A782.

Pett-Ridge, J. C., Derry, L. A. & Kurtz, A. C. 2009. Sr isotopes as a tracer of weathering processes and dust inputs in a tropical granitoid watershed, Luquillo Mountains, Puerto Rico. *Geochimica Et Cosmochimica Acta,* 73**,** 25-43.

Porder, S., Paytan, A. & Vitousek, P. M. 2005. Erosion and landscape development affect plant nutrient status in the Hawaiian Islands. *Oecologia,* 142**,** 440-449.

Prospero, J. M. 1999. Long-term measurements of the transport of African mineral dust to the southeastern United States: Implications for regional air quality.*Journal of Geophysical Research-Atmospheres,* 104**,** 15917-15927.

Prospero, J. M. & Lamb, P. J. 2003. African droughts and dust transport to the Caribbean: Climate change implications. *Science,* 302**,** 1024-1027.

Prospero, J. M., Landing, W. M. & Schulz, M. 2010. African dust deposition to Florida: Temporal and spatial variability and comparisons to models. *Journal of Geophysical Research-Atmospheres,* 115.

Riebe, C. S., Kirchner, J. W. & Finkel, R. C. 2004. Erosional and climatic effects on long-term chemical weathering rates in granitic landscapes spanning diverse climate regimes. *Earth and Planetary Science Letters,* 224**,** 547-562.

Scatena FN. Watershed scale rainfall interception on 2 forested watersheds in the Luquillo Mountains of Puerto-Rico. Journal of Hydrology. 1990;113:89-102.

Silver, W. L., Scatena, F. N., Johnson, A. H., Siccama, T. G. & Sanchez, M. J. 1994. Nutrient availability in a montane wet tropical forest - spatial patterns and methodological considerations. *Plant and Soil,* 164**,** 129-145.

Smith AL, Schellekens JH, Diaz ALM (1998) Batholiths as markers of tectonic change in northeastern Caribbean. In: Lidiak E.G., Larue DK (eds) Tectonics and geochemistry of the northeastern Caribbean. Geological society of America special paper. Boulder, Colorado, pp 99–122

Stallard, R. F. 2001. Possible environmental factors underlying amphibian decline in eastern Puerto Rico: Analysis of US government data archives. *Conservation Biology,*15**,** 943-953.

Stoorvogel, J. J., Vanbreemen, N. & Janssen, B. H. 1997. The nutrient input by Harmattan dust to a forest ecosystem in Cote d'Ivoire, Africa. *Biogeochemistry,* 37**,**145-157.

Swap, R., Garstang, M., Greco, S., Talbot, R. & Kallberg, P. 1992. Saharan dust in the amazon basin. *Tellus Series B-Chemical and Physical Meteorology,* 44**,** 133-149.

Tamayo, C. 2014. Geomorphic influences on soil weathering and nutrient status in a tropical forest. Undergraduate thesis, Brown University.

Tegen, I., Lacis, A. A. & Fung, I. 1996. The influence on climate forcing of mineral aerosols from disturbed soils. *Nature,* 380**,** 419-422.

Turner, B. F., Stallard, R. F. & Brantley, S. L. 2003. Investigation of in situ weathering of quartz diorite bedrock in the Rio Icacos basin, Luquillo Experimental Forest, Puerto Rico. *Chemical Geology,* 202**,** 313-341.

Vitousek, P. M., Porder, S., Houlton, B. Z. & Chadwick, O. A. 2010. Terrestrial phosphorus limitation: mechanisms, implications, and nitrogen-phosphorus interactions. *Ecological Applications,* 20**,** 5-15.

Walker, T. W. & Syers, J. K. 1976. Fate of phosphorus during pedogenesis.*Geoderma,* 15**,** 1-19.

White, A. F., Blum, A. E., Schulz, M. S., Vivit, D. V., Stonestrom, D. A., Larsen, M., Murphy, S. F. & Eberl, D. 1998. Chemical weathering in a tropical watershed, Luquillo mountains, Puerto Rico: I. Long-term versus short-term weathering fluxes.*Geochimica Et Cosmochimica Acta,* 62**,** 209-226.

White, E. J. & Turner, F. 1970. Method of estimating income of nutrients in a catch of airborne particles by a woodland canopy. *Journal of Applied Ecology,* 7**,** 441-&.

3.8 Tables

Table 1. Rare Earth Element, Nd, and Zr (ppm) in Soil Samples, Dust, and Bedrock Types

Sample#	Y	La	Ce	Pr	Nd	Sm	Eu	Gd
SM1	3.35	5.73	10.98	1.18	4.30	0.79	0.18	0.72
SM10	0.61	0.95	2.19	0.21	0.77	0.14	0.03	0.14
SM19	1.40	1.71	3.65	0.44	1.76	0.40	0.10	0.36
SM28	2.75	3.40	7.57	0.78	3.12	0.68	0.19	0.69
SM37	4.18	6.62	8.38	1.28	4.16	0.77	0.17	0.67
SM46	4.42	4.53	11.57	1.12	4.69	1.02	0.30	1.05
SM55	4.11	5.80	11.11	1.30	4.92	0.95	0.23	0.91
SM64	6.48	3.31	7.37	0.76	3.03	0.69	0.19	0.76
SM73	1.72	3.35	7.15	0.79	3.13	0.66	0.17	0.60
SM82	2.04	2.78	6.35	0.62	2.37	0.51	0.13	0.51
SM91	0.69	1.54	3.54	0.32	1.22	0.25	0.07	0.24
SM100	1.76	1.88	6.31	0.50	2.16	0.51	0.13	0.49
SM109	0.36	0.64	1.73	0.13	0.51	0.09	0.02	0.09
SM118	2.47	1.27	3.04	0.40	1.76	0.49	0.16	0.57
SM127	10.62	5.31	12.04	1.93	8.98	2.23	0.68	2.30
SM136	2.76	2.96	8.33	0.68	2.86	0.60	0.18	0.62
PR-CT-1	0.44	0.92	1.62	0.18	0.66	0.13	0.04	0.13
PR-CT-2	1.36	2.27	7.15	0.50	1.91	0.43	0.13	0.43
PR-CT-3	0.19	0.35	0.85	0.08	0.28	0.06	0.01	0.06
PR-CT-4	0.54	0.93	2.12	0.22	0.86	0.19	0.05	0.19
PR-CT-5	0.49	1.63	3.29	0.34	1.26	0.25	0.06	0.21
PR-CT-6	0.96	2.22	4.22	0.58	2.23	0.47	0.13	0.41
PR-CT-7	2.72	2.62	5.18	0.72	3.08	0.74	0.19	0.73
PR-CT-8	1.13	2.44	4.93	0.55	2.07	0.40	0.10	0.38
PR-CT-9	1.02	4.18	7.03	0.74	2.53	0.43	0.09	0.37
PR-CT-10	1.07	2.51	4.49	0.50	1.77	0.31	0.08	0.29
PR-CT-11	1.36	1.93	4.93	0.51	2.11	0.45	0.12	0.42
PR-CT-12	0.45	1.09	2.32	0.24	0.91	0.18	0.04	0.16
Dust	40.00	65.00	128.00	12.40	43.00	8.30	1.40	5.70
Quartz Diorite	13.73	8.24	16.27	2.01	7.86	1.77	0.61	1.80
Volcaniclastic	24.00	10.54	19.13	3.46	16.10	4.33	1.41	4.41
Mean Soil	2.23	2.69	5.64	0.63	2.50	0.53	0.14	0.52

Table 1 (cont.) Rare Earth Element, Nd, and Zr (ppm) in Soil Samples, Dust, and Bedrock Types

Sample#	Tb	Dy	Ho	Er	Tm	Yb	Lu	Zr	Nb
SM1	0.11	0.70	0.17	0.59	0.10	0.71	0.13	181.20	7.45
SM10	0.02	0.16	0.04	0.13	0.02	0.16	0.03	140.53	6.17
SM19	0.06	0.45	0.10	0.35	0.06	0.44	0.07	141.86	7.31
SM28	0.11	0.67	0.14	0.43	0.06	0.43	0.06	136.11	5.96
SM37	0.10	0.68	0.17	0.70	0.12	0.98	0.19	252.26	5.66
SM46	0.16	1.00	0.21	0.68	0.10	0.73	0.11	180.37	7.30
SM55	0.14	0.90	0.21	0.73	0.12	0.97	0.16	215.01	7.95
SM64	0.14	1.05	0.27	1.04	0.17	1.31	0.23	236.74	5.64
SM73	0.09	0.52	0.10	0.31	0.05	0.34	0.05	26.91	4.18
SM82	0.09	0.59	0.12	0.41	0.07	0.49	0.07	86.59	5.30
SM91	0.03	0.19	0.04	0.12	0.02	0.15	0.02	30.81	2.94
SM100	0.07	0.46	0.09	0.29	0.04	0.31	0.05	19.86	3.91
SM109	0.01	0.09	0.02	0.06	0.01	0.08	0.01	19.95	2.70
SM118	0.11	0.81	0.18	0.60	0.10	0.73	0.12	12.63	2.48
SM127	0.37	2.33	0.48	1.48	0.22	1.45	0.22	12.19	2.39
SM136	0.10	0.60	0.13	0.39	0.06	0.44	0.07	24.15	2.72
PR-CT-1	0.02	0.12	0.02	0.08	0.01	0.09	0.01	109.06	4.47
PR-CT-2	0.07	0.47	0.09	0.30	0.05	0.37	0.05	80.55	4.07
PR-CT-3	0.01	0.05	0.01	0.03	0.01	0.03	0.01	202.44	5.44
PR-CT-4	0.03	0.19	0.04	0.12	0.02	0.14	0.02	165.37	4.58
PR-CT-5	0.03	0.16	0.03	0.08	0.01	0.09	0.01	127.94	3.94
PR-CT-6	0.06	0.32	0.06	0.17	0.03	0.19	0.03	178.34	4.04
PR-CT-7	0.11	0.67	0.14	0.41	0.06	0.40	0.06	159.56	3.53
PR-CT-8	0.05	0.32	0.06	0.19	0.03	0.20	0.03	152.28	5.44
PR-CT-9	0.05	0.28	0.05	0.16	0.03	0.18	0.03	140.15	7.67
PR-CT-10	0.04	0.26	0.05	0.16	0.03	0.17	0.03	295.41	8.41
PR-CT-11	0.06	0.35	0.07	0.19	0.03	0.19	0.03	93.97	4.13
PR-CT-12	0.02	0.12	0.02	0.07	0.01	0.07	0.01	94.18	4.10
Dust	0.80	4.20	0.80	2.30	0.30	2.20	0.30	250.00	12.00
Quartz Diorite	0.30	1.85	0.42	1.23	0.23	1.49	0.27	99.85	1.87
Volcaniclastic	0.62	3.84	0.75	2.04	0.33	1.85	0.32	82.48	1.54
Mean Soil	0.08	0.52	0.11	0.37	0.06	0.43	0.07	127.25	5.03

Table 2. REE ratios of volcaniclastic soils normalized to REE concentrations in volcaniclastic bedrock

Sample#	Y	La	Ce	Pr	Nd	Sm	Eu	Gd	Tb	Dy	Ho	Er	Tm	Yb	Lu
SM1	0.14	0.54	0.57	0.34	0.27	0.18	0.12	0.16	0.18	0.18	0.22	0.29	0.30	0.38	0.40
SM10	0.03	0.09	0.11	0.06	0.05	0.03	0.02	0.03	0.04	0.04	0.05	0.06	0.06	0.09	0.09
SM19	0.06	0.16	0.19	0.13	0.11	0.09	0.07	0.08	0.10	0.12	0.13	0.17	0.17	0.24	0.22
SM28	0.11	0.32	0.40	0.22	0.19	0.16	0.14	0.16	0.18	0.17	0.18	0.21	0.19	0.24	0.20
SM37	0.17	0.63	0.44	0.37	0.26	0.18	0.12	0.15	0.16	0.18	0.23	0.34	0.37	0.53	0.58
SM46	0.18	0.43	0.60	0.32	0.29	0.24	0.21	0.24	0.26	0.26	0.28	0.33	0.31	0.40	0.35
SM55	0.17	0.55	0.58	0.38	0.31	0.22	0.16	0.21	0.23	0.23	0.27	0.36	0.36	0.53	0.49
SM64	0.27	0.31	0.39	0.22	0.19	0.16	0.13	0.17	0.23	0.27	0.36	0.51	0.52	0.71	0.70
SM82	0.08	0.26	0.33	0.18	0.15	0.12	0.09	0.12	0.15	0.15	0.16	0.20	0.20	0.27	0.23
Dust	1.67	6.17	6.69	3.58	2.67	1.92	0.99	1.29	1.29	1.09	1.06	1.13	0.90	1.19	0.93

Table 3. REE ratios of quartz diorite soils normalized to REE concentrations in quartz diorite bedrock

Sample#	Y	La	Ce	Pr	Nd	Sm	Eu	Gd	Tb	Dy	Ho	Er	Tm	Yb	Lu
SM73	0.13	0.41	0.44	0.39	0.40	0.37	0.28	0.33	0.29	0.28	0.24	0.25	0.20	0.23	0.19
SM91	0.05	0.19	0.22	0.16	0.16	0.14	0.12	0.13	0.11	0.10	0.09	0.10	0.08	0.10	0.09
SM100	0.13	0.23	0.39	0.25	0.27	0.29	0.21	0.27	0.24	0.25	0.23	0.24	0.19	0.21	0.18
SM109	0.03	0.08	0.11	0.07	0.06	0.05	0.03	0.05	0.05	0.05	0.05	0.05	0.04	0.05	0.05
SM118	0.18	0.15	0.19	0.20	0.22	0.28	0.27	0.31	0.38	0.44	0.43	0.49	0.42	0.49	0.44
SM127	0.77	0.64	0.74	0.96	1.14	1.26	1.11	1.27	1.23	1.26	1.16	1.20	0.93	0.98	0.81
SM136	0.20	0.36	0.51	0.34	0.36	0.34	0.30	0.35	0.32	0.33	0.31	0.32	0.26	0.29	0.26
PR-CT-1	0.03	0.11	0.10	0.09	0.08	0.07	0.06	0.07	0.07	0.07	0.06	0.06	0.05	0.06	0.05
PR-CT-2	0.10	0.28	0.44	0.25	0.24	0.24	0.21	0.24	0.25	0.25	0.21	0.24	0.22	0.25	0.20
PR-CT-3	0.01	0.04	0.05	0.04	0.04	0.03	0.02	0.03	0.03	0.03	0.02	0.02	0.02	0.02	0.02
PR-CT-4	0.04	0.11	0.13	0.11	0.11	0.11	0.09	0.11	0.10	0.10	0.09	0.09	0.08	0.09	0.08
PR-CT-5	0.04	0.20	0.20	0.17	0.16	0.14	0.10	0.12	0.09	0.09	0.07	0.07	0.06	0.06	0.05
PR-CT-6	0.07	0.27	0.26	0.29	0.28	0.27	0.22	0.23	0.19	0.17	0.14	0.14	0.12	0.13	0.11
PR-CT-7	0.20	0.32	0.32	0.36	0.39	0.42	0.32	0.41	0.38	0.36	0.33	0.33	0.26	0.27	0.23
PR-CT-8	0.08	0.30	0.30	0.27	0.26	0.23	0.16	0.21	0.18	0.18	0.15	0.15	0.12	0.13	0.12
PR-CT-9	0.07	0.51	0.43	0.37	0.32	0.24	0.15	0.21	0.16	0.15	0.13	0.13	0.11	0.12	0.10
PR-CT-10	0.08	0.30	0.28	0.25	0.22	0.17	0.12	0.16	0.14	0.14	0.13	0.13	0.11	0.12	0.10
PR-CT-11	0.10	0.23	0.30	0.26	0.27	0.26	0.19	0.23	0.20	0.19	0.16	0.16	0.13	0.13	0.12
PR-CT-12	0.03	0.13	0.14	0.12	0.12	0.10	0.07	0.09	0.08	0.07	0.06	0.06	0.05	0.05	0.05
Dust	2.91	7.89	7.87	6.18	5.47	4.68	2.30	3.16	2.63	2.27	1.93	1.87	1.30	1.48	1.10

Table 4. Important Element Ratios

Sample#	La/Yb	τNd (Nb)	%lossNd	%loss dust Nd
SM1	8.1	-94.5	-89.9	-97.7
SM10	5.9	-98.8	-98.2	-99.8
SM19	3.9	-97.7	-95.9	-98.9
SM28	7.8	-95.0	-92.7	-97.2
SM37	6.8	-93.0	-90.2	-93.3
SM46	6.2	-93.9	-89.0	-92.4
SM55	6.0	-94.1	-88.5	-93.1
SM64	2.5	-94.9	-92.9	-94.4
SM82	5.7	-89.4	-88.6	-96.1
SM73	9.8	-82.2	-85.0	-87.9
SM91	10.6	-90.1	-94.1	-95.1
SM100	6.0	-86.9	-89.6	-92.1
SM109	8.3	-95.5	-97.6	-99.2
SM118	1.7	-83.2	-91.6	-92.2
SM127	3.7	-10.9	-56.9	-59.4
SM136	6.8	-75.1	-86.3	-89.9
PR-CT-1	10.0	-96.5	-96.8	-98.4
PR-CT-2	6.1	-88.9	-94.9	-98.7
PR-CT-3	10.2	-98.8	-98.6	-99.6
PR-CT-4	6.6	-95.5	-95.9	-98.4
PR-CT-5	18.7	-92.4	-93.9	-98.6
PR-CT-6	11.7	-86.9	-89.3	-91.5
PR-CT-7	6.5	-79.3	-98.8	-92.6
PR-CT-8	12.3	-91.0	-90.1	-95.3
PR-CT-9	23.6	-92.2	-87.8	-95.9
PR-CT-10	14.5	-95.0	-91.5	-96.3
PR-CT-11	10.2	-87.9	-89.9	-97.0
PR-CT-12	15.8	-94.7	-95.6	-99.3
Dust	29.5	-	-	-
QD	5.5	-	-	-
Vol.	5.7	-	-	-

Table 5. Sample ε_{Nd} and %Dust Nd.

Sample#	ε_{Nd}	Nd (ppm)	%Dust Nd	Mass Dust (g)	Denudation Rates (m/Mya)	20cm Soil Res. Time (years)	% Soil Dust	Dust Dep. (g m^{-2} yr^{-1})
SM1	-8.1	4.3	77	74.1	-	-	8.2	-
SM10	-10.3	0.8	89	202.7	-	-	1.7	-
SM19	-7.2	1.8	73	58.0	-	-	3.2	-
SM28	-5.1	3.1	62	34.1	-	-	4.8	-
SM37	1.0	4.2	31	8.6	-	-	3.3	-
SM46	0.9	4.7	31	8.6	-	-	3.8	-
SM55	-0.8	4.9	40	12.9	-	-	5.0	-
SM64	3.0	3.0	21	5.1	-	-	1.7	-
SM82	-5.9	2.4	66	19.5	-	-	1.6	-
SM73	3.2	3.1	19	2.1	45-65	3077-4444	3.9	2.7-6.9
SM91	3.8	1.2	16	1.9	45-65	3077-4444	0.6	2.4-6.1
SM100	2.3	2.2	24	2.9	45-65	3077-4444	1.4	3.8-9.6
SM109	-6.2	0.5	68	21.7	45-65	3077-4444	0.8	28.3-70.6
SM118	5.5	1.8	8	0.7	45-65	3077-4444	0.4	1.0-2.4
SM127	5.9	9.0	6	0.4	45-65	3077-4444	1.8	0.5-1.2
SM136	1.9	2.9	26	3.2	45-65	3077-4444	2.0	4.2-10.4
PR-CT-1	-2.7	0.7	50	5.9	26	7692	0.9	7.6
PR-CT-2	-7.1	1.0	73	24.8	35	5714	1.8	43.2
PR-CT-3	-2.6	0.2	49	7.4	65	3076	0.2	24.2
PR-CT-4	-4.8	0.9	61	8.1	27	7407	1.3	11.0
PR-CT-5	-5.5	0.8	64	15.7	28	7143	1.3	22.0
PR-CT-6	3.0	2.2	20	1.0	33	6061	1.1	1.7
PR-CT-7	1.6	1.9	28	3.1	29	6897	1.3	3.9
PR-CT-8	-3.3	2.1	53	7.7	36	5556	2.7	13.9
PR-CT-9	-5.9	2.5	66	17.4	29	6897	4.0	25.2
PR-CT-10	-4.1	1.8	57	8.1	44	4545	2.5	18.0
PR-CT-11	-0.7	1.0	39	5.6	37	5405	1.0	10.4
PR-CT-12	-6.4	0.4	69	20.7	35	5714	0.7	35.8

Ranges of data comes from two estimates of soil residence time [Chabaux et al., 2013; Pett-Ridge et al., 2009]

Table 6. Soil environmental variables averaged from three pit sites.

Sample#	Slope (%)	Aspect (degrees)	Longitude (degrees)	Latitude (degrees)	Elevation (m)	Forest Type	Soil Class.	Bedrock Type	Annual Rainfall (mm)*
SM1	16.5	279.6	-65.8485	18.27728	797	Colorado	Oxisols	Volcaniclastic	4134
SM10	13.7	225.3	-65.826	18.31002	521	Colorado	Oxisols	Volcaniclastic	3786
SM19	12.1	234.7	-65.8397	18.26555	740	Colorado	Oxisols	Volcaniclastic	4071
SM28	6.3	121.6	-65.8297	18.32036	441	Tabonuco	Oxisols	Volcaniclastic	3658
SM37	11.6	186.6	-65.7412	18.31556	376	Tabonuco	Oxisols	Volcaniclastic	3538
SM46	20.0	12.2	-65.8159	18.31831	582	Tabonuco	Oxisols	Volcaniclastic	3873
SM55	8.7	288.3	-65.8183	18.30988	616	Colorado	Oxisols	Volcaniclastic	3919
SM64	14.1	209.9	-65.8525	18.27432	694	Tabonuco	Oxisols	Volcaniclastic	4017
SM82	13.4	160.2	-65.7703	18.3042	444	Tabonuco	Inceptisols	Volcaniclastic	3662
SM73	12.6	318.9	-65.7858	18.2961	778	Colorado	Inceptisols	Quartz Diorite	4113
SM91	7.2	65.1	-65.7956	18.29212	785	Colorado	Inceptisols	Quartz Diorite	4121
SM100	7.7	198.9	-65.7858	18.27137	661	Colorado	Inceptisols	Quartz Diorite	3977
SM109	18.8	266.1	-65.7944	18.27063	538	Colorado	Inceptisols	Quartz Diorite	3811
SM118	27.6	111.2	-65.803	18.26356	584	Tabonuco	Inceptisols	Quartz Diorite	3876
SM127	35.0	19.0	-65.7959	18.26788	565	Tabonuco	Inceptisols	Quartz Diorite	3849
SM136	14.5	166.6	-65.7935	18.26307	379	Tabonuco	Inceptisols	Quartz Diorite	3544
PR-CT-1	-	-	-65.7856	18.27099	678	Colorado	-	Quartz Diorite	3998
PR-CT-2	-	-	-65.786	18.27187	685	Colorado	-	Quartz Diorite	4006
PR-CT-3	-	-	-65.7872	18.27208	674	Colorado	-	Quartz Diorite	3993
PR-CT-4	-	-	-65.7877	18.27471	687	Colorado	-	Quartz Diorite	4009
PR-CT-5	-	-	-65.7883	18.27235	697	Colorado	-	Quartz Diorite	4021
PR-CT-6	-	-	-65.7906	18.28097	710	Colorado	-	Quartz Diorite	4036
PR-CT-7	-	-	-	-	-	Colorado	-	Quartz Diorite	-
PR-CT-8	-	-	-65.7963	18.29194	760	Colorado	-	Quartz Diorite	4093
PR-CT-9	-	-	-65.7977	18.29271	772	Colorado	-	Quartz Diorite	4107
PR-CT-10	-	-	-65.796	18.28943	815	Colorado	-	Quartz Diorite	4152
PR-CT-11	-	-	-65.7949	18.2905	795	Colorado	-	Quartz Diorite	4132
PR-CT-12	-	-	-65.7907	18.28843	668	Colorado	-	Quartz Diorite	3985

*estimated rainfall based on PRISM model [Daly et al., 2003]

Table 7. Soil Data from Tamayo Thesis [2014]

Site Name	Ridge Width (m)	Soil C (%)	HCO3-Pi (ppm)	NaOH-Pt (ppm)	τSi
PR-CT-1	17	4.3	0.8	49	-0.33
PR-CT-2	5	4.8	0.5	59	-0.46
PR-CT-3	9	5.2	0.9	61	-0.47
PR-CT-4	11	4.8	1.4	61	-0.45
PR-CT-5	14	5.6	0.9	47	-0.44
PR-CT-6	11	3.8	0.0	33	-0.29
PR-CT-7	21	6.0	1.1	46	-0.18
PR-CT-8	26	14.0	3.1	75	-0.62
PR-CT-9	54	13.5	3.7	79	-0.62
PR-CT-10	42	16.6	5.4	116	-0.68
PR-CT-11	15	4.1	0.4	38	-0.30
PR-CT-12	21	5.1	0.4	46	-0.40

3.9 Figures

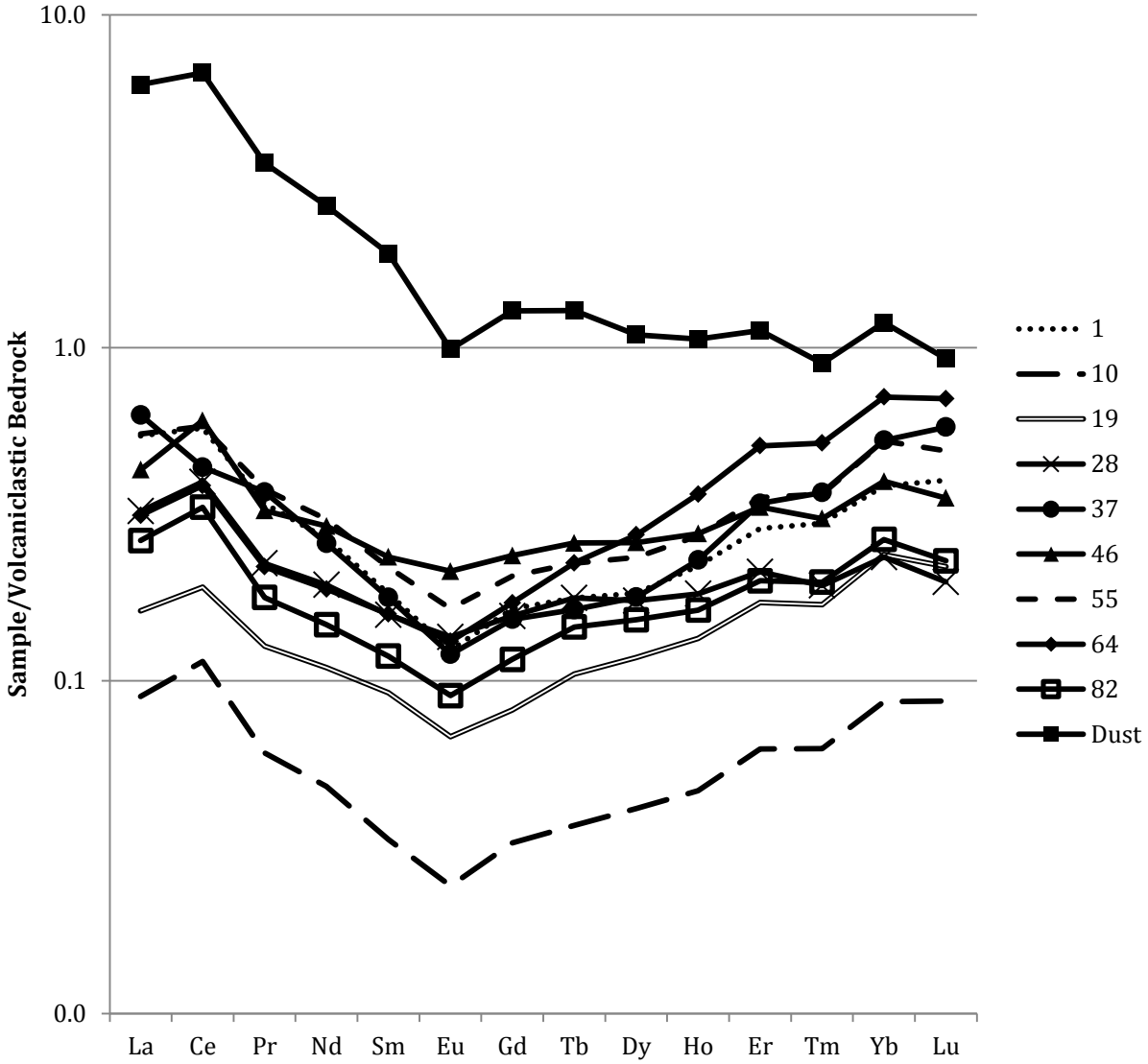

Figure 1. REE distribution of soils on volcaniclastic bedrock normalized to volcaniclastic bedrock concentrations of REEs.

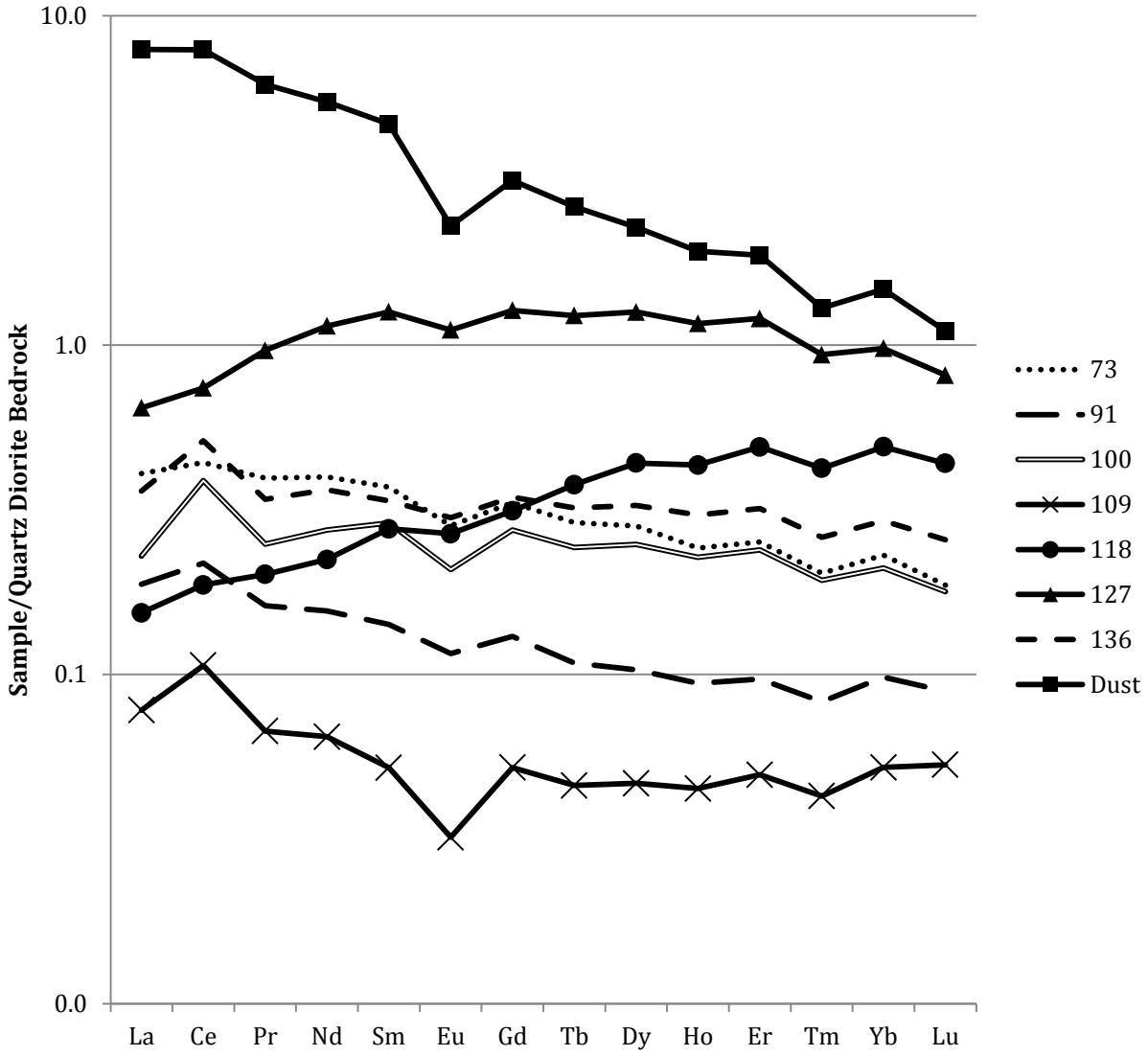

Figure 2. REE distribution of soils on quartz diorite bedrock normalized to quartz diorite bedrock concentrations of REEs.

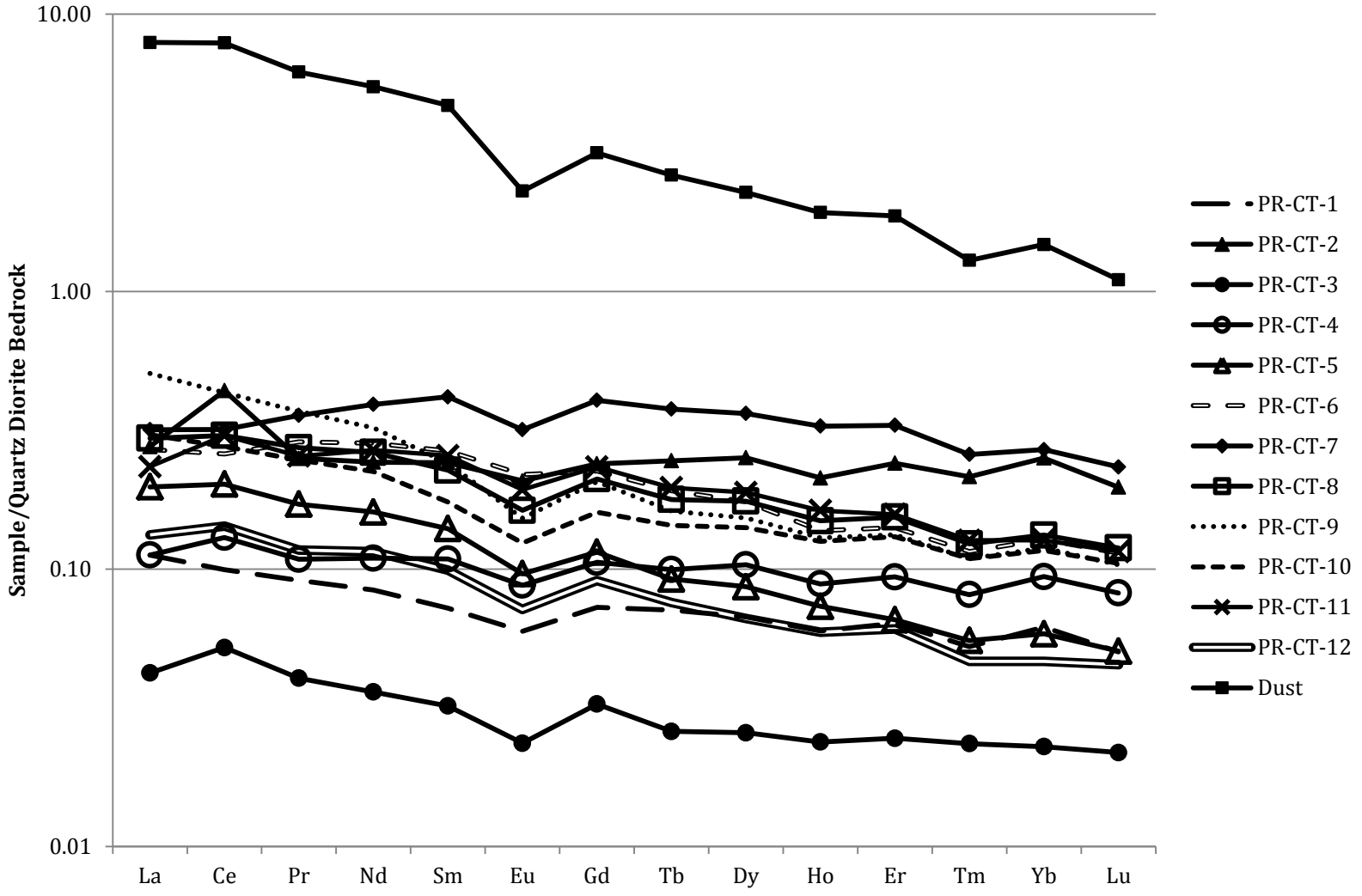

Figure 3. REE distributions of soils that were paired with ^{10}Be denudation rates normalized to quartz diorite bedrock concentrations of REEs.

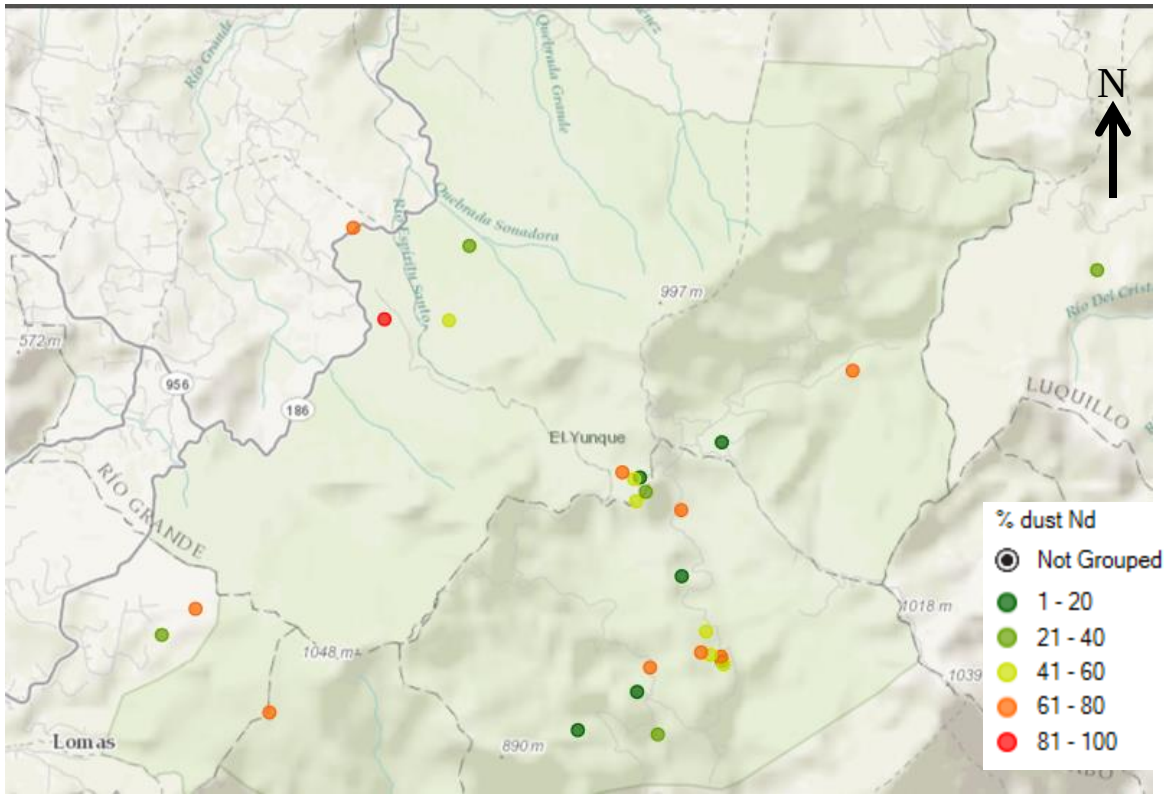

Figure 4. Map of El Yunque National Forest with locations of all 31 soil samples. Colors indicate the % of Nd that has been derived from dust, calculated using ƐNd values.

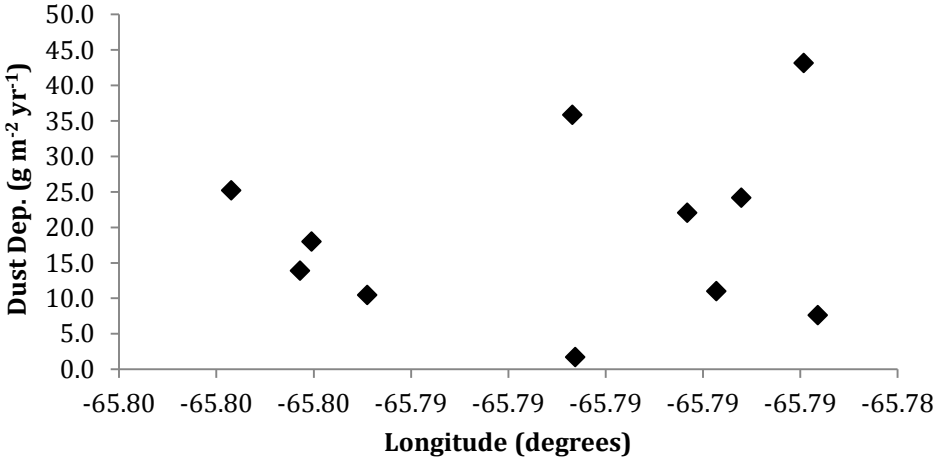

Figure 5. Longitude vs. the amount of dust deposition calculated from ƐNd on quartz diorite soils with associated 10Be denudation rates.

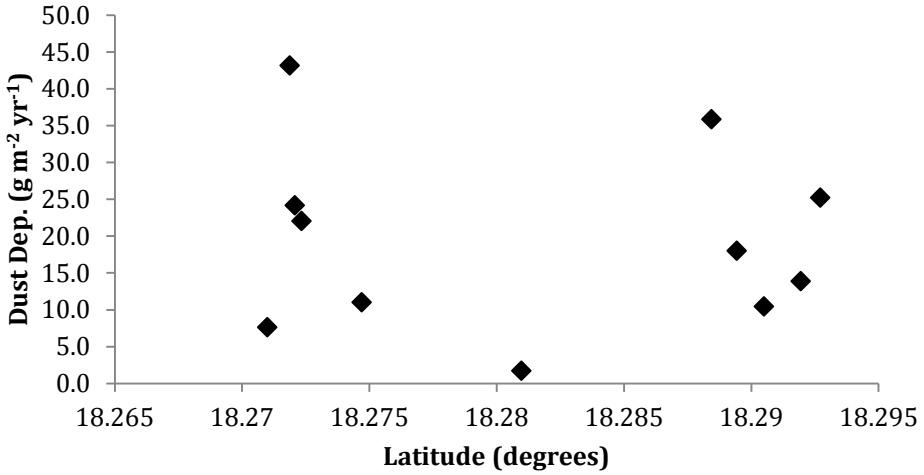

Figure 6. Latitude vs. the amount of dust deposition calculated from ƐNd on quartz diorite soils with associated 10Be denudation rates.

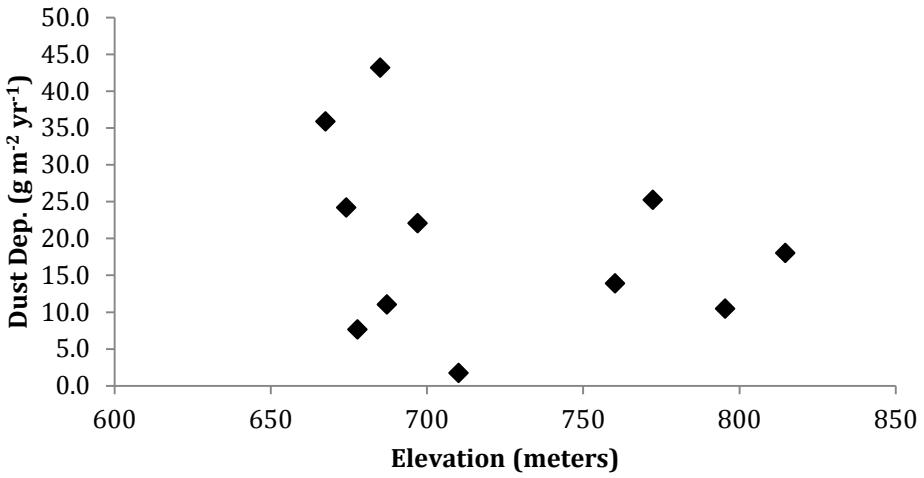

Figure 7. Elevation vs. the amount of dust deposition calculated from ƐNd on quartz diorite soils with associated ^{10}Be denudation rates.

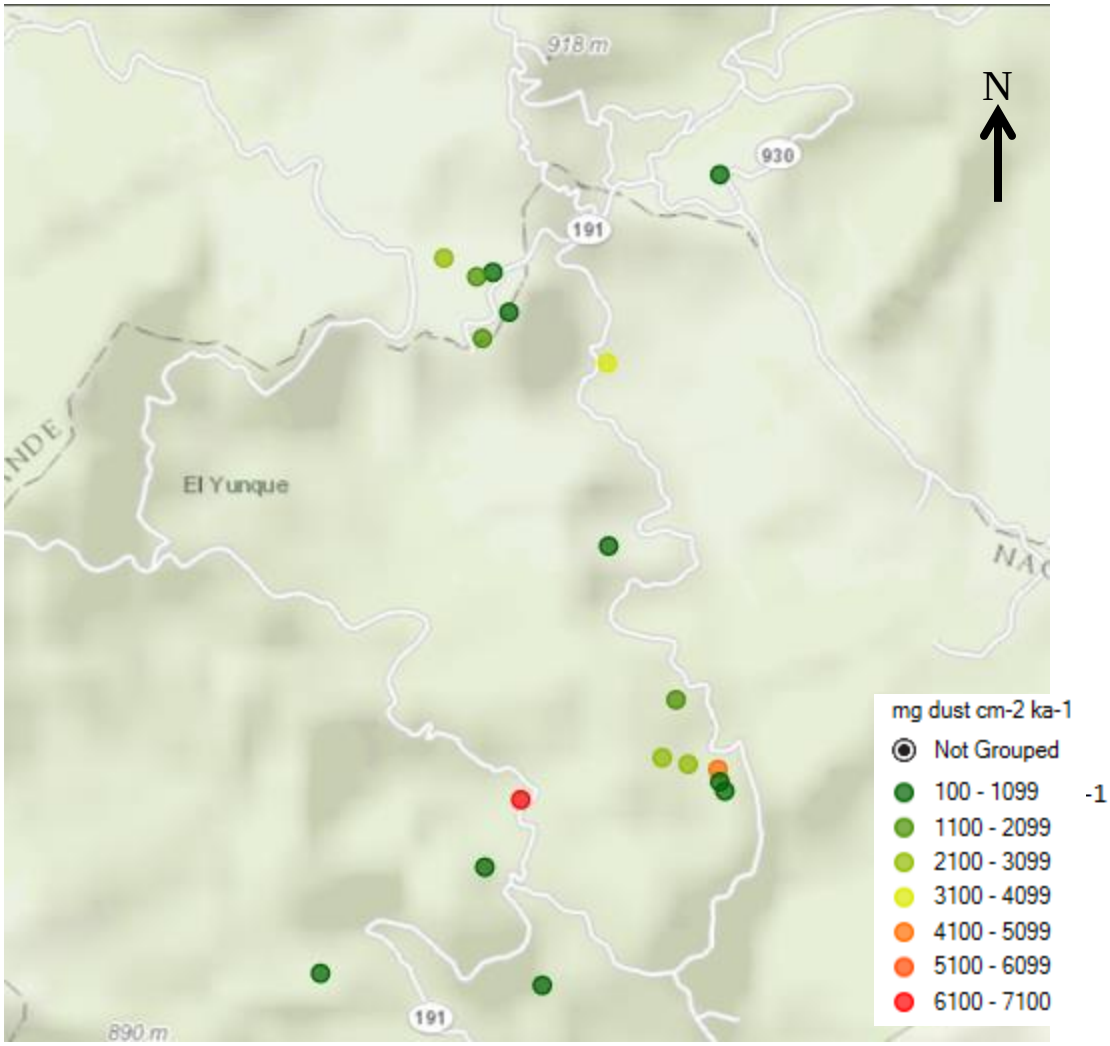

Figure 8. Map of El Yunque National Forest with locations of the 19 soils located on quartz diorite bedrock. Colors indicate rates of dust deposition calculated from ε$_{Nd}$, with low end estimates of soil residence times for soils unpaired with ^{e}Be data.

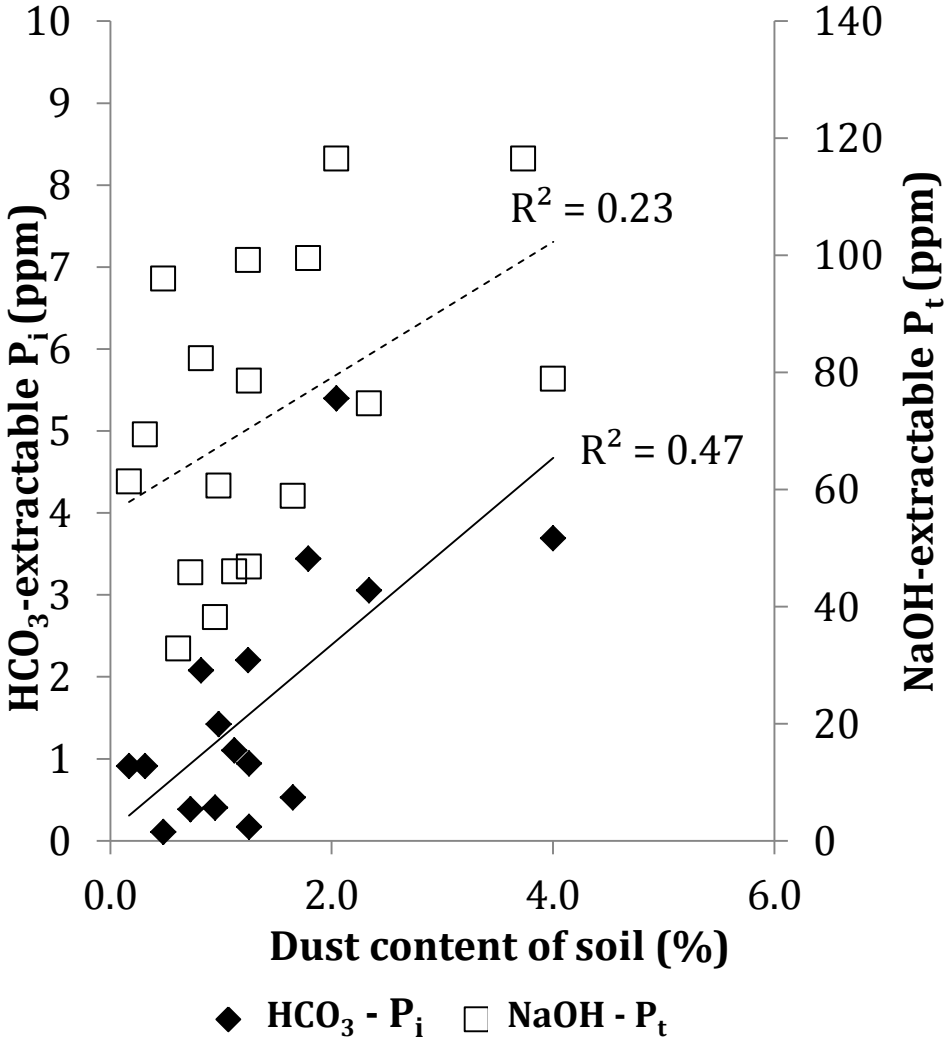

Figure 9. Current % dust content of quartz diorite soils plotted against $NaHCO_3$-extractable P (labile P) and NaOH - extractable P (organic P).

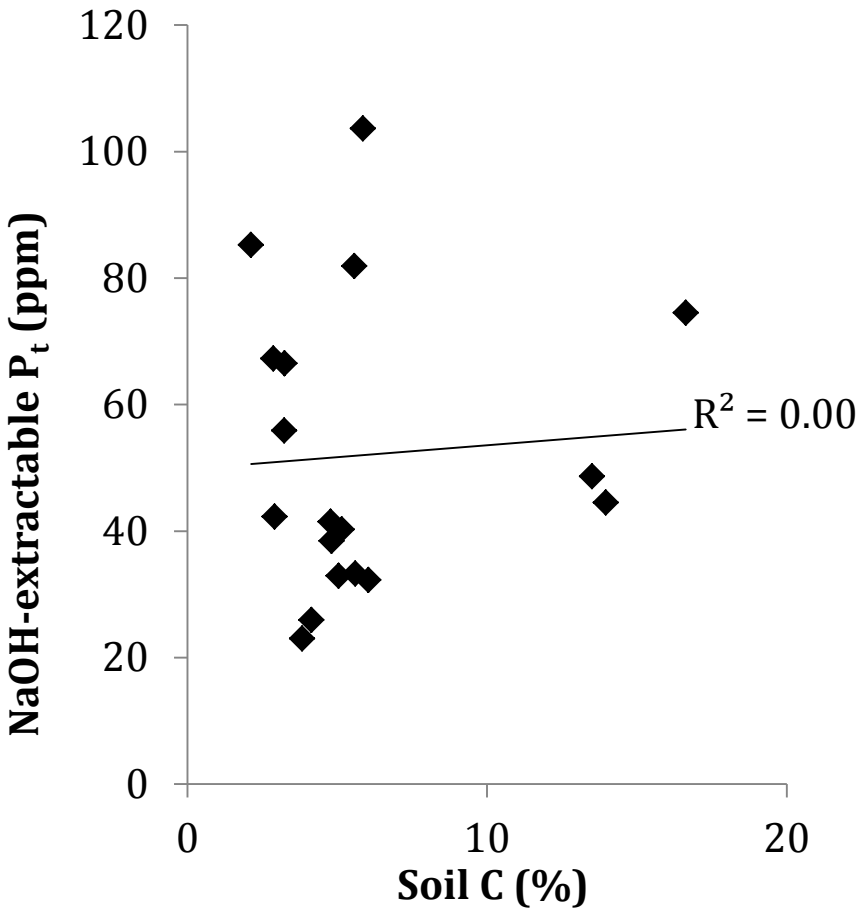

Figure 10. % soil carbon vs. NaOH - extractable P (organic P) for quartz diorite soils.

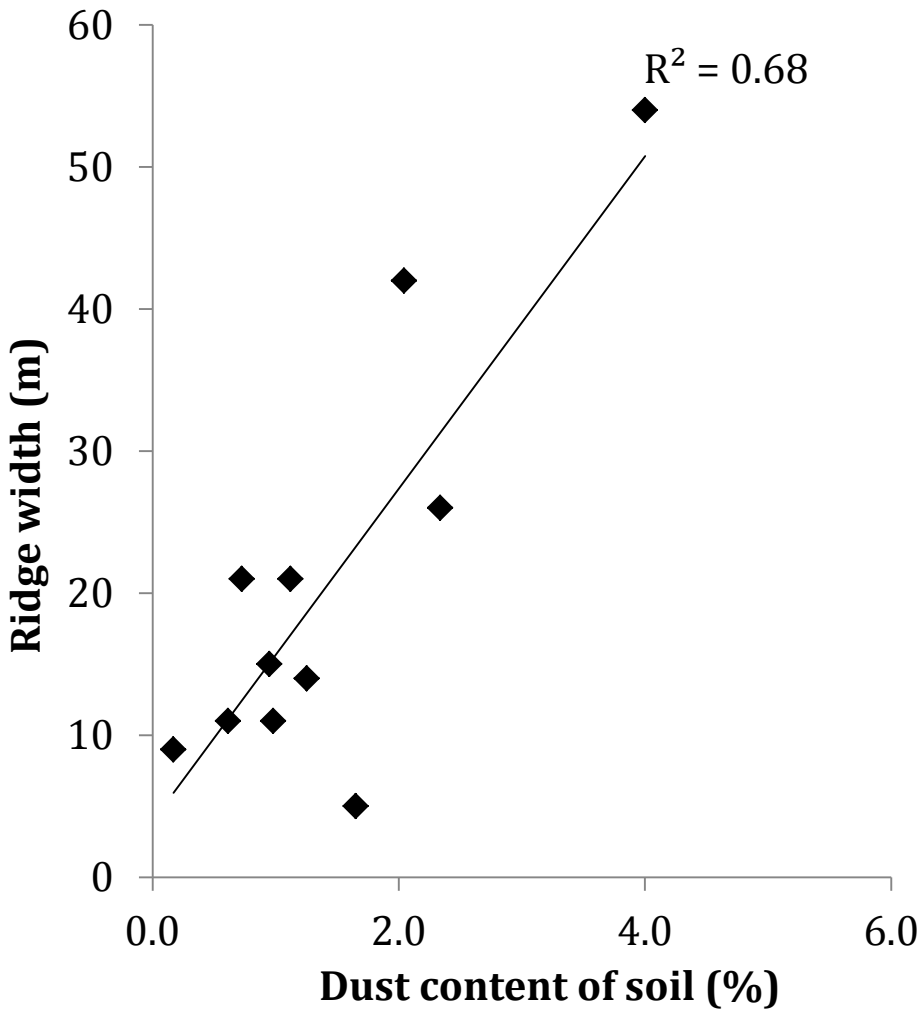

Figure 11. Current % dust content of soil vs. width of the ridges they formed on.

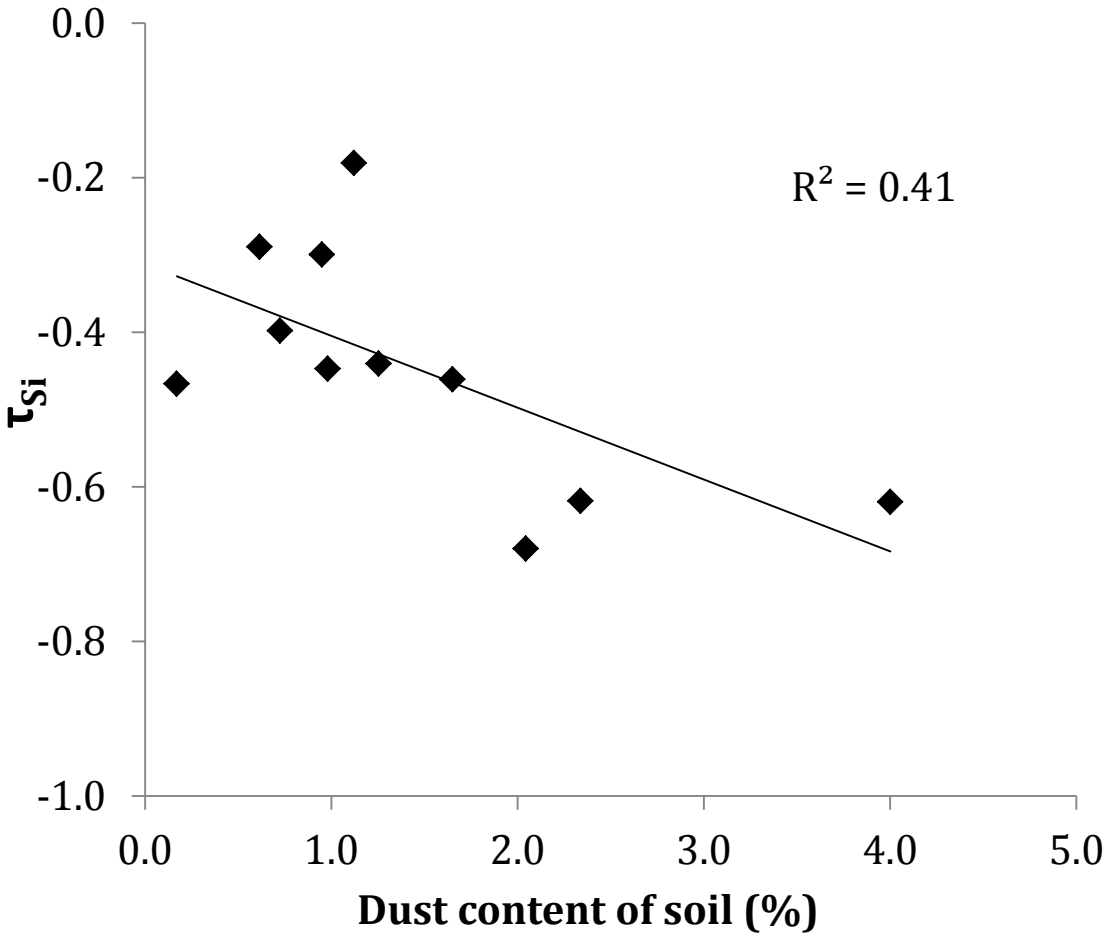

Figure 12. Current % dust content of soil vs. τSi, a measure of soil weathering based on the fraction of Si remaining in the soil relative to an immobile index element, Zr.

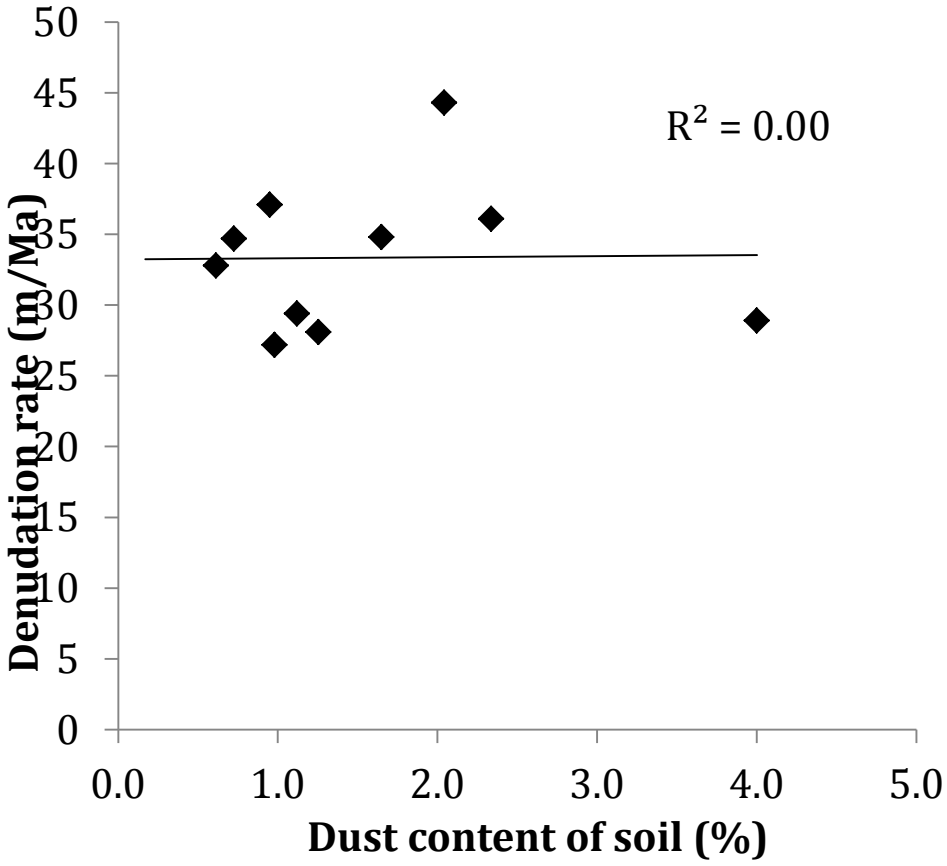

Figure 13. Current % dust content of soil vs. the denudation rates of soil calculated from ^{10}Be measurements.

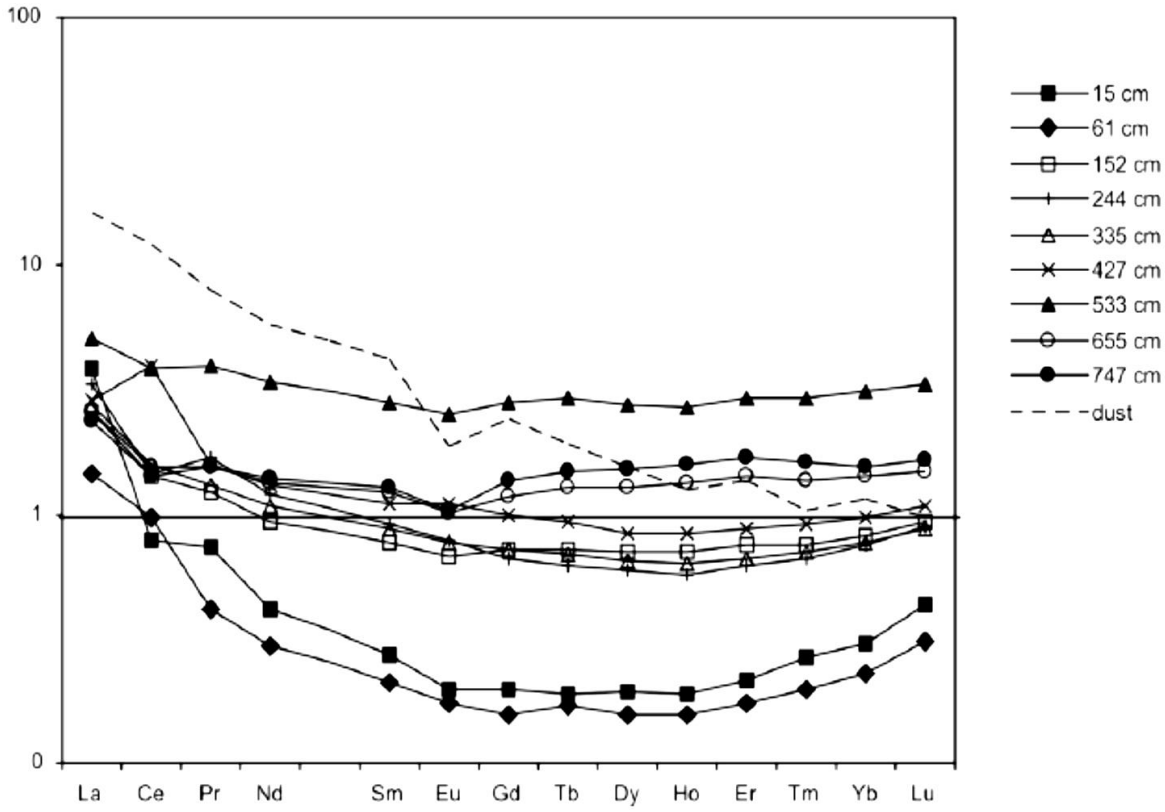

Figure 14. Distribution of REE in soil from different depths in the same profile normalized to the bedrock underneath.

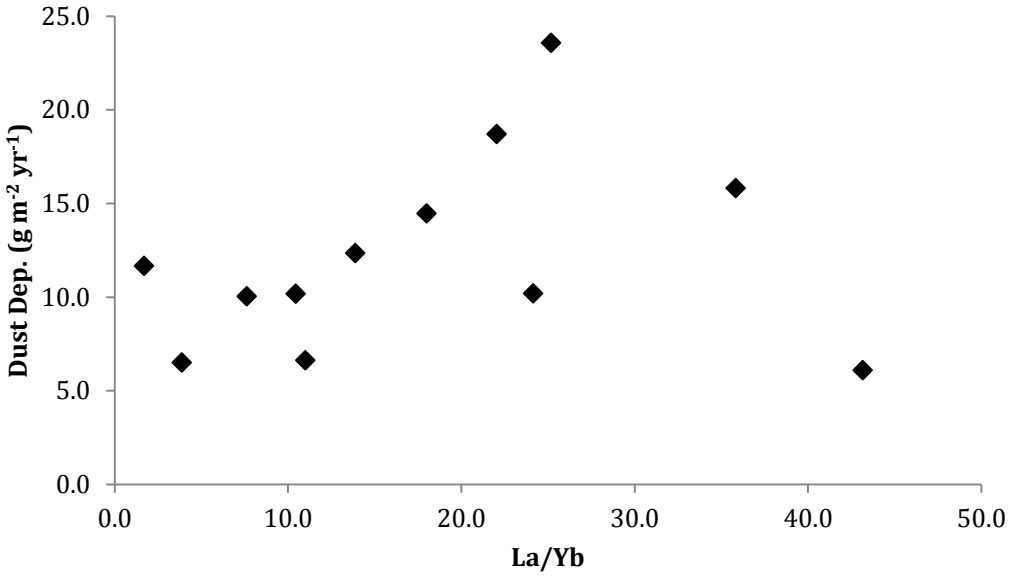

Figure 15. Rate of dust deposition calculated from εNd values vs. La/Yb in soils with precise denudation rates from ^{10}Be data.

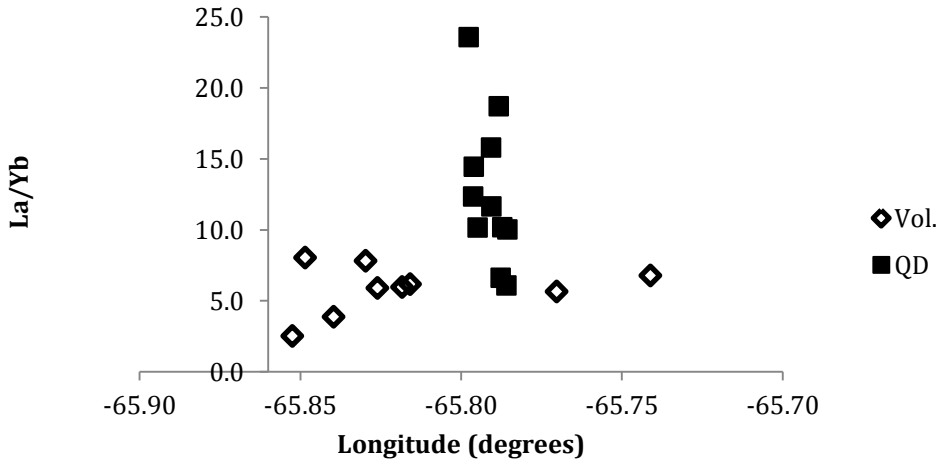

Figure 16. Longitude vs. La/Yb of all soils separated by bedrock type.

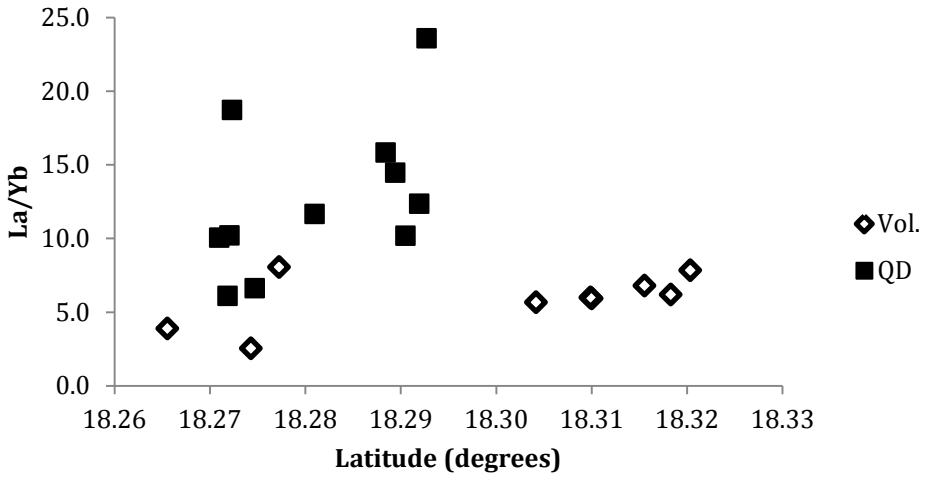

Figure 17. Latitude vs. La/Yb of all soils separated by bedrock type.

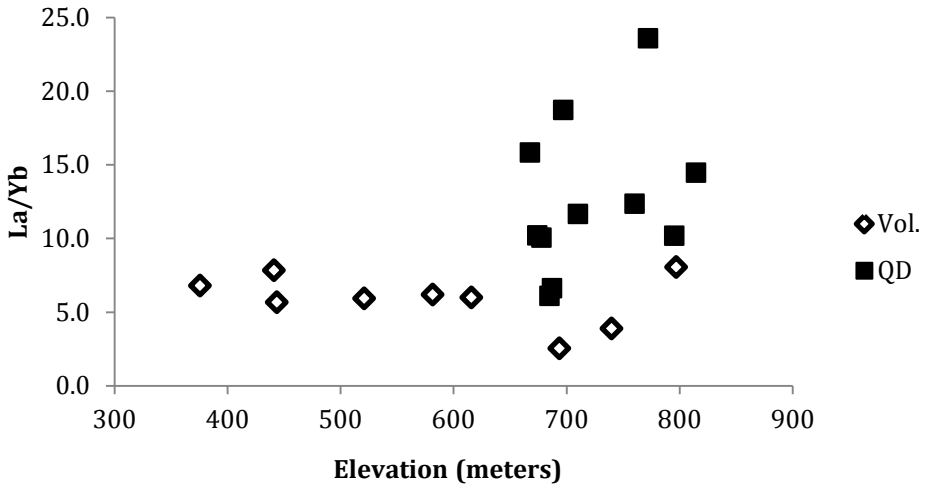

Figure 18. Elevation vs. La/Yb of all soils separated by bedrock type.

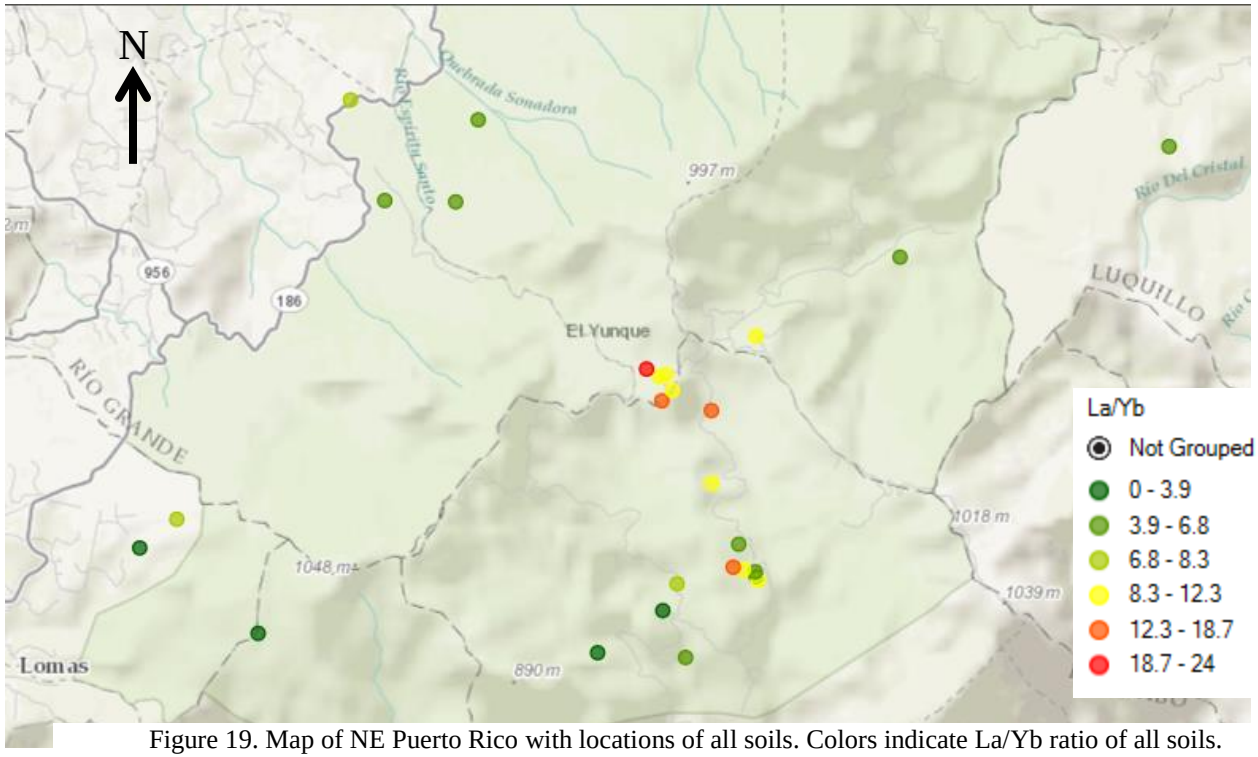

Figure 19. Map of NE Puerto Rico with locations of all soils. Colors indicate La/Yb ratio of all soils.

4 Thesis Conclusion

Mineral aerosols are implied to have a significant effect on the productivity of certain terrestrial ecosystems where rock-derived nutrients are limiting. But quantifying the rate at which mineral aerosols reach soil is a very difficult procedure, and is therefore rarely done multiple times in the same landscape. If the effect dust deposition has on terrestrial environments is to be investigated by future researchers, site specific dust deposition rates are required. In this thesis, I have presented evidence that the rates of dust deposition can be highly variable across small distances relative to what can be measured by satellite imagery. This spatial variability persists through timescales relevant to soil development, and is prominent enough to be detected on shorter timescales in rainwater.

When paired with records of airmass provenance, two rain chemistry datasets from two locations for twenty years reveals that dust deposition can double in as little as 10 km in the Luquillo Mountains of Puerto Rico. The seasonality of dust deposition in these rainfall datasets shows that deposition rates are linked to surface conditions in the Sahel region of Africa, and that any changes to surface conditions in the Sahel from agriculture or climate change will alter deposition rates in ecosystems across the Atlantic Ocean.

To obtain a longer record of dust deposition across a wider area, I quantified the dust present in soil using isotopic ratios of neodymium (Nd). Because the dust from the Sahara-Sahel region has an $^{143}Nd/^{144}Nd$ drastically different from the $^{143}Nd/^{144}Nd$ of the bedrock in Puerto Rico, a simple two endmember mixing model can be used to apportion the amount of Nd in soil that came from dust, and the amount that came from bedrock.

To calculate dust deposition rates, weathering and soil residence time needs to be accounted for. I estimated the weathering rate of dust derived Nd to be proportional to the weathering rate of bedrock derived Nd, and soil residence times were calculated from ^{10}Be measurements of soil denudation rates. Using this method shows there is at least a twenty-six fold variation in deposition rates across the approximately 100 km^2 of the Luquillo Mountains. Comparing the percentage of soil that is made from dust shows that the variability in dust deposition does influence the amount of plant-available phosphorus in the soil.

In this thesis, I have presented evidence that dust deposition varies on spatial scales not previously measured. This amount of spatial variability should serve as a cautionary message to other researchers investigating natural processes that are influenced by dust deposition. For example, the contribution of dust to terrestrial fertilization may be significant in one location of a landscape, but insignificant in another. The contributions of dust should be well quantified on small spatial scales before concluding whether or not it plays a significant factor in ecosystem processes.